An in-depth investigation on the inhibitory activity of a native cave fungus against *Pseudogymnoascus destructans*.

By
Jennifer Lynn Kolwich

A Thesis Submitted to
Saint Mary's University, Halifax, Nova Scotia
in Partial Fulfillment of the Requirements for
the Degree of Master of Science in Applied Science.

August 2021, Halifax, Nova Scotia

Approved: Dr. Clarissa Sit
Supervisor
Department of Chemistry

Approved: Dr. Christa Brosseau
Supervisory Committee Member
Department of Chemistry

Approved: Dr. Genlou Sun
Supervisory Committee Member
Department of Biology

Approved: Dr. John Sorensen
External Examiner
Department of Chemistry
University of Manitoba

Date: August 20, 2021

An in-depth investigation on the inhibitory activity of a native cave fungus against *Pseudogymnoascus destructans*.

By Jennifer Lynn Kolwich

Abstract

A metabolite-based treatment for *Pseudogymnoascus destructans*, the causative agent of bat White-nose syndrome, was isolated from a soil fungus native to Eastern Canada. Three application methods were modelled using media-based assays to determine how the treatment could be applied *in situ*: an environmentally-applied prophylactic, a topically-applied prophylactic, and a topical post-infection treatment. *P. destructans* growth was effectively slowed in all three models.

After separation and characterisation, an active molecule in the metabolite-based treatment was determined to be griseofulvin, a known antifungal compound. This compound was tested against *P. destructans* using the topically-applied prophylactic method and proved to be more potent than the crude metabolite mixture.

To identify the mechanism of action of the metabolite-based treatment, transcriptome analysis was performed on control and treated groups of the target fungus *P. destructans* and a non-target Pseudogymnoascus species. To date, transcript reads were aligned and quantified. Further differential expression analysis must be completed.

August 20, 2021

Acknowledgements

First and foremost, I would like to thank my supervisor, Dr. Clarissa Sit, for her guidance, effort, and patience in her mentorship of me throughout my bachelor's and master's degrees. The opportunities she has granted me are numerous, and have helped shape me as a researcher, learner, and teacher. I would also like to thank the faculty and staff in the Department of Chemistry at Saint Mary's University, who have helped me grow and learn, and have supported me and my goals over the last seven years. In particular, Dr. Clarissa Sit, Mary Sheppard, and Dr. Kai Ylijoki for allowing me countless opportunities to develop my science communication skills in my pursuit of teaching and a very special thank you to Patricia Granados and Alyssa Doué, not only for instrument and technical support, but also for emotional support. I couldn't have asked for better technicians (or cheerleaders)!

I would also like to thank the other students who contributed to this work: Tanner George for his enthusiasm at taking my mystery crystals trudged out of a messy fungal metabolite soup and identifying them so quickly; Tanisha Ballard, who was an invaluable resource during crunch time; and of course my partner in crime (or at the very least, in slime), Lindsay Donovan who helped plan and carry out much of the work completed on this project.

I would like to acknowledge NSERC and the FGSR for financial support.

I would also like to thank my committee members Dr Christa Brosseau and Dr Genlou Sun for their time and expertise throughout this process.

I would like to thank my family and friends for their constant support and apologise for making all of them listen to me rant about bats and bread mould for the better part of four years. Completing a master's during a global pandemic certainly made it a challenge to stay sane, but they kept me afloat. Finally, and most importantly, I would like to thank my parents Kevin and Colinda for their love, support, and unwavering belief in me and my abilities. I know I will always be okay, as long as I have them in my corner.

Table of Contents

List of Abbreviations

BLAST	Basic Local Alignment Search Tool
cDNA	complementary Deoxyribonucleic Acid
CFU	Colony Forming Unit
COSY	correlation spectroscopy
d	doublet
DAD	Diode Array Detector
DEPT	Distortionless Enhancement by Polarisation
DGE	Differential Gene Expression
ESI	Electrospray Ionisation
GC	Gas chromatography
GO	Gene Ontology
HMBC	Heteronuclear Multiple Bond Correlation
HPLC	High Performance Liquid Chromatography
HRMS	High-Resolution Mass Spectrometry
HSQC	Heteronuclear Single Quantum Correlation
Indels	Insertion-Deletion events
IR	Infrared Spectroscopy
LC	Liquid Chromatography
m	medium (IR)
m	multiplet (NMR)
MIC	Minimum Inhibitory Concentration
MMP	Maximal Mappable Prefix
m.p.	melting point
NMR	Nuclear Magnetic Resonance Spectroscopy
NOESY	Nuclear Overhauser Effect Spectroscopy
Pb	*Pseudogymnoascus bhattii*
PCA	Principal Component Analysis
PCR	Polymerase Chain Reaction
Pd	*Pseudogymnoascus destructans*
PolyA	Polyadenylated
Pp	*Pseudogymnoascus pannorum*
Pr	*Pseudogymnoascus roseus*
Prep-TLC	Preparatory Thin-Layer Chromatography
QC	Quality Control
qPCR	quantitative Polymerase Chain Reaction
QTOF	Quadrupole Time-of-Flight
RIN	RNA Integrity Number
RNA	Ribonucleic Acid
RNA-Seq	RNA Sequencing
rRNA	ribosomal Ribonucleic Acid
s	strong (IR)
s	singlet (NMR)
S9	*Penicillium canescens* Strain S9
SBS	Sequencing by Synthesis
TIC	Total Ion Chromatograms
TLC	Thin-Layer Chromatography
UV-vis	Ultraviolet-visible Absorption Spectroscopy
VOC	Volatile Organic Compound
vs	very strong
w	weak
WNS	White-nose Syndrome
YMA	Yeast Mold Agar
YMB	Yeast Mold Broth
ε	molar absorptivity coefficient

List of Tables

List of Figures

Chapter 1: Introduction

1.1 Project Overview

North American Bat White-nose Syndrome (WNS) is a devastating disease caused by the fungus *Pseudogymnoascus destructans* (*Pd*). Responsible for the deaths of millions of bats, WNS has led to the decline and regional extinction of bat populations throughout eastern North America.[1] As of May 2021, the disease has been detected in 37 US states and seven Canadian provinces.[2]

Effective treatment and prevention of the disease requires an understanding of its cause, mechanism, and geographical reach. In the early 2010s, much of the foundational work was done in this area, including determining the cause of the disease, tracking the sites affected by the disease, revealing the origin of the fungus, and identifying the mechanism by which the disease leads to mortality. Currently, work on WNS is focused on controlling the spread of the disease between contaminated sites, as well as looking for treatments to help mitigate the damage in affected areas, thus allowing for the revival of lost populations. These treatments have focused not only on the bats themselves but also on contaminated cave sites.

The story of WNS is one that is still actively unfolding. While the cause and origin of the disease have been determined, the inability of many classical immunity models to solve this issue makes it unique and challenging—requiring creativity and patience in pursuit of a solution. Currently, one of the most promising solutions lies in utilising pre-existing microbe-microbe interactions to limit the spread and impact of the disease. Direct probiotic application and microbially-produced volatile organic compound-based fumigation are two of the main microbially-derived treatments for WNS that have been

investigated. However, these generally involve microbes not native to the bats or their environment, and the treatments are usually not assessed for selectivity against *Pd*. Therefore, the invasive and non-specific nature of these treatments poses a risk, as they may further disrupt the already fragile microbiome of bats that are infected or at risk of infection with *Pd*. Furthermore, most efforts in the direct application of probiotics have neglected to identify the active compounds responsible for inhibition. Without understanding the compound(s) responsible for the inhibition, the mechanism of the inhibition, and therefore the full ramifications of the treatment, cannot be fully understood.

By investigating microbes native to North American bats and their environments and elucidating the identity of antimicrobial compounds they produce, there is an opportunity to discover potential treatments that are both effective and specific towards invasive microbes, like *Pd*. Not only could they have potential in treating WNS, but they could be applied more broadly to other infectious diseases.

1.2 Objectives of Thesis

1.2.1 Research Questions

The overarching research question of this project is as follows:

"Can microbes taken from bat skin and cave areas produce effective natural products with antifungal activity against the fungus infecting North American bat populations, Pseudogymnoascus destructans?"

Within this question, the following intermediate questions were used to guide and design project goals and methods:

- **What species of microbes live on bat skin and in their cave environments?** Are any of them known antifungal producers? Are any genetically similar to *Pd*?
- **Do any of these microbes show inhibition against *Pd*?** Is it due to metabolites or resource competition? Is it innate or induced?
- **How could the metabolites be applied as real-world treatment?** Are they stable? Should they be applied to cave environments or bats themselves? Do they work effectively as a WNS preventative or a post-infection treatment?
- **What are the active molecules causing inhibition?** Do they work independently or synergistically? What is their structure?
- **What are the mechanisms of action of the active compounds against *Pd*?** Which genes, organelles, or metabolic pathways are being targeted by the compounds?

1.2.2 Foundational Work

The majority of the work on the first two research questions was completed and outlined in the author's honours thesis, "Discovery of antifungal compounds from the immunobiome of North American bat species threatened by fungal infection with *Pseudogymnoascus destructans*."[3] The key methods and outcomes are summarised below.

Isolation of Environmental Strains

With the aid of collaborators, strains of culturable microbes were collected from Eastern Canadian bats and cave environments. The McMaster Bat Lab swabbed the wings and muzzles of 40 *Eptesicus fuscus* (big brown bats) originating from Ontario, Canada to

collect cutaneous microbes and collaborators at the Myron Smith Lab at Carleton University provided samples collected from soil and rock substrates in and near cave environments in Quebec and Ontario, Canada. These environmental microbe samples were isolated to purity and identified by Sanger sequencing. *Pseudogymnoascus destructans* (the causative agent of WNS) and *Pseudogymnoascus bhattii*, which are not native to Eastern Canada, were obtained from strain libraries. Two species of *Pseudogymnoascus* that are native to Eastern Canada, *Pseudogymnoascus pannorum* and *Pseudogymnoascus roseus*, were also collected from the cave regions in Quebec and Ontario, Canada by the Smith Lab.

Preliminary Pairwise Testing

The compiled isolate strain library was tested against four strains of *Pseudogymnoascus*: *Pseudogymnoascus destructans* (*Pd*, the WNS fungus), *Pseudogymnoascus bhattii* (*Pb*), *Pseudogymnoascus pannorum* (*Pp*), and *Pseudogymnoascus roseus* (*Pr*). The testing process involved a method called pairwise testing, whereby one strain is inoculated on one side of the media, and another is inoculated on the opposite side. Pairwise testing allows for the visualisation of inhibitory activity by one strain against another. This inhibition was quantified by measuring the diameter of each strain while grown pairwise and comparing it to the diameter of strain grown on its own. Each isolate strain from the compiled library was tested against each of the Pseudogymnoascus strains. The pairwise testing for *Pb* and *Pp* occurred at room temperature, while the tests against *Pd* and *Pr* occurred at 12 °C, based on allowable growth temperatures.

The strains with the best overall inhibition scores were F1, F3, S2, S8, and S9, all of which were fungal isolates. These five strains showed the highest potential for inhibition of the *Pseudogymnoascus* strains and were determined to be the most likely source of anti-*Pseudogymnoascus* metabolites. However, this preliminary testing only revealed that inhibition occurred, but did not give any information about the nature of the inhibition. It is possible that the isolate strain was able to effectively compete with the *Pseudogymnoascus* strains by consuming resources and space faster, thus limiting the *Pseudogymnoascus* growth via resource competition. Conversely, the inhibition may have been a result of the secretion of metabolites from the isolates, which were able to limit the growth of the *Pseudogymnoascus* strains; these molecules may be innately produced by the isolate strain regardless of its circumstances, or only excreted when induced by the presence of a competing force.

Extraction of Metabolites

For subsequent bioactivity and chemical testing, metabolites were extracted from the media of the pure isolate strains; F1, F3, S2, S8, and S9. Each of the pure isolate strains were allowed to grow on media for two weeks; then, metabolites were extracted by soaking the agar media in organic solvents. The extracted solvent and metabolites were gravity filtered to remove the bulk particulate matter and the solvent was removed by rotary evaporation. The extracted solids were redissolved in methanol and filtered through a 0.22 μm filter to sterilize the sample. This prevents any cells of the isolate strains from growing in and contaminating subsequent assays using the metabolites.

Metabolite-supplemented Media Testing

By testing the metabolites directly against the *Pseudogymnoascus* strains, it was determined whether the observed inhibition of the five isolate strains was due to inhibitory molecules being secreted into the media by isolate strains or simply due to the presence of two growing stains competing for space and resources.

To test this, the four *Pseudogymnoascus* strains were grown on media that was supplemented to a concentration of 100 μg/mL with the cell-free metabolite solution extracted from the isolate strains, removing the factor of resource competition. The metabolite extract was added to the molten media and mixed in before it solidified. The area of the growth of the *Pseudogymnoascus* strains was measured after ten days and converted to coverage scores: a percent ratio based on the total coverage on the supplemented media to the growth of each respective *Pseudogymnoascus* on control media. Low *Pseudogymnoascus* coverage indicated significant inhibitory activity by the isolate strains' metabolites, and thus a high chance of interference competition.

Overall, F1, F3, S2, and S8 showed minimal inhibition of growth (all with >60% coverage). The metabolites of S9 showed nearly complete inhibition of growth of *Pb* and *Pd* (with 4 and 3% coverage, respectively) and moderate inhibition of *Pp* and *Pr* (with 52 and 50% coverage, respectively, Figure 1.1). These results indicated that F1, F3, S2, and S8 only inhibited the *Pseudogymnoascus* strains via resource competition or that the inference activity is not innate. Since the experiment was performed using the extracted metabolites of the pure isolates, as opposed to ones originating from pairwise tested strains, the inhibitory metabolites of the isolate strains may only be produced when induced by the

presence of the *Pseudogymnoascus* strains. Conversely, S9 did show innate activity, with active biomolecules clearly being produced by the pure isolate.

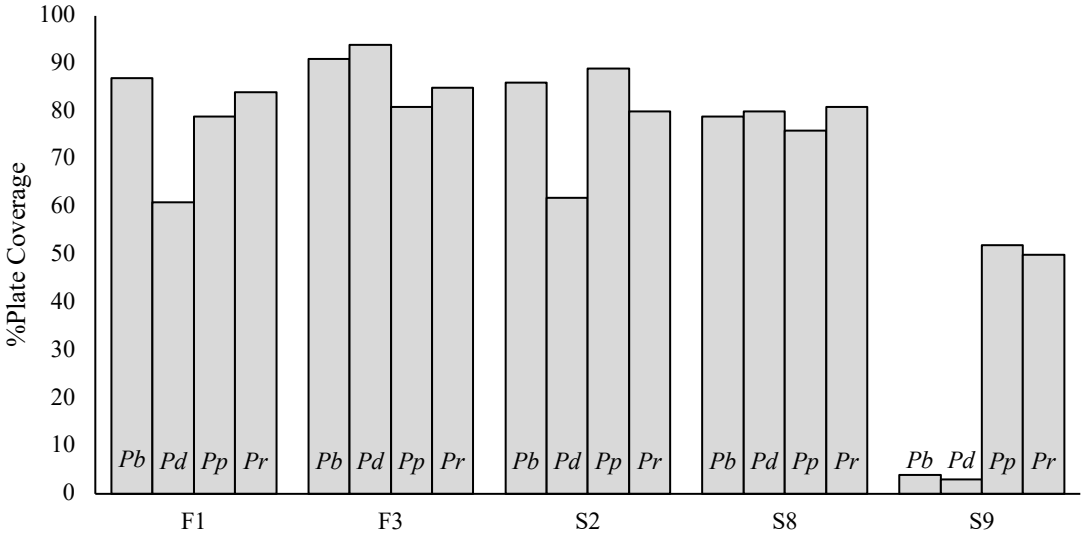

Figure 1.1. Percent coverage of Pseudogymnoascus strains, *Pb, Pd, Pp, and Pr* on media supplemented with the extracts from the media of isolate strains F1, F3, S2, S8, and S9. The coverage scores were a percent ratio based on the total coverage of the respective Pseudogymnoascus on un-supplemented media.

The metabolites from the S9 supplemented plates were re-extracted after the *Pseudogymnoascus* strains had grown, then re-supplemented into new media, where the *Pseudogymnoascus* strains were inoculated again; this process occurred twice to test if the inhibitory activity could be sustained. After each extraction, the metabolites were also analysed by reverse-phase liquid chromatography paired with a diode array detector (LC/DAD) to visualise changes in the chemical profile of the metabolites.

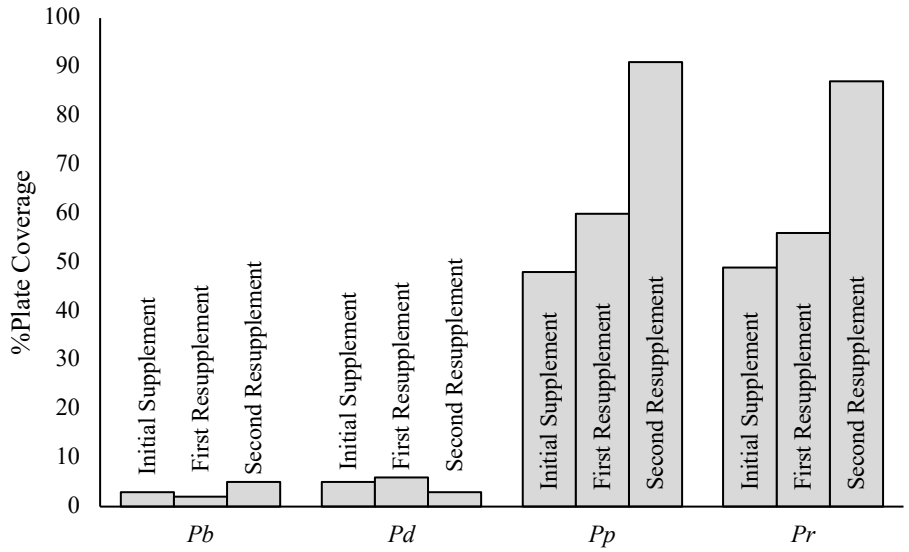

Figure 1.2. Percent coverage of *Pseudogymnoascus* strains, *Pb, Pd, Pp, and Pr* on media supplemented with the extracts from S9. Metabolites were reextracted from the media after growth and supplemented into new media and growth was measured. The coverage scores were a percent ratio based on the total coverage of the respective *Pseudogymnoascus* on un-supplemented media.

The S9 re-supplementation revealed that with repeated extraction, the S9 metabolites retained strong activity against *Pb* and *Pd,* with coverage scores of 5 and 3% respectively on the second resupplementation; however, the activity was progressively lost against *Pp* and *Pr*, with coverage scores of 91 and 87% respectively on the second resupplementation (Figure 1.2). The inhibition in *Pb* and *Pd* was retained after eight weeks, after which the experiment was concluded. Furthermore, the chemical profiles for the S9 metabolites extracted from the control, *Pb*, and *Pd* media remained fairly consistent each round, but degradation of a specific peak (molecular ion: 569 m/z) was visible in both the *Pp* and *Pr* chromatograms.

The limited inhibition of *Pp* and *Pr* as well as the degradation observed in the chemical profiles reveals that fungal species native to the same region as S9 may have

developed a mechanism to overcome its inhibitory metabolites. However, the active S9 compounds were able to remain stable and retain activity over multiple extractions and rounds of *Pseudogymnoascus* growth for the non-native species, *Pb* and *Pd*.

The conclusion of the honours thesis was that the compounds of S9 have strong potential as a treatment for WNS as they show strong, specific inhibition toward invasive *Pseudogymnoascus* species, while only moderately affecting native species. This work established a microbe library of bat-associated microbes and identified a potential candidate, S9, a strain of *Penicillium canescens* isolated from a cave site in Eastern Canada, as a microbe able to use specific and innate interference competition against *Pd*. The activity and identity of the S9 metabolites will be the focus of the work outlined in this Master of Applied Science thesis.

1.3 Scope of Thesis

The remainder of the thesis is divided into four sections, with all references appearing at the end of the document in Chapter 6. Chapter 2 is a review of relevant literature used to guide the direction and design of the research completed in this project. Chapters 3 to 5 represent major research projects undertaken during the course of the Master of Applied Science program. In Chapter 3, various assay methods were designed and implemented to model the efficacy of the S9 metabolites as a real-world treatment. Chapter 4 focuses on the separation and testing of the S9 metabolites, as well as characterisation of one of the isolated active compounds. Chapter 5 presents a mini-review on the methodology used in transcriptomic analysis and how it can be used to identify the mechanism of action of the inhibitory S9 metabolites; in this section, only early-stage methods and results are discussed due to delays in the project as a result of the COVID-19 Pandemic. Together, these chapters draw on the conclusion of the prior research by exploring the potential of the S9 metabolites as a treatment and beginning to identify the chemical and biological nature of the inhibition.

Chapter 2: Literature Review

2.1 An Introduction to Bats

2.1.1 Diversity and Significance of Order Chiroptera

Chiropterans, or bats, are incredibly diverse and unique creatures. With over 1250 species, Chiroptera is the second largest order of class Mammalia, making up over 20% of all mammalian diversity.[4,5] As the only mammals capable of sustained flight, bats are evolutionarily distinct, with no close relatives.[6] The significance of the ecological roles bats play in our world is often underappreciated. As a keystone species, bats are vital to the balance of many ecosystems. Their roles include seed dispersal, pollination, insect control, and fertilisation.[7,8] Fruit-eating and nectar-feeding bats play a key role in plant reproduction and population maintenance; without them, the foundation of the food chain would collapse, devastating the ecosystem. Bats are also responsible for the pollination of many crops used for food, medicine, and resources. Insect-eating bats help control the population of disease-carrying insects, as well as agricultural pests. Some bats are even able to consume their weight in insects per night. In fact, it is estimated that bats save the United States agricultural industry $3.7 billion per year through reduced crop damage by agricultural pests and limiting pesticide use.[8]

The adaptive variety within this order is also astounding; bats range in size from just 1.5 grams to over a kilogram, with species living in habitats extending from tropical rainforests to North of the arctic circle.[4] One key behavioural adaptation of bats living in colder climates is hibernation. During colder months, in the absence of accessible food and water sources, bats will enter a metabolic state known as torpor, spanning from a few days

to months.[9] In this state, the bat's body temperature drops from its euthermic state to the ambient temperature of the hibernacula, or hibernation site, as low as -2.5°C.[10,11] While hibernating, the bat's metabolism drops to nearly 1% of their euthermic state, requiring the limitation of some energy-intensive functions, including immune, pulmonary-respiratory, and circulatory functions. For small mammals like bats, heart and breathing rates are dropped from 200-300 beats per minute and 100-200 breaths per minute, down to just 3-5 beats per minute and 4-6 breaths per minute, respectively.[11] To ensure survival through the overwinter period, bats will build up fatty tissue stores prior to entering the torpid state. Burning these high caloric density triglycerides via fatty acid oxidation is an effective method for hibernators to not only produce energy, preventing them from actively requiring food during the resource-scarce winter period, but also water, which can replace a fraction of what is lost during respiration (Figure 2.1).[12]

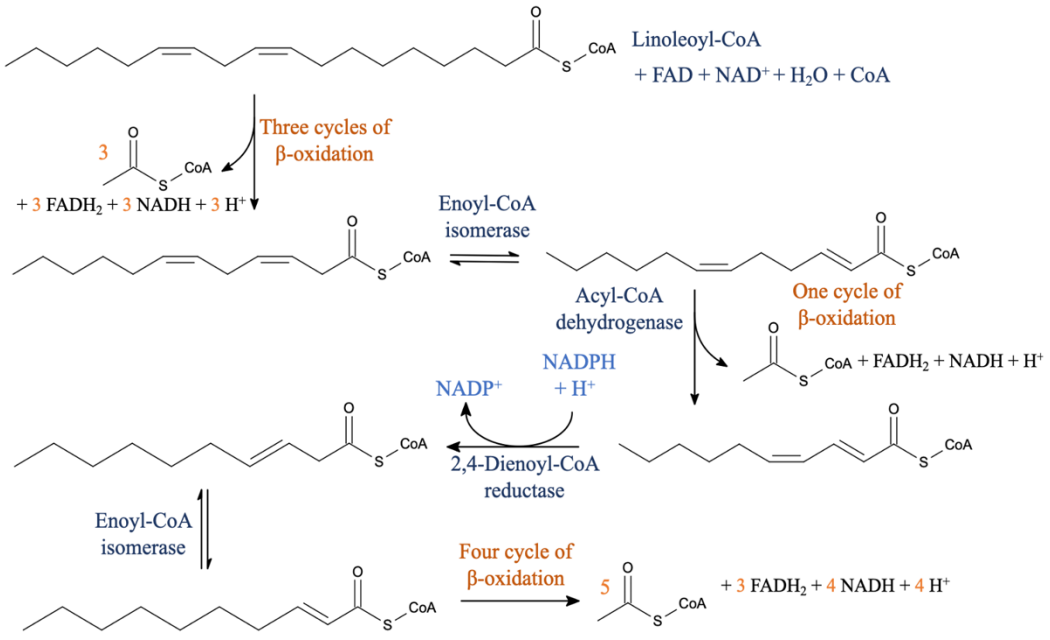

Figure 2.1 Catabolism of Linoleic acid via β-oxidation.[13] The β-oxidation of 1 mol of linoleic acid, a common storage molecule for bats,[12] results in a net of 9 mol of Acetyl CoA, 7 mol of $FADH_2$, and 7 mol of NADH. After combined reactions in the electron transport system and oxidative phosphorylation, this yields 118 mol of ATP and 140 mol of water.

2.1.2 Physiology and Anatomy of Bats

The most significant structural feature responsible for the majority of bat physiological function is the wing membrane.[14] The wings not only serve as locomotive limbs, but the distinctive wing membrane called the patagium functions in thermoregulation, passive gas exchange, and water balance. The skin of the patagium is highly folded and four to eight times larger than the rest of the body's surface. The patagium is also ten times thinner than the skin on the rest of the body, consisting of two epidermal layers, which encase highly vascularised connective tissue; the shallow depth of this vascularisation allows for passive gas exchange across the surface of the wings and the establishment of thermal equilibrium with the environment during hibernation. However, due to the high surface area, up to 99% of the water loss in a hibernating bat occurs as evaporative water loss at the patagium, though the sebaceous and apocrine glands on the wing provide a moisturising and waterproofing layer on the surface of the skin to minimise this as much as possible. This secreted layer is also thought to interact with the skin microbiome of bats by providing nutrients to beneficial microbes; this sustained microflora equilibrium helps protect the bats from invading pathogens.[14] However, as is evident by the outbreak of North American Bat White-nose Syndrome (WNS), the mechanism of microbial protection is imperfect.

2.2 White-Nose Syndrome

2.2.1 Discovery and Impact

White-nose Syndrome is a fungal infection that has devastated many North American bat populations in the past decade. First documented in 2006 in Howes Cave outside Albany, New York, WNS has spread to 37 US states and seven Canadian provinces, as of May 2021.[2,15] Population losses have been so extreme that some species have even been classified as regionally endangered or extinct. In Nova Scotia, WNS was first detected in 2011, and led to the loss of 95% of the population in the five largest hibernation sites by the end of the 2012/2013 winter season.[16,17] After 2013, half of Nova Scotia's bat species were classified as endangered as a result of the disease.[17]

The issue was first detected in 2007 when observed winter flying in bat populations was ten times higher than the 25-year record, and surveyed caves experienced population losses exceeding 75%. Then in 2009, Blehert *et al.* first named and described the disease.[15] White-nose Syndrome is characterised by the growth of a powdery white fungus of the muzzle (or nose, Figure 2.2), ears, and patagium of torpid bats.[15] Despite the name of the disease, it is the presence of the fungus on the wings, not the nose, that leads to the observed mortality. Due to their physiological significance, the colonisation of fungus on the wing tissue leads to a destructive cascade of physiological effects, which ultimately leads to death by starvation or dehydration (Figure 2.3).[14]

Figure 2.2. Little Brown Bat with WNS, New York, Oct. 2008. Credit: Ryan von Linden/New York Department of Environmental Conservation

2.2.2 Mechanism of Disease

First, the fungal hyphae invade the hair follicles, the sebaceous glands, and the apocrine glands. The glandular disruption prevents the protective secretions, causing the bat to become more susceptible to evaporative water loss. The hyphae then extend through the epidermis into the vascular and connective tissue, limiting circulation and leading to tissue death. The disruption of circulation and damage to the surface of the wing prevents passive gas exchange, leading to an accumulation of carbon dioxide in the blood. The increased water loss and blood carbon dioxide lead to states of hyperkalemia (salt imbalance) and acidemia (low blood pH).[14,18,19] The interruption to passive respiration and acidemia induces hyperventilation. Not only does hyperventilation cause further dehydration due to pulmonary evaporative water loss as a result of breathing, but it is also a metabolically expensive action. This leads to depletion of fat reserves, even before torpor patterns are disrupted. Due to hyperventilation, dehydration, or hunger, bats will arouse mid torpor, requiring them to reheat to euthermic temperature, increase their heart rate, resume active pulmonary gas exchange, and forage for food and water.[19] The arousal further depletes fat stores, and as

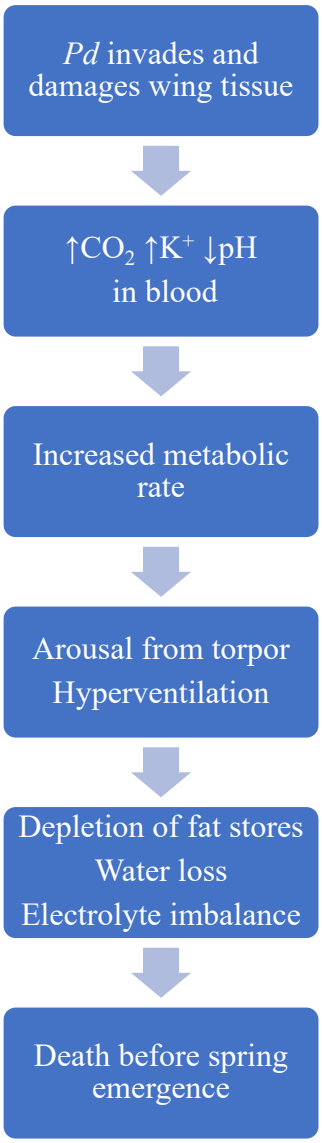

Figure 2.3. Disease cascade in bat WNS.

bats are normally unsuccessful at finding food mid-winter, they have no means to re-establish these stores enough to survive through the remaining hibernation period.[20] Ultimately, the disease leads to starvation or dehydration during hibernation, before the bats can emerge in the spring.

2.3 *Pseudogymnoascus destructans*

2.3.1 Classification and Description

In 2009, Blehert *et al.* also speculated on the causative agent of the disease. It was found that the presence of the fungus *Geomyces destructans* (later reclassified as *Pseudogymnoascus destructans, or Pd,* in 2013) was associated with the disease.[15,21] This previously uncharacterised fungus was initially identified as a close relative to genera *Geomyces* and *Pseudogymnoascus* based on analyses of the internally transcribed spacer (ITS) region and small subunit ribosomal RNA gene sequences.[22] *Pd* is a slow-growing, powdery, white-grey fungus that forms circular, convex colonies on solid nutrient media (Figure 2.4) and bears distinctive asymmetrically curved conidia.[22,23] The fungus is psychrophilic, meaning it grows at low temperatures; *Pd* can grow from 4-20°C—a range inclusive of most North American hibernacula temperatures—and its optimal growth occurs between 12.5-15.8°C.[24] The fungus is also saprotrophic, meaning it gains nutrients from decaying organic matter; in the case of the disease, this is the bat's tissue.[23,25]

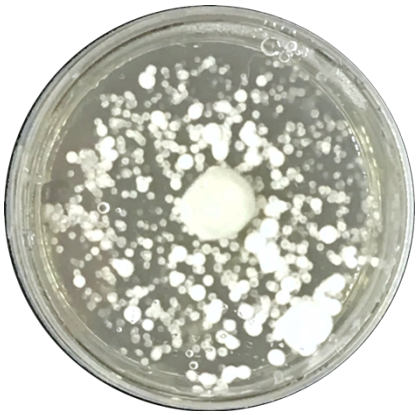

Figure 2.4. *Pd* on agar media.

2.3.2 Establishment as a Primary Pathogen

At this point, the presence of *Pd* was associated with WNS, but no strong evidence existed to indicate the fungus was the causative agent of the disease. There was doubt that it was the causative agent, as *Pd* was found in Europe with no associated mortality.[26] Koch's postulates for identifying a primary pathogen are as follows: the pathogen must be present in every instance of the disease, the live pathogen can be isolated from a diseased host, the inoculation of a healthy host with the pathogen is sufficient to cause the disease, and the live pathogen can be re-cultured from this host.[27] Blehert *et al*. confirmed the first two postulates in 2009, but it was not until 2011 that *Pd* was confirmed to be the causative agent of White-nose Syndrome. Lorch *et al.* experimentally inoculated healthy little brown bats (*Myotis lucifugus)* with pure cultures of *Pd*. This inoculation successfully induced WNS in bats, and live *Pd* could be cultured from diseased bats, meeting the remaining criteria of a primary pathogen.[27]

While the determination of the primary pathogen answered the question of what causes the disease, it does not explain why the disease appeared so suddenly in 2006, or why the same fungus is present in Europe without any associated mortality.

2.4 Origin of White-nose Syndrome

2.4.1 Endemic and Novel Pathogen Hypotheses

Early in WNS research, there were two prevailing hypotheses: the endemic pathogen hypothesis and the novel pathogen hypothesis.[28] The endemic pathogen hypothesis postulates that *Pd* is native to North America but underwent a genetic mutation that caused the development of characteristics resulting in a strain that was more pathogenic

to bat populations. This theory was quickly disproven since no close relatives to *Pd* exist in North America.[21] The only strain of *Pd* was determined to be clonally spread from the origin point.[29,30] Furthermore, only a single mating type has ever been found on the continent, an unusual feature for a native pathogen.[31] In contrast, the novel pathogen hypothesis states that *Pd* is an invasive species introduced to North America from a different geographic region. This hypothesis is supported by the sudden outbreak in an isolated area and clonal spread, as the fungus was likely transplanted into the Albany region by anthropogenic cave activity and spread by tourist activity. The established presence of the fungus in Europe was a good starting point for locating the origin of the pathogen, assuming it was introduced.

2.4.2 Presence of White-nose Syndrome in Europe

Pd was genetically confirmed to be widespread in Europe, and could be found in Germany, the United Kingdom, Hungary, Switzerland, France, the Czech Republic, Slovakia, Estonia, Ukraine, Poland, the Netherlands, and Belgium. [26,32–34] Furthermore, photographic evidence from these sites indicates that the characteristic white muzzles of WNS could be seen on bats dating back to 1995 in Slovakia, 2003 in the Netherlands, 2007 in Germany, 2008 in France, Romania, and Belgium, 2009 in Turkey, and 2010 in Ukraine and Poland. [26,34] However, during these periods, no significant mortality events were associated with the disease in individuals that were tracked and photographed.[26,35] It was speculated that the lack of mortality could be attributed to the lower pathogenicity of the European strains of the fungus. However, in 2012, North American bats were experimentally infected with the most common European strain of *Pd*, and it was found that this was sufficient to cause both the disease and similar mortality to the North

American strain.[36] If the difference in mortality could not be attributed to the pathogenicity of the fungus, it was argued that it must be due to differences in resistance in bat populations themselves. Thus, it was proposed that the resistance to the disease by the European bat species is a result of long exposure and co-evolution of the bats and the fungus.[35]

2.4.3 Discovery of Origin

Aside from the fact that fungus is widespread, further evidence exists to support the long-standing presence of *Pd* in Europe. Two mating types of the fungus were found to be present in Europe; thus *Pd* was able to participate in sexual recombination by a heterothallic mating system—whereby different sexual structures exist in different individuals.[31] Eight haplotypes, or genetic variations, of *Pd* were observed in Europe; interestingly, the most common European haplotype exactly matched the single haplotype that spread throughout North America.[37] In-depth phylogenetic analysis and molecular dating revealed that *Pd* in Europe showed genetic divergence in the last century (which included the emergence of the strain later found in North America) and diverged from *Pd* populations in Asia over 3000 years ago.[38] Together, this evidence confirms that *Pd* originated and evolved in the Palearctic region and was only introduced to North America in recent years.

2.5 Resistance to White-nose Syndrome

To understand the mechanism of resistance developed by bats in Europe, comprehensive immunological investigations were performed to compare affected and unaffected bats in North America and Europe. It was initially believed that the mortality was a result of decreased immune function in the torpid state. Pathogen resistance normally requires a coordinated and adapted immune response, whereby innate immune mechanisms are targeted to mount an effective and appropriate immune response. However, it was found

that North American bats that succumbed to the disease mounted a greater immune response than their European and surviving counterparts.[39,40] This could indicate that while immune regulation is still occurring in the torpid bats, the response is not specific or efficient enough, leading to unnecessary metabolic strain.

2.5.1 Inflammatory Immune Response

Histological evidence suggests that, while in the torpid state, North American bats seem to lack an inflammation response, as there is little damage or emaciation in affected bats prior to their first arousal.[39] Upon return to the euthermic state, however, they experience intense neutrophilic inflammation and wing tissue begins to emaciate. The bats are infected during torpor while their immune system is in a suppressed state to conserve energy, but upon arousal and return to an immunocompetent state, the immune system detects the late stage infection and mounts a severe, reactionary immune response; this is known as an immune reconstitution inflammatory response.[39] However, it was determined that while torpid, innate immune-response genes are activated in the affected bats.[41,42]

Other studies have indicated variable responses in affected bats, but some trends include elevated white blood cell count associated with increased body temperature during torpor (20°C), although no difference in circulating immunoglobins could be observed.[43] These responses together are not indicative of a true inflammatory response; the elevated temperatures are likely responses to the upset physiological balance and a diminished ability to thermoregulate. The increased white blood cells are likely a response to this elevated temperature and thus increased circulation, as opposed to an immune response.[43] Another study found increased activation of cathelicidins, pro-inflammatory cytokines, and inflammatory response modulators, without follow-up by an actual effective immune

response. Together, this evidence revealed that an inflammatory response is being genetically signalled and mounted but not effectively carried through.[41,42] One proposed issue is inappropriate targeting, as the gene expression of these inflammation factors occur primarily in the lungs.[41] Thus far, there is no evidence that *Pd* infects the lungs. As such, this response may be a non-specific host response to unknown fungal invasion, or it may successfully be preventing the establishment of spores in the lung tissue. Regardless, this response does not prevent infection and spread on the surface of the wings, as it was observed that, despite cytokine and chemokines being appropriately expressed, there is no recruitment of immune cells to the infection site on the patagium.[41]

2.5.2 Antibody-mediated Immunity

To understand the role of antibodies in WNS survival, populations of WNS-affected bats from North America and Europe were compared.[44] Affected North American bats were shown to have higher expression of anti-*Pd* than affected European bats. Furthermore, increased production of certain anti-*Pd* antibodies was correlated with decreased mass indicating, in this case, that antibody production is connected to a poor prognosis.[40,44] However, an immune response comparison between affected populations within North America revealed that infected bats that continued to successfully emerge from hibernation in regions of North America where *Pd* has been present longest also had higher antibody levels than emerging bats in more recently infected regions, providing little clarity to the role of antibodies in long-term WNS resistance.[44]

Since classical host-immunity models were not able to explain the reduced severity of infection in some populations, researchers began looking to external factors that might play a role in defence and resistance.

2.6 Microecological Defenses: Immune-Relevant Microbe-Microbe Interactions

2.6.1 The Immunobiome Theory

Advancements in therapeutic agents for microbial pathogens have historically focused on derivatising and synthesising existing antimicrobial structures, like penicillin. However, penicillin and most other known antimicrobials were initially discovered as natural products biosynthesised by microbes themselves.[45] Since microbes cannot engage in classical "fight-or-flight" behaviour, when they are threatened by the introduction of other microbes, they require other means to maintain their access to nutrients and space required for reproduction. Somewhat counterintuitively, microbes will actually produce antimicrobials; these antimicrobials are usually expressed at low levels, to prevent adjacent colonisation by other microbes. Thus, microbes play a role in the control and prevention of infection, adjacent to the immune system. The establishment of this "immunobiome" relies on the selective evolutionary and ecological pressure guided by the micro-ecology on or in a host—adapting in response to changes in the environment or even new pathogens (Figure 2.5).[46] The microorganisms that inhabit a host can be beneficial, benign, or pathogenic, and are categorised based on how each microbe impacts the host. However, these host-microbe relationships are not static.

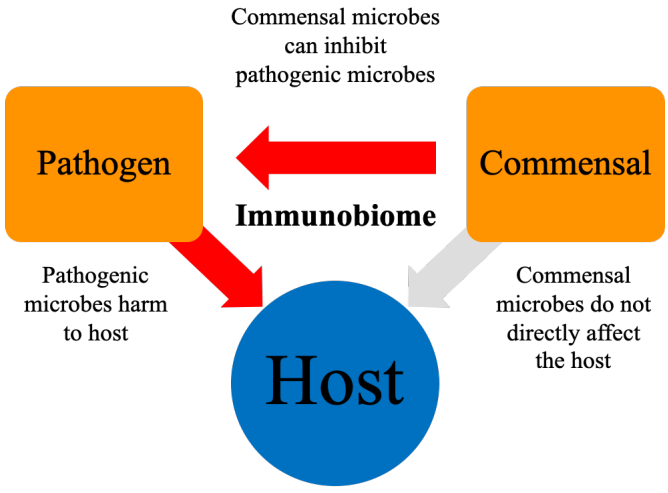

Figure 2.5. Host-microbe interactions that form the basis of the immunobiome.

For example, a benign microbe may become pathogenic if its growth is not controlled, or if it moves to a different part of the host. In this model, the host provides a habitat for the important microbe ecosystem that may, in turn, provide protection from pathogen invasion. This protection is not intended to benefit but is a fortuitous consequence of competition between microbe species. Some microbes use a method called resource competition to prevent the colonisation of non-native species, where the microbe's rate of nutrient and space consumption is fast enough to prevent the strong colonisation of other species. Another form of protection includes metabolic secretions by microbe species, which can nourish and contribute to host barriers, or act as antimicrobials to prevent other microbes from over-utilising the shared nutritional sources; this is referred to as interference competition. These bioactive metabolites may be the key to new therapeutics for infection-based diseases, like WNS.[46]

In the case of pressure from an invasive pathogen, immunobiotic microbes are not generally equipped with suitably effective antimicrobials. This leads to the loss of many species in the immunobiome and creates a dysbiotic state, meaning a state of microbial imbalance. If the dysbiosis is reversed by the reestablishment of the microbial equilibrium, the infection could be controlled. The microbes that are resilient against the invasion present an interesting case; they are either producing more broadly effective antimicrobials, or they are utilising alternative defences that may have been locked in previously silent genes. In both cases, pathogen pressure and the unique make-up of each immunobiome may present a fascinating source of microbes for targeted natural product searches.

Evidence suggests that the skin microbiota of persistent or surviving WNS-positive populations have altered microbial diversity and are more abundant in beneficial microbes compared to populations that have yet to be exposed to the disease. This microbial protection has re-established naturally in some populations, but not at a high enough rate to restabilise bat populations.[47] Researchers in the WNS field began looking for suitable probiotic organisms that show specific activity against *Pd*, but approaches regarding where to look for these microbes, and how they could be applied to the WNS issue differed.

2.6.2 Applying Microbe Ecology to White-nose Syndrome

The first reported use of microbe-derived treatments against *Pd* occurred in 2014, when Cornelison *et al.* tested known fungistatic volatile organic compounds (VOCs) reported to be produced by soil bacteria against *Pd*. [48] To test the effect of the VOCs on *Pd* growth, *Pd* was inoculated onto nutritional media, then placed in a contained airspace that was shared with a filter disk soaked with different concentrations of the selected VOCs: decanal, 2-ethyl-1-hexanol, nonanal, benzothiazole, benzaldehyde, and N,N-dimethyloctylamine. Mixed VOC trials were also performed on the mycelial plugs, whereby each possible combination of two of the six VOCs was co-tested. All six tested VOCs showed complete inhibition of conidial growth and mycelial extension at the highest concentration (30 μL of VOC) for 9 days. Three of the co-tested VOCs pairs were able to exhibit synergistic inhibition, whereby the observed inhibition was greater than the combined inhibition of each of the pure VOCs. The proposed utilisation of this technique involves supplementing cave soil with bacterial strains known to produce these mixtures of VOCs to limit the growth of *Pd* and thus the fungal load experienced by bats. This method overcomes the challenge of dealing with highly migratory species; while it does not limit

the spread while migrating, it would help reduce disease severity in caves during hibernation.[48]

Cornelison *et al.* continued studying volatile-based inhibition of *Pd* using bacteria *Rhodococcus rhodochrous* using contact-independent assays. This is a soil microbe known to reduce fruit ripening and was chosen for its ability to produce an array of VOCs. Nutritional media plates of *Pd* and established *R. rhodochrous* were placed in a shared airspace, and *R. rhodochrous* was able to cause complete inhibition of conidial growth in *Pd*. This experiment was able to establish that the concentration of VOCs released by bacteria was sufficient to limit *Pd* growth, thus making the soil supplementation a viable solution.[49] Unfortunately, the soil microbe used in this study was not native to the affected bat cave environments and the specificity of the fungistatic action to *Pd* was not established. Thus, applying the microbe to affected cave areas may further disturb the already fragile micro-ecosystem of bats with WNS.

Treatments derived from cave-adjacent soil and substrate microbes may be better tolerated by the micro-ecosystem. In 2015, Zhang *et al.* isolated a *Trichoderma polysporum (Tp)* strain from a cave affected by WNS and the strain was cocultured with *Pd* in a contact-dependent study.[50] This was done on both nutrient media, as well as in a sterile soil sample, to mimic a natural setting. The plate coculture revealed that the *Tp* strain restricts the growth of *Pd*, keeping its growth static after 28 days and extreme inhibition (99.98%) was observed in the soil samples based on the DNA quantification. To identify the active compound responsible for the inhibition, compounds were extracted from pure *Tp* and tested directly against *Pd* using a disk diffusion bioassay. The extract was also tested against a related species *Pseudogymnoascus pannorum (Pp)*, commonly found in cave areas, as well as other

common cave fungi. The crude extract showed inhibitory specificity towards *Pd*, as *Pp* and the other common cave fungi were unaffected by the extract. The extract then underwent reverse-phase HPLC fractionation and the collected fractions also underwent disk diffusion assay testing to determine which fraction was responsible for the inhibitory activity. Two high-polarity fractions and four low-polarity fractions were shown to have activity against *Pd*, but the identities of the six fungistatic compounds in the fractions were not determined.[50]

This work was continued in 2018, by Singh *et al.,* where the same *Trichoderma polysporum* strain was tested to see how it would interact with *Pd* in the presence of the native soil microbes.[51] Soil samples were collected from three caves affected by WNS: two samples from each site were treated with just *Tp*, two with just sterile water, two were supplemented with addition *Pd* and treated with *Tp* (1:1 *Pd*/*Tp*), and two were supplemented with *Pd* and treated with sterile water. *Tp* induced 100% killing of native *Pd* in the unsupplemented sample. Additional enrichment trials were performed at 1:10 and 1:100 *Pd*/*Tp*, which showed low initial inhibition (50 and 67% killing, respectively), but at five weeks increased to 95 and 84% killing, respectively. Furthermore, the treatment with *Tp* was found to have no significant effect on the soil microbe diversity or abundance. This cave-associated fungus exhibits effective and specific inhibitory activity against *Pd*, making it a good candidate for soil supplementation in WNS affected caves.[51]

In 2017, Micalizzi *et al.* examined both contact-dependant and independent inhibition of *Pd* using 301 microbe strains sourced from various environmental substrates in Quebec and Ontario.[52] Through contact-dependant cocultures, 145 microbe strains that inhibited the growth of *Pd* were identified. Fifty-three strains show complete or nearly

complete (greater than 85%) inhibition of *Pd* in contact dependant cocultures and the 28 most effective strains underwent contact-independent testing. Seven of the tested strains produced VOCs that were able to effectively inhibit *Pd* growth for six to ten days. Analysis of VOCs from inhibitory strains identified four bioactive volatiles: 2-methyl-1-propanol, 2-methyl-1-butanol, propanoic acid, and 1-pentanol. All four volatiles were tested directly against *Pd*, and complete inhibition occurred for all VOCs. Effective contact-dependant strains were also investigated in spent-media assays to test for the presence of secreted, soluble inhibitory metabolites. The spent media of several isolates showed inhibition against *Pd*, but not the closely related species *Pseudogymnoascus pannorum* or *Pseudogymnoascus roseus.* The contact-independent strains producing inhibitory VOCs and soluble metabolites provide strong candidates for isolating effective and specific anti-*Pd* natural products. However, the identification of the compounds from the spent media was hindered because the compounds were difficult to isolate without affecting the activity.[52]

Hoyt *et al.* isolated cutaneous bacteria directly from hibernating bats to investigate the anti-*Pd* activity. This method was chosen, as these strains have a higher chance of being well-tolerated in the bat microbiome if applied as direct probiotic treatments.[53] Cutaneous bacteria were collected from the forearm and muzzle of several bat species, including *Eptesicus fuscus, Myotis leibii, Myotis lucifugus,* and *Myotis sodalist*. Six *Pseudomonas* strains were isolated and tested for contact-dependent activity by coculturing against *Pd* on solid nutrient media, with two isolates, Pf1 and Pf2, showing optimal inhibition, even at low concentrations. Both strains were able to suppress the growth of *Pd* for the duration of the experiment, 42 days.[53]

Later, the efficacy of one of these *Pseudomonas* isolates (called *Pf1)* as an *in vivo* treatment was tested.[54] Bats were treated using pre-exposure and simultaneous inoculation techniques, as well as control and sham inoculations. It was determined that when the bats were inoculated concurrently with *Pf1* and *Pd,* disease severity was reduced in terms of mortality, wing lesions, surface fungi, UV fluorescence, and torpor bout duration. While simultaneous inoculation reduced severity, it was found that pre-treatment with *Pf1* actually increased severity in all aspects except mortality, which experienced no significant change from untreated, *Pd* infected bats.

Together, these investigations support the value of investigating microbe-derived treatments for bat WNS. However, they also highlight the unique challenges and considerations involved in actually applying these treatments. First, there is a strong argument for utilising microbes associated with bats or their environments, as they are less likely to cause harm to the bats or their microbiome. WNS was caused by the introduction of a novel microbe, and adding another as a potential solution could have unintended consequences that cannot be predicted. Second, it is important to consider the specificity of any potential treatment. To be effective, the treatment must have antifungal activity to inhibit the growth of *Pd*, but if this activity also affects other beneficial microbes, it may cause further dysbiosis of the bats and leave them open to other opportunistic pathogens. Finally, there are multiple ways a microbially-derived treatment can be applied: treating the cave by inoculating the soil has the potential to limit the spread of the fungus to bat colonies hibernating in that site,[55] while applying the treatment to the bats themselves provides more direct protection, especially for bat populations that are more susceptible to the disease.

Chapter 3: Application Assays for an S9-based Treatment

3.1 Overview

The metabolites of a *Penicillium canescens* strain, S9, exhibit characteristics that make it a strong candidate for the basis of potential WNS treatment, including stability, specificity, and potent antifungal activity.[3] However, before the metabolites can be tested *in situ*, it must first be established how and when they would best be applied. Should they be applied to cave environments or bats themselves? Do they work more effectively as a WNS preventative or a post-infection treatment? To answer these questions, media-based assays were designed and carried out against *Pseudogymnoascus destructans*, the WNS fungus, and *Pseudogymnoascus roseus*, a non-pathogenic species native to North America. The growth patterns of these fungi were examined and compared to determine the effectiveness and specificity of the treatment toward *Pd*.

3.2 Background

3.2.1 Cultivation of Filamentous Fungi

Filamentous fungi, or more commonly, moulds, are multinucleated organisms comprised of filaments or hyphae. These hyphae are tubular structures made up of cells separated by septa, with pores that allow for transport along the cells of the filament. Vegetative hyphae are the portions of the hyphae that anchors the mould and absorbs nutrients, whereas aerial hyphae produce spores for asexual reproduction. The network of connected hyphae is known as the mycelium. The mycelium grows, spreads, and penetrates substrates by elongation at the tips of the hyphae.[56]

Most moulds are saprotrophic, or acquire nutrients by decomposing organic matter through the secretion of enzymes like proteases, lipases, and amylases, to obtain amino acids, fatty acids, and sugars. In the lab, growth medium is used to support the propagation of moulds; these media contain various elements to support the nutritional needs of the mould.[57] Sugars, like dextrose, are commonly found in media as the primary carbon source. A peptone, or enzymatic digests of protein, provides additional carbon, nitrogen, and amino acids, which the fungi may not be able to produce on their own. Additional ingredients, like salts or extracts from other organisms can be added to support growth of specific types of microbes. Yeast malt (or mold) media, known as YM is formulated with dextrose and peptone, as well as extracts from yeast and malt, which provide additional carbon, amino acids, vitamins, and trace elements, to support the growth of yeasts and moulds.[57] Agar is another component commonly added to media as a solidifying agent. Solid media helps mimic surfaces on which some microbes naturally grow and allows for easy cultivation, isolation, and collection of microbes.

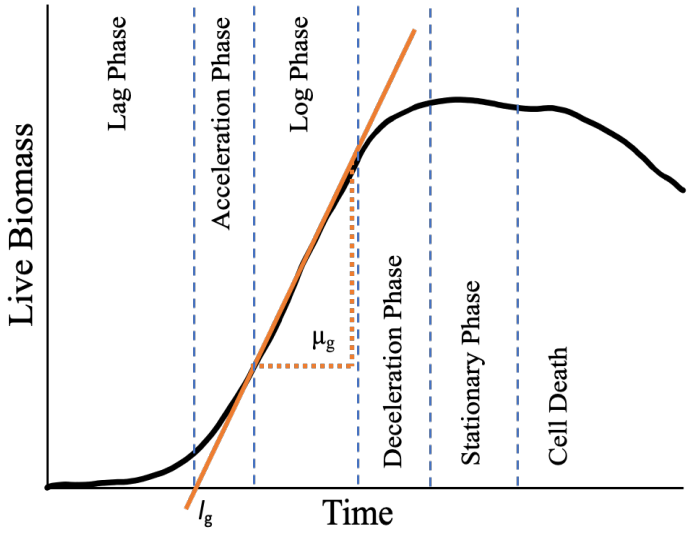

Figure 3.1. Phases of fungal growth with respect to time; μ_g is the maximum growth rate and l_g is the lag time.

Mould propagation occurs in five phases: the lag phase, the acceleration phase, the exponential (or log) phase, the deceleration phase, and the stationary phase (Figure 3.1).[56] The lag phase is the period when the fungi are becoming accustomed to their environment

and is characterised by little to no growth. This is followed by the acceleration phase, whereby some, but not all viable fungi begin to grow. Once all fungi begin growing, the log phase begins. The log phase maximum growth rate can be determined by measuring the slope of the linear portion of the graph (μ_g), while the x-intercept of this line (l_g) marks the time at which the fungus exits the lag phase. Log phase marks the steepest increase in fungal growth, which continues until nutrients start to become limited and some fungi begin to die off. At this point, the deceleration phase leads into the stationary phase, where the slow growth due to low nutrients is offset by cell death, causing the curve to level off. Once all nutrients are depleted and growth has stopped, existing cells will slowly die off.

3.2.2 Quantification of Filamentous Fungi

When propagating microbes in the lab, it is important to be able to quantify them to maintain healthy, viable stocks and obtain consistent results when performing multiple growth-based experiments over a long period of time or with different stocks. Metrics of quantifying filamentous fungi include counting colony-forming units (CFUs), counting viable spores, or measuring dry biomass. To calculate CFUs via inoculum quantitation, multiple dilutions of a fungal stock are made and plated. The number of colonies formed on each dilution plate are then counted and used to obtain a CFU per millilitre quantity for the dilutions.[57] This method is not commonly used as it is time-consuming—especially for slow-growing fungi—and, depending on the morphology of the hyphae, it can be difficult to reliably distinguish individual colonies.

Counting viable spores is more common, whereby a spore suspension of the fungus is prepared, and a very small volume is added to a device called a hemocytometer, which is then viewed under a microscope. The counting chamber of a hemocytometer is divided

into four 4x4 grids, and the spores within the grids are counted, while number of spores touching the borders are divided by two. Using this method, the number of viable spores per millilitre can be estimated.[58]

Finally, the growth of filamentous fungi can be measured based on the change in dry biomass. This method is primarily used to understand the growth in batch liquid cultures, where aliquots are taken at various points in growth, and the mycelia are filtered and oven-dried to determine mass of mycelia per millilitre of liquid stock. In smaller scale experiments, this is not feasible since removing 1 mL aliquots may deplete the entire sample. However, Langvad established that the dry mass of filamentous fungi in a sample is linearly related to the absorbance of a liquid sample at 630nm.[59] Once a calibration curve is established for the species of fungus under investigation, the concentration of the liquid sample can be estimated non-destructively using an absorbance reading.

3.3 Results and Discussion

3.3.1 Quantification and Propagation of Fungi in Liquid Stocks

To quantify the fungal concentration of *Pd* and *Pr* liquid stocks used to inoculate the assays, a calibration curve was created to relate absorbance at 630nm and dry mass per millilitre for each of the fungi. The dry mass measured for both the *Pd* and *Pr* liquid stocks showed a strong linear relationship with the absorbance reading at 630 nm, with R^2 values of 0.999 and 0.998, respectively (Figure 3.2). Based on the curves, *Pd* and *Pr* samples yield 4.35 mg/mL and 4.46 mg/mL of dry mass per absorbance unit when measured at 630 nm. This is fairly consistent with the relationship established by Langvad, where the average was 4.2 mg/mL per absorbance unit for the fungi tested.[59]

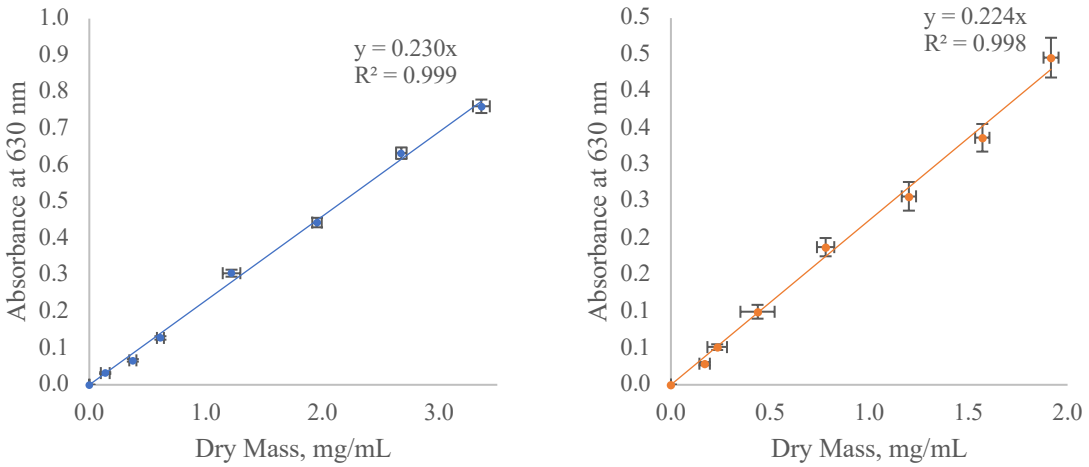

Figure 3.2. Calibration curves for the determination of the concentration of fungal dry mass in liquid stocks for *Pd* (blue) and *Pr* (orange). The horizontal error bars represent the standard deviation from the mean for the dry mass measurements (n=3) and the vertical error bars represent the standard deviation in the absorbance readings (n=10).

For subsequent experiments, the assays needed to be inoculated with fungal liquid stocks with comparable concentrations and growth phases for consistent results. Log phase growth was an ideal stage as the rate of cell propagation in culture remains consistent and linear over the entire period. To establish a timeline for the propagation and to determine when log phase began and ended for *Pd* and *Pr*, the absorbance of freshly made fungal stocks were measured at regular intervals until the curve entered stationary phase. The log phase of the liquid stock of *Pd* ranged from Days 2 to 10, with a growth rate of 0.094 absorbance units per day, or 0.41 mg/mL of *Pd* dry mass per day, consistent with reports that it is a slow-growing species (Figure 3.3). The log phase of *Pr* ranged from Days 1 to 5, with a growth rate of 0.200 absorbance units per day, or 0.89 mg/mL of *Pr* dry mass per day, more than twice as fast as *Pd*. Based on these results, *Pd* and *Pr* liquid stocks were prepared five to seven and three to five days prior to use in subsequent experiments

respectively, and made up to concentrations of 1.7 ± 0.1 mg/mL of fungal dry mass in fresh YMB prior to plate inoculation.

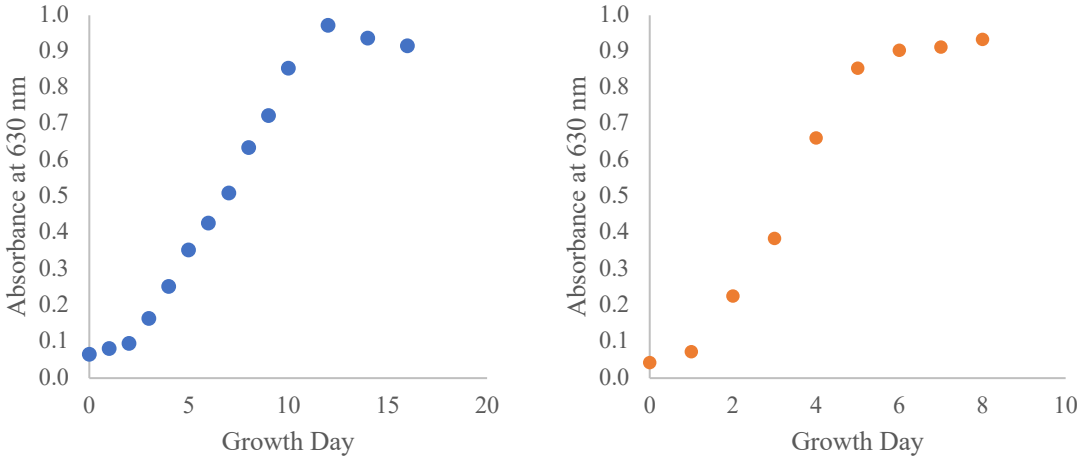

Figure 3.3. Average growth curves (n=10) for the determination of the log phase growth time span in liquid stocks for *Pd* (blue) and *Pr* (orange).

3.3.2 Prophylactic and Post-infection Treatment Modelled with Media-based Assays

For preliminary investigations, media-based assays are used to develop antimicrobial treatments prior to *in situ* testing.[50,51,53,54] When designing these assays, it is important to consider the following questions:

- What are the infection dynamics of the pathogen? How is it normally transmitted?
- How and when will the treatment be applied? What concentration is appropriate?
- What are the impacts on non-targets? Is it safe for the host?

In the case of bat White-nose syndrome, *Pd* remains dormant in bat cave environments and since the fungal portion of the microbiome is primarily dictated by environmental fungi, the bats pick up the fungus from contact with the caves and one another prior to hibernation.[55,60,61] However, it is not until hibernation begins, and the temperature of the bats drop to below 20°C during their torpid state, that *Pd* begins to grow

and infect the tissue. Since fungal load is one of the key factors linked to mortality, reducing the ability of the *Pd* to propagate in the early stages would be ideal to reduce disease severity and increase chances of survival.[35]

In this preventative intervention model, the treatment would be applied prior to *Pd* invasion and propagation. In the case of WNS, the treatment could be applied pre-emptively to either the cave environment or to the bats themselves, prior to hibernation. Since cave soil is the primary reservoir in the environment for dormant *Pd*, one application method could involve mixing the proposed inhibitory treatment into the top layers of soil in the bat caves.

Environmental Prophylactic Application via Supplemented Media Assays

The media-based assay used to test the viability of the treatment for this application was supplemented media testing, where the cell-free S9 extract was mixed into the media matrix, then inoculated with the *Pseudogymnoascus spp*. This established whether the proposed treatment could limit the growth of the pathogen when diluted in a nutrient-rich matrix.

First, an effective concentration for supplementation had to be established. The ideal supplementing concentration, in micrograms of S9 extract per millilitre of YMA media, was one where the target fungi, *Pd*, experienced marked inhibition, but the control fungi, *Pr,* experienced minimal inhibition. To establish an effective concentration, molten agar was supplemented with of 0, 25, 50, 75, 100, 150, 200, 250, 500, and 1000 µg of crude S9 solid per millilitre agar, poured into 96 well plates, and inoculated with *Pd* and *Pr.* Photographic data was collected and analysed each day to quantify the growth of the fungi. The area of the fungi relative to the well (%Area, see Section 3.6.5 for details) was

calculated for each concentration, day, and fungus and plotted to observe trends (Figure 3.4).

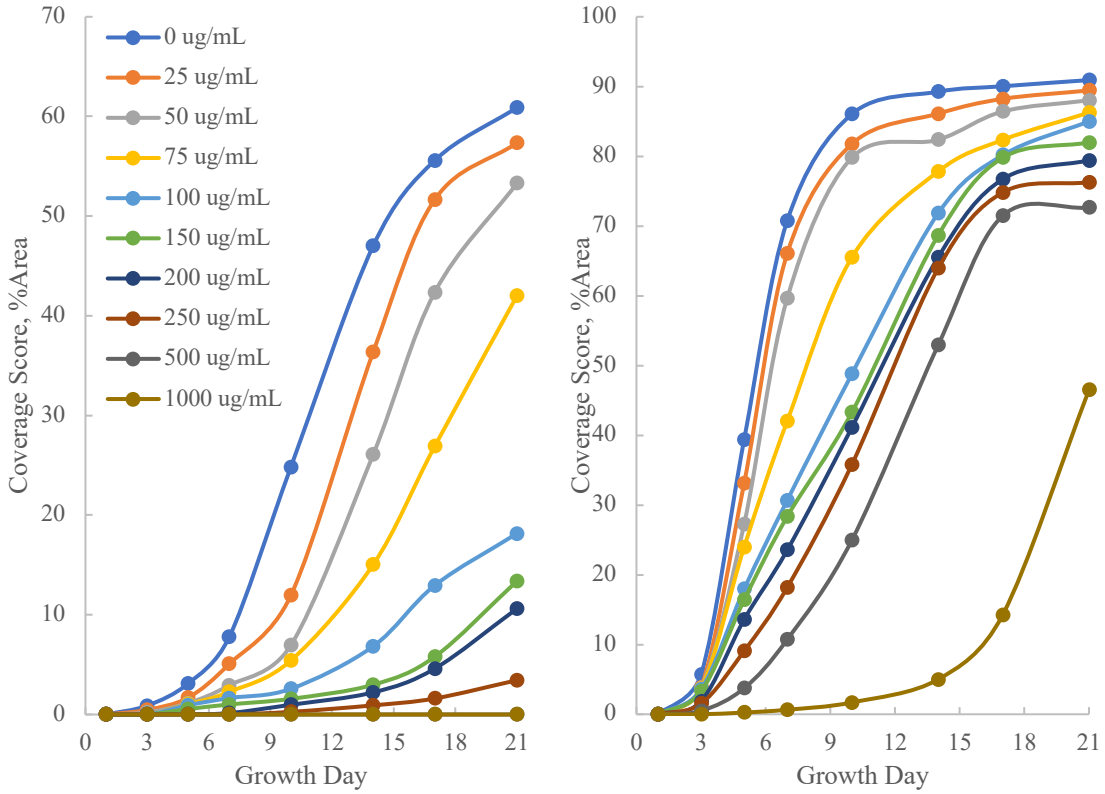

Figure 3.4. Growth curves of percent plate coverage of *Pd* (left) and *Pr* (right) on various concentrations of S9 extract supplemented media.

For *Pd*, even the lowest concentration of S9 supplement (25 µg/mL) showed evidence of fungistatic effect; *Pd* experienced extended lag-phase growth, with the control (0 µg/mL) and the 25 µg/mL treatment entering log phase in 5.6 and 7.8 days respectively, and dramatically slower log phase growth (or decreased slope) in samples supplemented with 75 µg/mL and greater were observed (Table 3.1 and Figure 3.4). For all media concentrations greater than 50 µg/mL of S9 metabolites, *Pr* experienced noticeably slowed log phase growth rate. Lag time increased noticeably (>1 day) at the 250 µg/mL (3.9 days) and 1000 µg/mL concentrations (15.2 days) compared to the 0 µg/mL control (2.6 days).

Table 3.1. Growth data for *Pd* and *Pr* on S9 extract supplemented media.

Concentration of S9 in media, µg/mL	*P. destructans*		*P. roseus*	
	Growth rate, %Area/day	Lag time, days	Growth rate, %Area/day	Lag time, days
0	5.60	5.6	16.26	2.6
25	5.69	7.8	15.55	2.8
50	5.04	8.7	13.98	2.9
75	3.85*	10.1	8.80	2.4
100	1.60*	9.6	6.16	2.2
150	1.51*	13.9	5.84	2.3
200	1.22*	13.9	5.76	2.7
250	0.46*	-	6.15	3.9
500	0.00*	-	5.79	5.0
1000	0.00*	-	8.06*	15.2

* Deceleration was not observed. All points following acceleration were used to calculate slope.

An overall growth score for *Pd* and *Pr* at Days 10 and 21 were calculated for each concentration by averaging the growth score of the same well over the specified time period to obtain an overall growth measurement, then taking the average and standard deviation of the replicates. The scores were then normalised to the control growth (0 µg/mL) for *Pd* and *Pr* and compared using a *t*-test method. All concentrations of S9 extract above 50 µg/mL had a statistically significant impact ($P < 0.005$) on the growth of *Pd* on Days 10 and 21 (Figure 3.5), while concentrations of 100 and 150 µg/mL were necessary to cause significant differences in growth in *Pr* on Days 10 and 21, respectively.

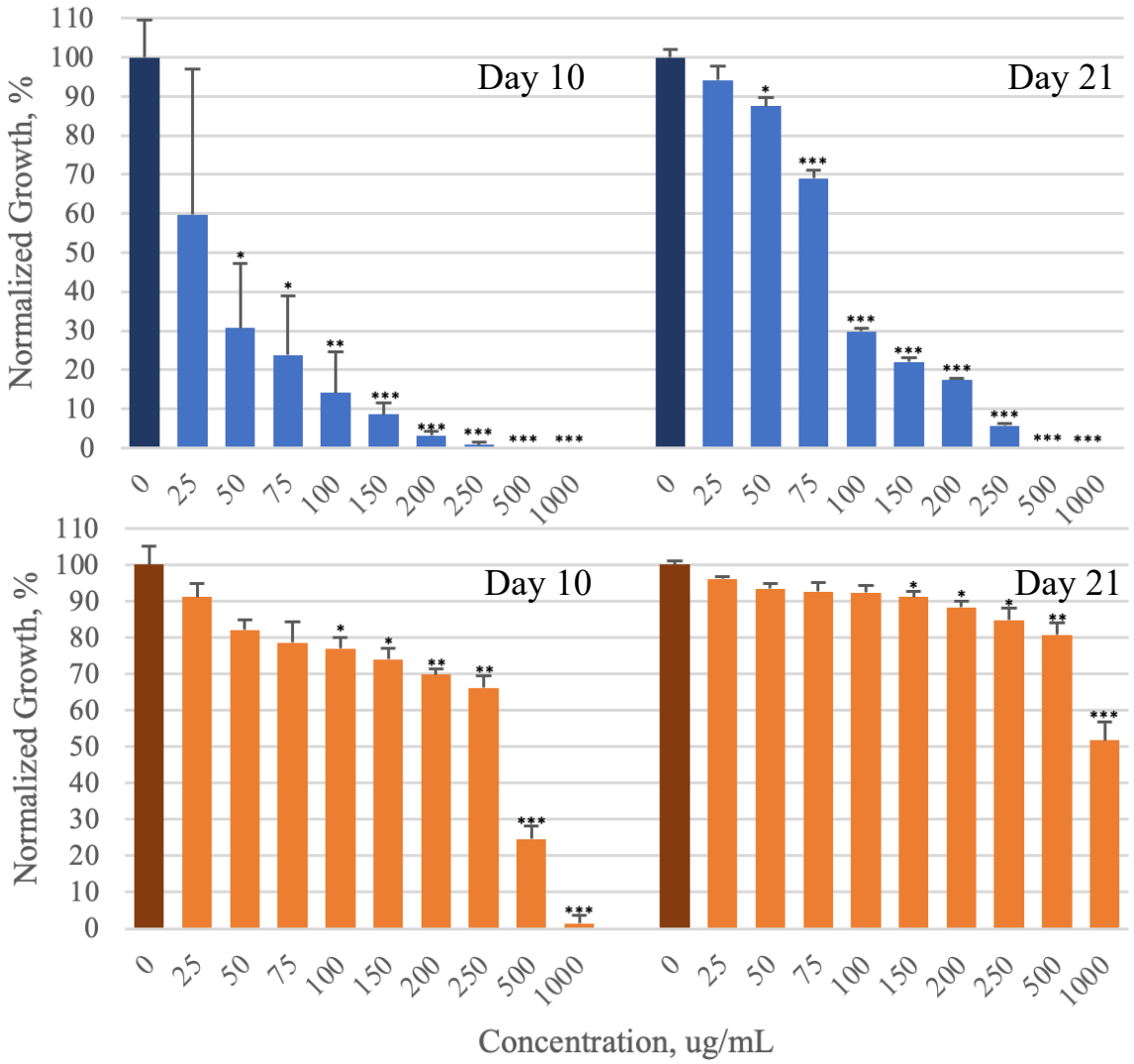

Figure 3.5. Normalised growth at Days 10 and 21 for *Pd* (blue) and *Pr* (orange) on various concentrations of S9 extract supplemented media.. The error bars represent the standard deviation for the averaged overall growth measurements (n=3). Data were analyzed using a *t*-test method. * $P < 0.005$, ** $P < 0.001$ and *** $P < 0.0001$.

For the Day 10 and Day 21 data, inhibition scores were also calculated; the inhibition at Day 10 was used to guide the concentration chosen for the subsequent supplementation-resupplementation experiment as ten days will be used as the length of each round of growth. It is important that the chosen concentration shows visible growth by Day 10, so it is not mistaken for an incomplete inoculation of the well but shows enough

initial inhibition to be able to observe any loss of activity in the resupplementation portion of the experiment. Based on Figure 3.6, 100 µg/mL was chosen as the supplementing concentration for the subsequent experiment as marks the point at which *Pd* curve begins to level off toward complete inhibition while still exhibiting unambiguous visible growth; this concentration shows 89.6 and 43.3% inhibition of *Pd* and *Pr,* respectively.

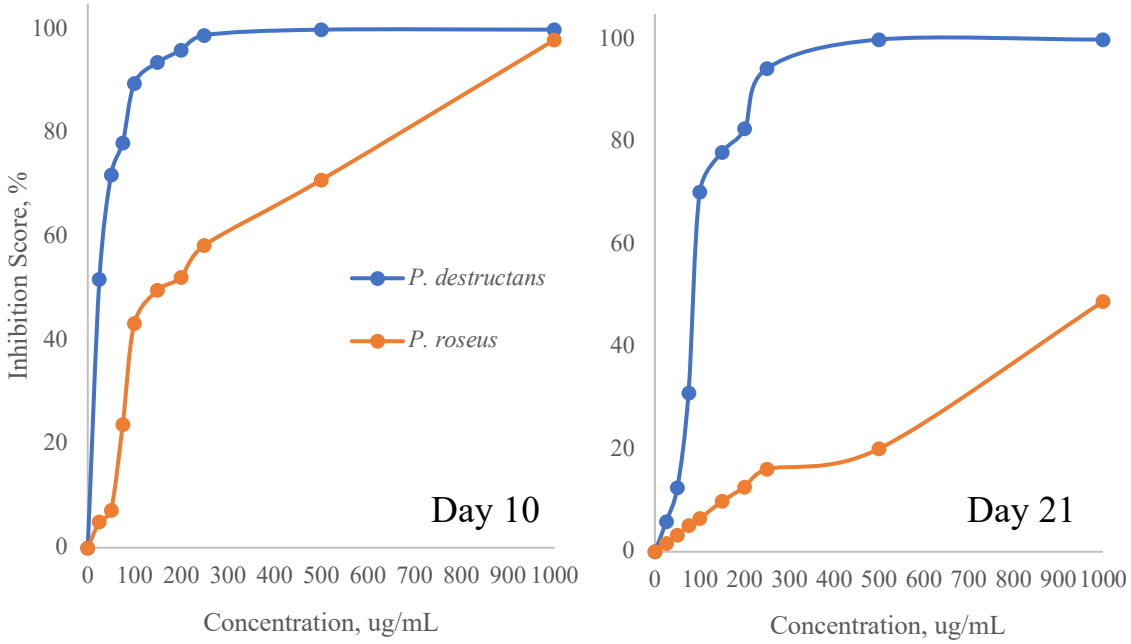

Figure 3.6. Inhibition scores for Days 10 and 21 *Pd* (blue) and *Pr* (orange) grown on various concentrations of S9 extract supplemented media.

Percent inhibition was calculated for Day 21 growth to understand how the S9 treatment performs long term at each concentration. In order for this application method to be feasible for real world use, the treatment must be stable and robust—or able to have continued activity against the pathogen over a long period of time. Figure 3.6 reveals that, while activity is mostly maintained in *Pd* (70.1% inhibition at 100 µg/mL), it is almost completely lost in *Pr* (6.5% inhibition at 100 µg/mL) by day 21. The minimum inhibitory

concentration (MIC) capable of complete inhibition of *Pd* was 500 µg/mL on Days 10 and 21. MIC was not reached for *Pr* in the range tested in this assay. Since complete inhibition was maintained at the 500 µg/mL and greater in *Pd* at Day 21, the metabolites may have exhibited fungicidal activity at this concentration, but since a sample of *Pd* was not collected from the to test for viability it cannot be confirmed whether the mycelia and conidiospores were actually killed, or just strongly inhibited long term. Furthermore, since the liquid stocks consisted of whole fungi samples, the differences in how the treatment affected hyphal growth and conidiospore germination could not be observed. Due to the complete inhibition of all growth at the 500 µg/mL and greater concentration, it can be confirmed that the treatment can inhibit both hyphal extension and germination, but the extent to which it affects each individually was not explored. Based on this, it is possible that fungicidal activity could be occurring at a lower concentration for one of the two reproductive methods, while the observed growth is a result of the other, but this would require further investigation to confirm.

To further test the robustness of the S9 treatment against multiple encounters with pathogens, *Pd* and *Pr* were allowed to grow on 100 µg/mL S9 media for ten days (R1), and then the metabolites were extracted from agar and resupplemented into new media and reinoculated (R2 and R3) to see if the treatment could withstand multiple rounds of inoculation and growth cycles. Consistent with the results from the prior honours work, activity was relatively well maintained in *Pd*, but was progressively lost in *Pr* (Figure 3.7).[3] The treated *Pd* growth on Day 10 increased from 6.1% to 12.6% in the R1 and R3 trials, indicating a small loss in activity in each resupplementation, but all three rounds retained significantly decreased growth when compared to the control. However, while the first two

rounds of *Pr* growth (R1 and R2) were significantly lower than the control at 38.0 and 76.4%, respectively, the final round (R3) showed no significant difference from the control, at 96.0% growth.

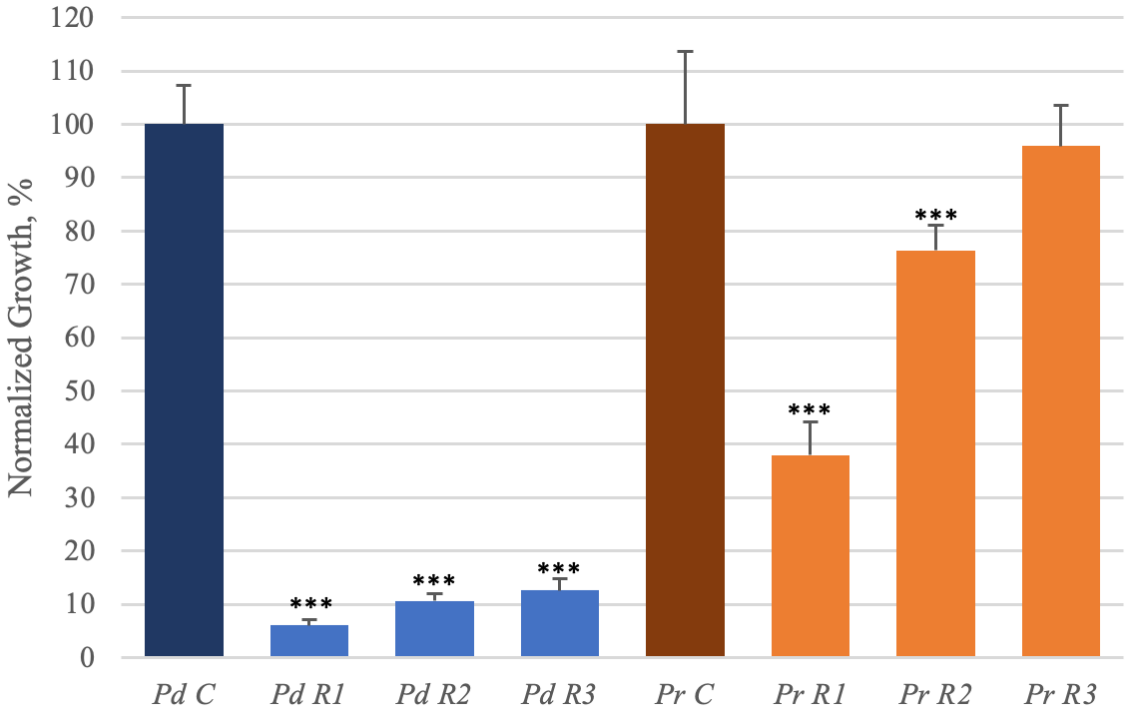

Figure 3.7. Normalised growth scores of Day 10 *Pd* (blue) and *Pr* (orange) on 100 µg/mL S9 extract supplemented media (R1) and Day 10 growth for two rounds of resupplementation (R2 and R3). The error bars represent the standard deviation for the averaged overall growth measurements (n=96). Data were analyzed using a *t*-test method. *** $P < 0.0001$.

In prior work, reduced activity was proposed to be a result of the degradation of the active compounds by native species like *Pr*. Species native to the same region may have encountered S9 and its metabolites in their shared environment prior to collection and isolation, and developed mechanisms of resistance against its antifungal activity.[3] This was supported by LC/DAD/MS profiles which showed successive loss of peaks at retention times 5.4, 6.0, 11.6, 12.1, and 17.7 min in the profile of *Pr* and another native species *Pseudogymnoascus pannorum*, but not in the control media or *Pd* and another non-native

species *Pseudogymnoascus bhattii*.[3] While this degradation ability by native species is beneficial at preventing the disruption of the existing micro-ecosystem, it may pose a challenge to implementing the treatment in a mixed microbe environment like cave soil. This is especially problematic, as *Pd* grows very slowly and would only make up a small portion of the fungi in the soil. This means that faster growing native fungi may degrade the active compounds before they can affect *Pd* propagation. Instead, the compound-based prophylactic may be more effective if applied to a substrate where *Pd* growth dominates, like the bats' themselves.

Direct Prophylactic Application via Thin Film Media Assays

In the case of direct application on the bats, the compound would need to be topically applied to the bats' skin just after the bats enter hibernation, but before *Pd* can establish on the wings. The direct treatment of the bats would not be expected to have the same longevity as treating the environment, since it may be diluted or lost in water that condenses on bats in the cold humid hibernacula. However, this application method would have the most direct effect on fungal load on the wings. A representative media-based assay for this involves applying a solution of the treatment to the surface of the media just prior to inoculation with *Pd*.

Thin films consisting of 0, 5, 10, 25, 50, 75, 100, 150, 200, and 250 µg of crude S9 solid were applied to 24 well plates (surface area of 1.9 cm^2) and inoculated with *Pd* and *Pr.* Fungistatic activity was observed for both fungi at all concentrations. For *Pd*, a dramatic successive decrease in rate with increased concentration was observed, with little change in lag time (Table 3.2 and Figure 3.8). For *Pr,* a gradual successive decrease in growth rate

was observed, with minimal variation (± 1 day) in lag time from the control (2.6 days) until the 250 µg S9 film (6.1 days).

Table 3.2. Growth data for *Pd* and *Pr* on media treated with S9 extract as thin films.

Mass of S9 in film, µg	Surface concentration of S9, µg/cm²	*P. destructans*		*P. roseus*	
		Growth rate, %Area/day	Lag time, days	Growth rate, %Area/day	Lag time, days
0	0.0	5.64*	5.4	16.89	2.6
5	2.6	4.03*	5.1	16.05	2.6
10	5.3	2.81*	4.7	15.86	2.7
25	13.2	1.31*	5.1	11.95	2.7
50	26.3	0.24*	-	9.88	2.6
75	39.5	0.28*	-	6.72*	2.3
100	52.6	0.10*	-	6.48*	3.1
150	78.9	0.00*	-	4.79*	3.3
200	105.3	0.00*	-	2.84*	3.4
250	131.6	0.00*	-	2.14*	6.1

* Deceleration was not observed. All points following acceleration were used to calculate slope.

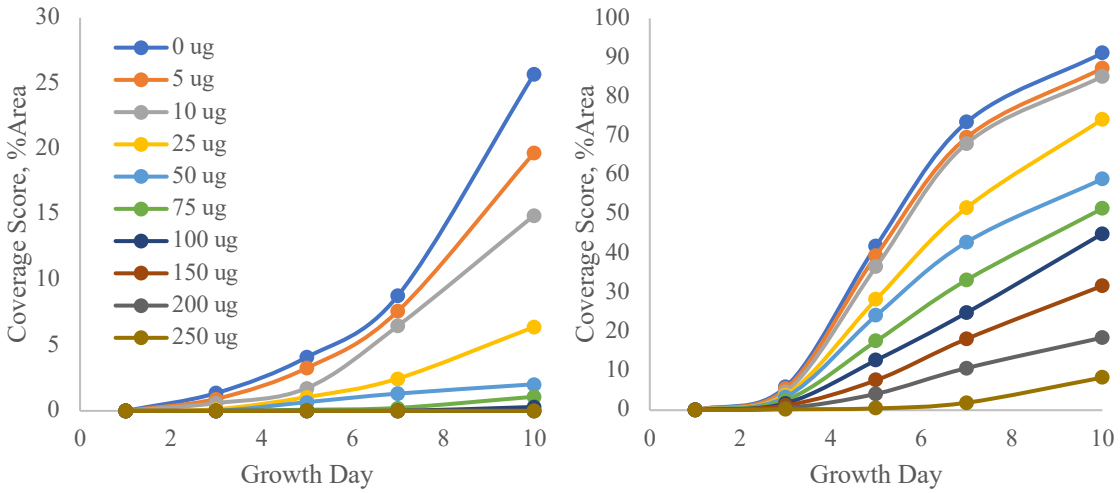

Figure 3.8. Growth curves of percent plate coverage of *Pd* (left) and *Pr* (right) on various masses of S9 extract applied to the media as thin films.

Based on the normalised growth score on Day 10, all films of S9 extract above 10 and 25 µg applied mass had a statistically significant impact on the growth of *Pd* and Pr, respectively (Figure 3.9)

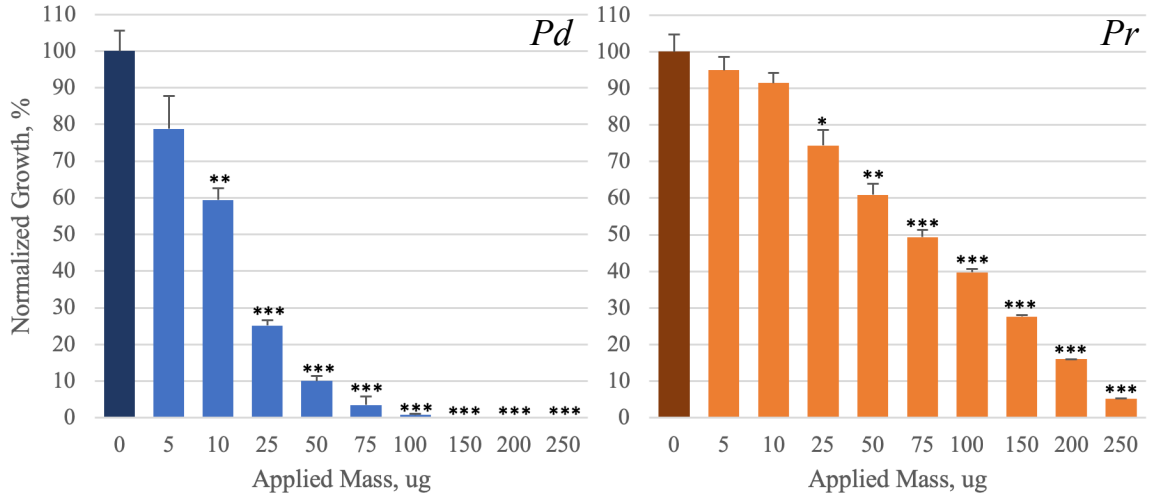

Figure 3.9. Normalised growth scores of Day 10 *Pd* (blue) and *Pr* (orange) grown on various masses of S9 extract applied to the media as thin films. The error bars represent the standard deviation for the averaged overall growth measurements (n=3). Data were analyzed using a *t*-test method. * $P < 0.005$, ** $P < 0.001$ and *** $P < 0.0001$.

Minimum inhibitory concentration on Day 10 of growth was achieved with the 150 µg film or 78.9 µg/cm^2 surface concentration for *Pd*, while the MIC was once again outside the range tested for *Pr* (Figure 3.10).

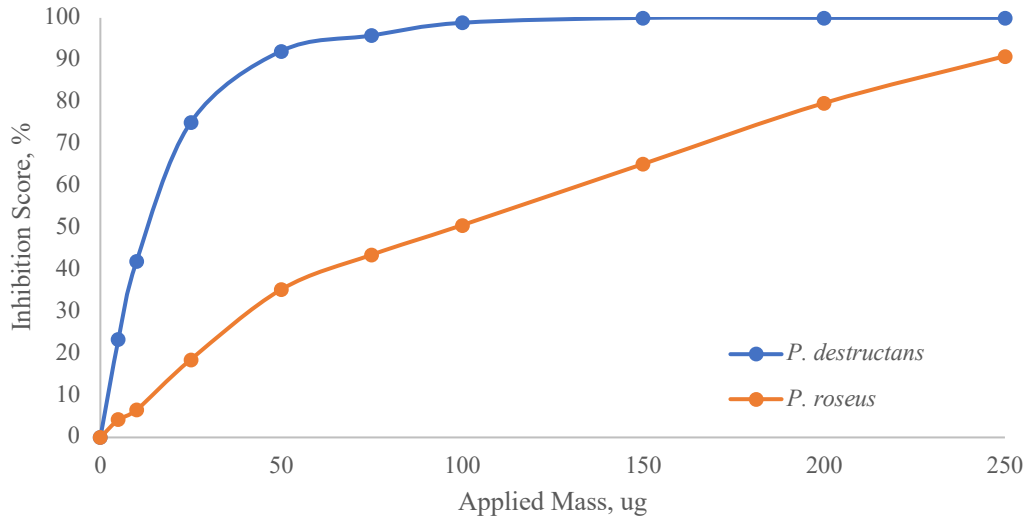

Figure 3.10. Inhibition scores for Day 10 *Pd* (blue) and *Pr* (orange) grown on various masses of S9 extract applied to the media as thin films.

Direct Post-infection Application via Drop-Treated Radial Growth Assays

Finally, to establish whether the treatment could effectively limit the propagation of actively growing *Pd*, 50 µL of sterile 25 mg/mL S9 extract (in methanol) was applied to the surface of established *Pd* and *Pr* plates. The S9 and methanol (control) treated areas were transferred to new plates as mycelial plugs after one day and allowed to grow for 21 days; the growth measured from the mycelial plugs was due to radial extension of hyphae. For *Pd*, the treatment resulted in a delayed log-phase (12.2 days) compared to the methanol control (5.5 days); a slightly decreased growth rate was also observed for the treated fungus compared to the control, at 1.49 and 1.73%/day respectively (Figure 3.11). For *Pr,*

however, treated growth varied only slightly from the control, with a minor decrease in log phase growth rate at 8.41%/day for the treated and 9.99%/day for the untreated fungi, and virtually no change in lag time, at 4.4 and 4.5 days respectively.

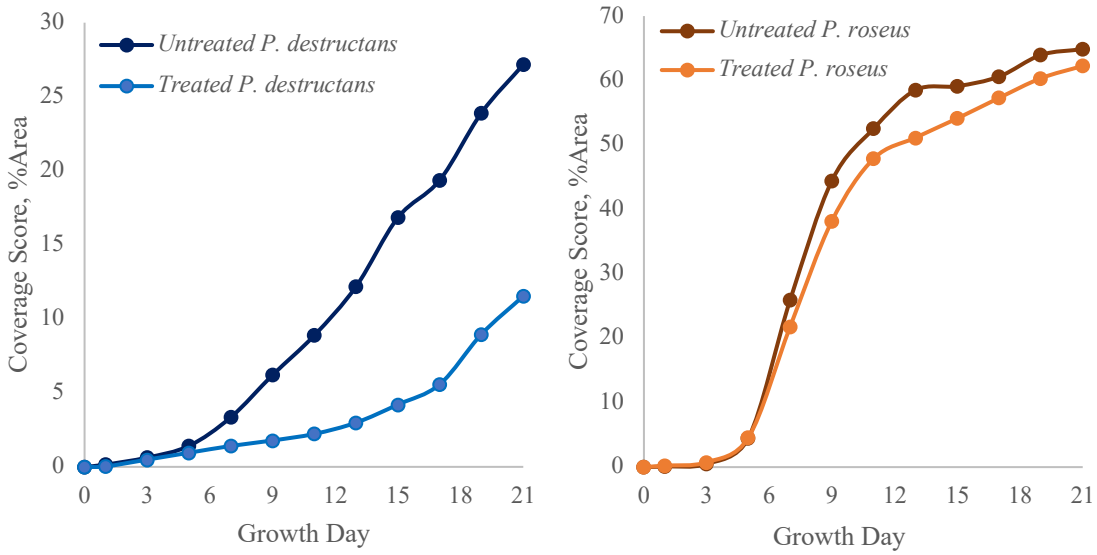

Figure 3.11. Growth curves of percent plate coverage of *Pd* (left) and *Pr* (right) propagated from solid fungal stocks treated topically with 25 mg/mL S9 extract (treated) and methanol (untreated).

The S9 treatment showed significant inhibition against *Pd* at Days 9 and 21, with decrease in overall growth of 60.3% and 66.6%, while *Pr* only experienced a 13.2% and 8.4% decrease, respectively (Figure 3.12). The delayed log phase growth in the treated *Pd* samples was the major contributor to the observed inhibition, since growth rate was only minimally affected once the fungus entered log phase. Based on this data, the treatment shows short-term fungistatic effect on mycelial growth by slow hyphal extension of established *Pd*. This result is promising for the use of S9 as a topical treatment for bats and caves with established *Pd* growth, as it could be used to control fungal load in affected caves, thus potentially reducing mortality.

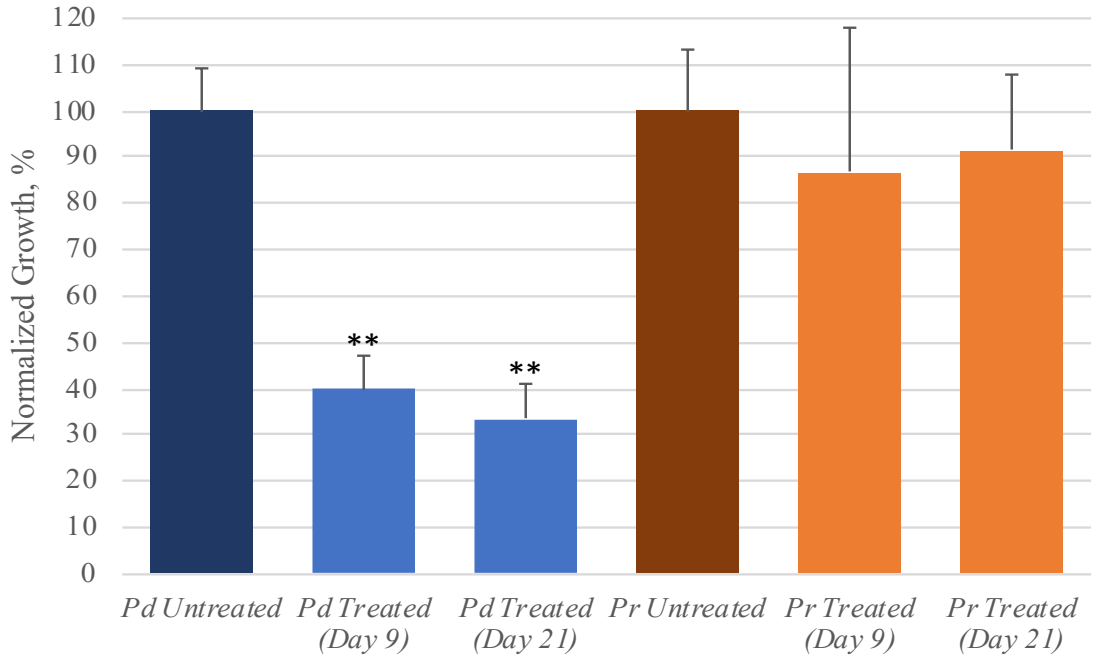

Figure 3.12. Normalised growth scores for Day 9 and 21 *Pd* (blue) and *Pr* (orange) when propagated from solid fungal stocks treated topically with 25 mg/mL S9 extract (treated) and methanol (untreated). The error bars represent the standard deviation for the averaged overall growth measurements (n=3). Data were analyzed using a *t*-test method.
** $P < 0.001$

3.4 Conclusions

All three of the media-based assays—environmental prophylactic, topical prophylactic, and topical treatment—showed promising results for their respective uses. The crude S9 metabolites in all assays were extremely effective against *Pd*, but demonstrated only moderate ability against *Pr*. Overall, the S9 metabolites appear to be fungistatic against *Pd*, as they extend the lag phase and slow the rate of log phase growth in all assays compared to their respective controls, with this effect intensifying at increasing concentrations. This leads to limited or delayed propagation, rather than complete death of the mycelia (fungicidal). In terms of long-term bat population survival, a fungistatic

treatment has advantages over a fungicidal one, since low level exposure may lead to the development of resistance in affected colonies—whether immune-based or immunobiome based. Furthermore, while activity against *Pd* remained comparatively strong and stable during the long-term growth experiments, activity against *Pr* decreased significantly over time. This is promising, as it reveals that, while non-target microbes may be slightly affected by the S9 based treatment, they also seem to have a better chance at re-establishing growth and overcoming the inhibition. Overall, these results support the efficacy of using compound-based treatments derived from microbes native to the bat cave region as a means to prevent microbiome disruption.

3.5 Future Work

The mechanism by which the S9 metabolites affect the growth of *Pd* and other fungi should be further explored. While fungistatic activity was confirmed in this study, identifying whether the S9 treatment has fungicidal capabilities and at what concentration would be useful in determining *in situ* dosing levels. Furthermore, while the topical post-infection treatment indicated that S9 is fungistatic with regards to the growth of the mycelia by hyphal extension, it has not been determined whether the compounds are affecting conidiospore germination in a fungistatic or fungicidal manner for the prophylactic assays, as the liquid stocks used to inoculate them contained both spores and mycelia. Understanding the effects of the doses on hyphae and spores separately may inform choices on the timing of dosing and how it would best be applied depending on the level and stage of *Pd* growth in bat caves.

While media-based testing is helpful as a preliminary representation of application methods, further experiments must be conducted to more accurately model the *in situ* applications. For example, for the environmental prophylactic application, the treatment should be tested against *Pd* in an actual soil matrix with other representative soil microbes native to the region. This would not only further inform the efficacy of the treatment in complex matrices, but also how the microbiome might be affected by the treatment, or how the treatment might be impacted by the presence of native microbes—especially those with the ability to degrade the compounds.

Finally, the compounds would have to be tested for topical and oral toxicity in bats if it is to be used as a direct treatment, as bats participate in extensive grooming. To ensure the treatment does not cause extensive disruption to the microbiota, the effect of the compound on microbe diversity in healthy bats should also be established.

3.6 Experimental

3.6.1 General Microbiology

All microbiology work was completed in a Containment Level 2 laboratory in accordance with the guidelines and practices outlined by the Public Health Agency of Canada. This lab is fitted with an ESCO Class II, Type A2 biological safety cabinet (BSC) for sterile work with microbes.

Sterile, disposable culture plates, tubes, serological pipettes, and inoculation loops were used for making and inoculating cultures and assays. Media and non-sterile items (media bottles, glassware, micropipettes, micropipette tips, etc.) to be used in the BSC were sterilised using a Gentinge SL5000 autoclave set to a 30-minute liquid cycle, during which a minimum temperature and pressure of 121.1 °C and 15 psi respectively were held for 30

minutes. The outside of all items placed in the BSC were also surface decontaminated by spraying with a solution of 70%v/v ethanol.

Autoclaved BD Difco™ Yeast Mold Broth (YMB; 3.0 g yeast extract, 3.0 g malt extract, 5.0 g peptone, and 10.0 g dextrose per 1 L deionised water; pH 6.2 ± 0.2) and Yeast Mold Agar (YMA; same formulation as YMB with 20.0 g EMD Millipore Agar Powder added per litre; pH 6.2 ± 0.5) were used to make liquid and plate cultures respectively. All small-volume media additives or treatments (<10 mL) were sterilised by filtration through 0.22 µm cellulose acetate syringe filters into autoclaved vials for later use in assays or directly into sterile media. Ampicillin trihydrate was added to the media of fungal storage stocks to limit bacterial growth. A Danby Refrigerator (Model: DCR059WE; 48 L capacity) affixed with an Inkbird Thermostat Controller (Model: ITC-308) was kept at 14.0 ± 1.0 °C and used to incubate all liquid stocks, plates, and assays.

For frozen stocks, a solution of 50% glycerol was prepared using molecular biology-grade glycerol and deionised water, filtered through a 0.22 µm nylon filter top into a pre-sterilised bottle. A Z-SCI Twincore ultra-low temperature freezer kept at -80.0 °C was used to store frozen stocks.

3.6.2 Acquisition of fungi and stock maintenance

Penicillium canescens (S9), *Pseudogymnoascus destructans* (*Pd*), and *Pseudogymnoascus roseus* (*Pr*) were sent as isolated cultures on BD Difco™ Potato Dextrose Agar plates from collaborators in Myron Smith's Lab at Carleton University (Ottawa, Ontario). *Pseudogymnoascus destructans* (strain US-15) was originally obtained from Agriculture and Agrifood Culture Collection, Ottawa, ON, Canada. *Penicillium*

canescens and *Pseudogymnoascus roseus* were originally isolated from soil from a rock outcropping in Gatineau, Quebec.

Each of the fungi was propagated on solid YMA plates (containing 100 μg/mL ampicillin) using an inoculation loop to collect spores from the surface of the fungi and streaking them on the surface of the new plates. These plates were incubated for two weeks at 14.0 ± 1.0 °C; this temperature was chosen as it falls within the optimal growth range of *Pd* (12.5-15.8 °C)[24], which is the most temperature-dependant of the three fungi. Unless otherwise stated, assume stocks and assays are being incubated and stored at this temperature.

Colonies of fungi (~7 mm in diameter) were excised from the agar plates with the back of a sterile Pasteur pipette and a scalpel, placed in 10 mL liquid YMB cultures (containing 50 μg/mL of ampicillin), and vortexed to make the primary liquid stocks. Primary liquid stocks were tested every month for viability and contamination by using them to inoculate solid plates. These stocks were stored in the 14 °C incubating fridge and used to make secondary working liquid stocks and new primary stocks. New primary stocks were made when the volume of the old stocks reached less than 2 mL or when one of the primary stocks became contaminated. Working stocks were prepared three to seven days prior to use. New liquid stocks were prepared by placing 1 mL of uncontaminated, viable liquid stock into 9 mL of fresh YMB (with 50 μg/mL of ampicillin for new primary stocks).

Frozen stocks were prepared by adding 0.5 mL of primary liquid stock and 0.5 mL of 50% sterile glycerol solution to a 2 mL cryovial, mixing thoroughly, and incubating for one week; frozen stocks were then moved to the -80 °C freezer for long term storage. Solid plates were repropagated on fresh media when necessary (every 3-6 months) and kept as a

precaution, in the case that the liquid or frozen stocks become contaminated or lose viability.

3.6.3 Quantification and Propagation of Fungi in Liquid Stocks

For the *Pd* and *Pr* fungi, three liquid stocks were prepared by mixing 5 mL of seven-day incubated liquid stock with 45 mL of fresh YMB. These new stocks were allowed to incubate for an additional seven days, and then were used to prepare 35 mL each of a dilution series of 0, 5, 10, 20, 40, 60, 80, and 100% stock in YMB. A BIOCHROM NovaSpec Plus Visible Spectrophotometer and a quartz cuvette (10 mm pathlength) were used to measure the absorbance of a portion of each sample; the absorbance at 630 nm (zeroed using fresh YMB) was collected ten times for each sample to account for heterogeneity. To determine the dry mass associated with each sample, three 10.0 mL samples of each aliquot were collected on desiccator-dried, pre-weighed filter paper (Whatman No 1) by vacuum filtration. The mycelia and filter paper were rinsed with deionised water to ensure any residual media components were removed from the collected fungi. The filter papers with the collected fungi were placed in a desiccator for 24h, then weighed to determine dry mass per millilitre of sample. The absorbance and mass data were plotted against one another to confirm linearity and determine slope.

For all subsequent experiments where liquid stocks were used to inoculate plates, the absorbance at 630 nm was measured for the stocks on the day of inoculation, and converted to mass of fungi per millilitre of stock (in mg/mL) using the slope of the calibration curve.

Growth curves in liquid were also prepared for *Pd* and *Pr* by adding 1 mL of a mature liquid stock to 9 mL of fresh YMB. Using the aforementioned method, absorbance

readings were collected until three consecutive days of stationary phase data were collected. Measurements were daily from days zero to ten, then every second day until the termination of the experiment.

3.6.4 Extraction of Metabolites

Since the inhibition caused by S9 was determined to be the result of compound-based interference competition, the metabolites were extracted from the growth media of S9 for subsequent testing and analysis. The extraction was completed using a 2:1:1 methanol, ethyl acetate, and chloroform mixture. The combination of extraction solvents was chosen to maximise extracted compounds. Methanol is a protic, polar solvent, chloroform is a non-polar solvent, and ethyl acetate is a mildly polar aprotic solvent; based on the principle "like dissolves like", molecules will be extracted most optimally by the solvent to which they are most similar. All organic solvents used for extraction were ACS Grade and purchased from Fisher Scientific.

To ensure high metabolite yield, ten 12-well plates of S9 were allowed to grow for two weeks. The agar media was removed from the plate and soaked in an equal volume (~500 mL) of the solvent mixture for two hours before the metabolite-rich solvent was collected by vacuum filtration. The soaking and filtration process was repeated two more times, and the filtrate was pooled into a round bottom flask. The solvent was removed by rotary evaporation. Then, the extracted solids were redissolved in methanol, filtered through a 0.22 μm filter to remove any cells, and made up to a concentration of ~25 mg/mL for stock.

3.6.5 Data Collection and Analysis

For all subsequent assays, fungal growth data was collected by photographing the plates on selected growth days. The plates were placed on an LED lightbox (LitEnergy A4, 4000 Lux) to increase contrast between the translucent media and opaque fungal colonies (Figure 3.13a). The camera (iPhone XS) was secured to a ring stand 20 cm above the photo surface and set to a 1.5x zoom setting. Placing the camera higher and zooming in reduced the distortion of the wells closer to the edges of the image caused by parallax.

The photos were processed in the graphical design program Affinity Designer to prepare for analysis. The photos for each assay set were compiled into single image files, scaled so the wells or plates were the same size, and rasterised to create a pixel image. A mask layer was created based on the rim of each well to only show the area of the photograph inside each well. Using a non-contiguous, colour-based threshold selection tool, the fungal colony from each well was selected and filled in with black using the flood-fill tool (figure 3.13b). Adjustments to the threshold level were made until all visible fungal colonies were filled in. The area inside the wells that did not contain fungal colonies was selected and deleted. An image slice of the mask and filled in fungi were exported as binary, 8-bit images.

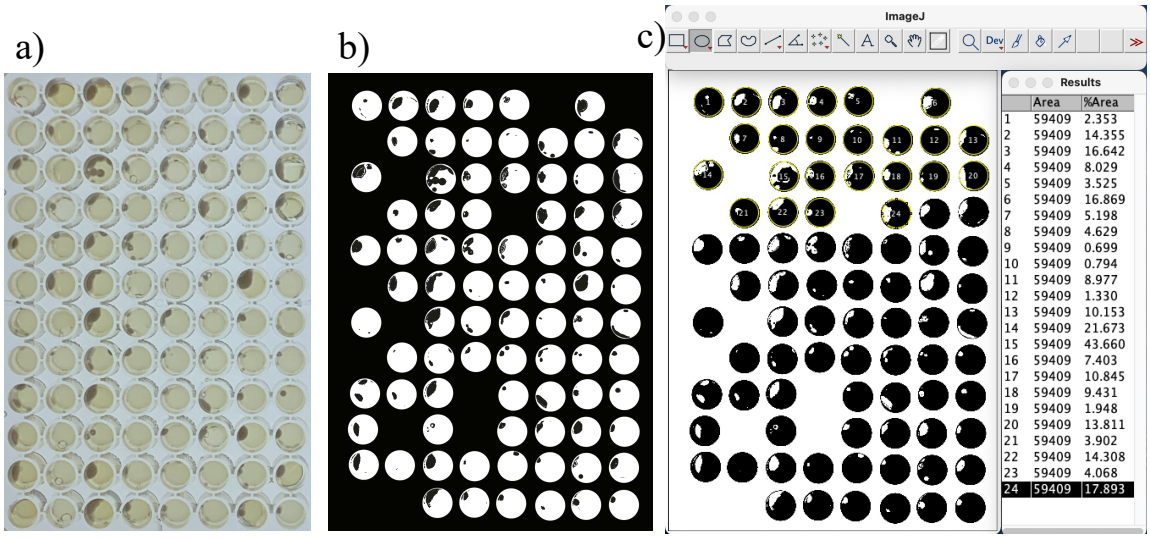

Figure 3.13. Photo data processing workflow.

Using ImageJ, the mask files were used to create a selection, thus setting the selection to include only the area within the wells, then this selection was applied to the colony images.[62] The colony images were inverted, then measured for %Area, which gave the value for the amount of the well area covered by the fungal colony; this is referred to as a coverage score (Figure 3.13c).

$$\%Area = \left(\frac{White\ Pixels}{Pixels\ in\ Selection}\right) \times 100$$

Coverage scores were plotted over multiple days to compare growth trends between treatments and controls. To determine log phase growth rate, the slope of the tangent of the growth curve was taken. The first point after visible acceleration and the last point before visible deceleration on the curve were used to find the slope of the tangent (μ_g, in %Area/day). In some cases, deceleration was not observed, so all points following acceleration were used (indicated by *). The x-intercept of this line was used to determine the lag time (l_g, in days), where the lag phase ends and growth acceleration into the log

phase begins. For curves with slopes less than 1%/day, lag time was not calculated. Coverage scores were converted to inhibition scores using the equation:

$$\%inhibition = \left(1 - \frac{\%Area_{Treatment}}{\%Area_{Control}}\right) \times 100,$$

where $\%Area_{Treatment}$ was the average coverage score for the treatment of interest and $\%Area_{Control}$ is the average coverage score of the associated control wells. Inhibition scores were calculated for selected days to draw conclusions about and compare different treatments.

Overall growth scores were calculated by averaging the growth score of the same well over the specified time period to obtain an overall growth measurement, then taking the average and standard deviation of the replicates.[63] Each of the treatment scores were normalised to the overall growth of an appropriate control set using the following equation:

$$\%Normalized\ Growth = \left(\frac{Average\ Growth_{Treatment}}{Average\ Growth_{Control}}\right) \times 100$$

Then, the mean normalised growth values of each treated and control set were compared using an unpaired *t*-test method (two sample, assuming unequal variance) to calculate *P* values and identify significant growth differences.

3.6.6 Environmental Prophylactic Application via Supplemented Media Assays

Pd and *Pr* were grown in triplicate on YMA media supplemented to a concentration of 0, 25, 50, 75, 100, 150, 200, 250, 500, and 1000 µg/mL with the crude S9 extract. The media was supplemented by adding an appropriate volume of the methanolic S9 stock into the molten YM agar (~50 °C) and mixed by swirling (Figure 3.14a), then pouring the media into well plates (Figure 3.14b). Liquid cultures of *Pd* (1.71 mg/mL) and *Pr* (1.69 mg/mL) were used to inoculate wells in triplicate with a volume of 25 µL per well on the sets of

supplemented plates (Figure 3.14c). The plates were photographed on Days 1, 3, 5, 7, 10, 14, 17, and 21 of growth and the average coverage scores were plotted to visualise the effect of each concentration on propagation.

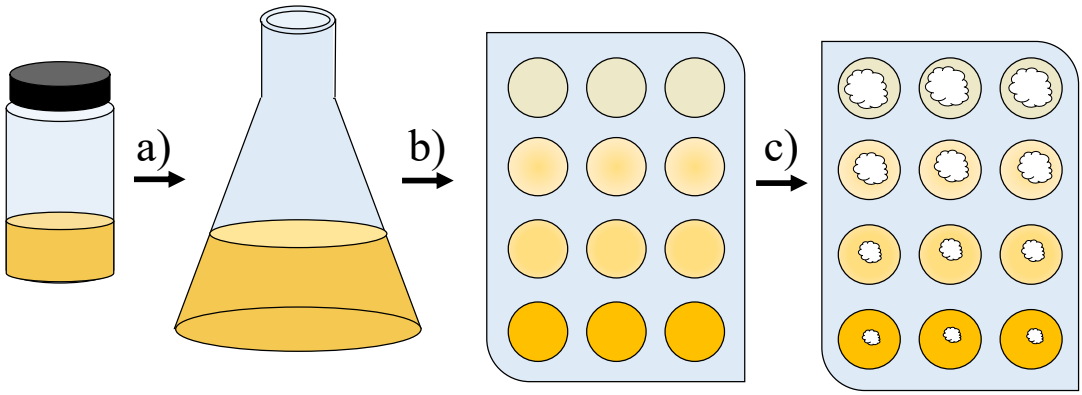

Figure 3.14. Supplemented media testing workflow.

For the supplemented media experiment and subsequent resupplementations, the assays were completed on 96-well plates. This experiment involved multiple rounds of extraction from the media, so a smaller volume of media, both in total and per well was ideal to minimise the amount of extracting solvent used and extracting time required. Ninety-six well plates were chosen, as they only require 100 µL of media per well, for a total of 9.6 mL of media per plate, while giving 96 independent inoculation points, or replicates. A twelve well plate by comparison requires a minimum of 1 mL per well, at 12 mL per plate, and only 12 replicates.

Sets of 96-well plates containing S9-supplemented YMA media at 100 µg/mL (4 mL of 25 mg/mL S9 extract in MeOH per litre media) and of control YMA (with 4 mL of sterile MeOH per litre media) were prepared. Liquid cultures of *Pd* (1.61 mg/mL) and *Pr* (1.64 mg/mL) were each used to inoculate two control and two S9-supplemented plates

with an inoculation volume of 2 µL per well. The plates were incubated at 14.0 ± 1.0 °C, and photographs were taken on Days 1, 3, 5, 7, and 10.

On Day 10, the media was removed from each plate and placed into separate centrifuge tubes containing 10 mL of the solvent mixture used in Section 3.6.4, and then vortexed for 1 minute to aid in metabolite extraction. For each tube, the metabolite-rich solvent was collected by gravity filtration. The mixing and filtration process was repeated four more times with fresh solvent mix. The pooled solvent was removed by rotary evaporation, and the extracted solids were redissolved in 0.5 mL methanol and filtered through a 0.22 µm filter to remove any cells. The entire extract was added to 9.6 mL of molten YM agar (~50 °C) and pipetted into a new 96-well plate. Liquid cultures of *Pd* and *Pr* made to the same concentration used in the initial inoculation, and a volume of 2 µL per well was added to the resupplemented plates. The plates were incubated at 14.0 ± 1.0 °C, and photographs were taken on Days 1, 3, 5, 7, and 10.

Extraction, resupplementation, and inoculation were repeated two additional times. Growth curves based on average coverage score for each round of supplementation and control growth were created and percent inhibition was calculated for the Day 10 growth of each round.

3.6.7 Direct Prophylactic Application via Topical Thin Film Media Assays

Pd and *Pr* were grown in triplicate on YMA media with S9 metabolites applied to the surface of each well. Dilutions of the S9 extract were prepared and filtered through 0.22 µm cellulose acetate syringe filters into autoclaved vials. A volume of 100 µL of each dilution was applied to the surface of six wells each, which were tilted to ensure even coverage of the extract on the surface of the well (1.9 cm^2, Figure 3.15a). The solvent was

allowed to evaporate, leaving behind 0, 5, 10, 25, 50, 75, 100, 150, 200, and 250 µg films of the S9 metabolite solids evenly coating the surface of the wells (Figure 3.15b). Liquid cultures of *Pd* (1.71 mg/mL) and *Pr* (1.69 mg/mL) were used to inoculate wells in triplicate on each of the surface concentrations using a volume of 25 µL per well (Figure 3.15c) The plates were incubated at 14.0 ± 1.0 °C, and photographs were taken on Days 1, 3, 5, 7, and 10. Growth curves were created, and Day 10 percent inhibition was calculated for each surface concentration.

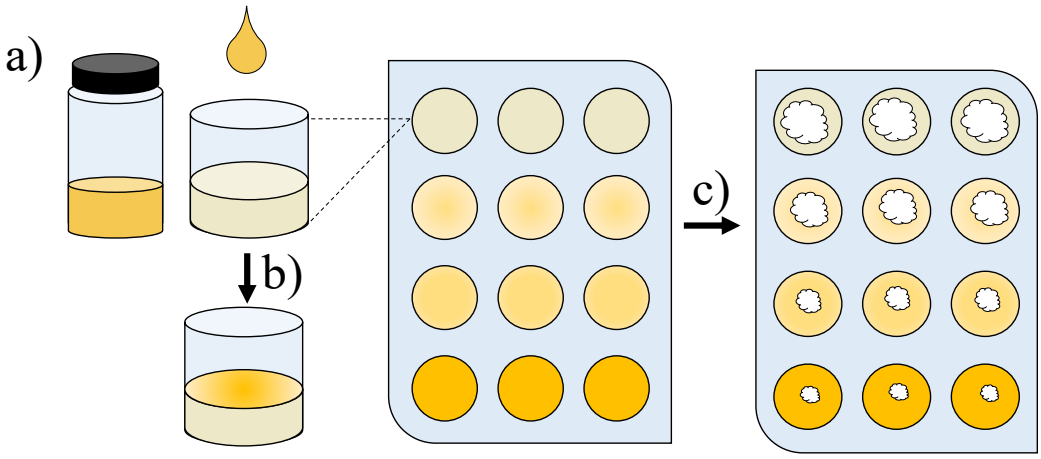

Figure 3.15. Thin film testing workflow.

3.6.8 Direct Post-infection Application via Drop-Treated Radial Growth Assays

Six YMA plates each of *Pd* and *Pr* were prepared from liquid stocks (1.71 and 1.69 mg/mL, respectively) and were allowed to grow for two weeks. For each set, three plates were treated by dropping 50 µL of sterile 25 mg/mL S9 extract in methanol on the surface of the fungi (Figure 3.16a). The remaining three plates were treated with sterile methanol as a control. The treated plates were incubated for one day (Figure 3.16b), then plugs of the fungi at the treatment site were removed using the back ends of autoclaved glass pipettes and placed on fresh YMA plates as mycelial plugs (Figure 3.16c). The plates were

incubated at 14.0 ± 1.0 °C and photographed on Day 0 and each odd growth day up to Day 21. For analysis, only the colony extending from the initial plug was thresholded. Discontiguous colonies were removed from the measured area for the coverage scores, as these would have been a result of conidiospore germination rather than hyphal extension. The Day 0 coverage score for each plate was subtracted from coverage score calculated for each day, and average adjusted coverage scores were plotted to visualise the effect of the topical treatment on mycelial growth by hyphal extension. For the Day 9 and Day 21 data, inhibition scores were also calculated to understand how the S9 treatment performs short and long term.

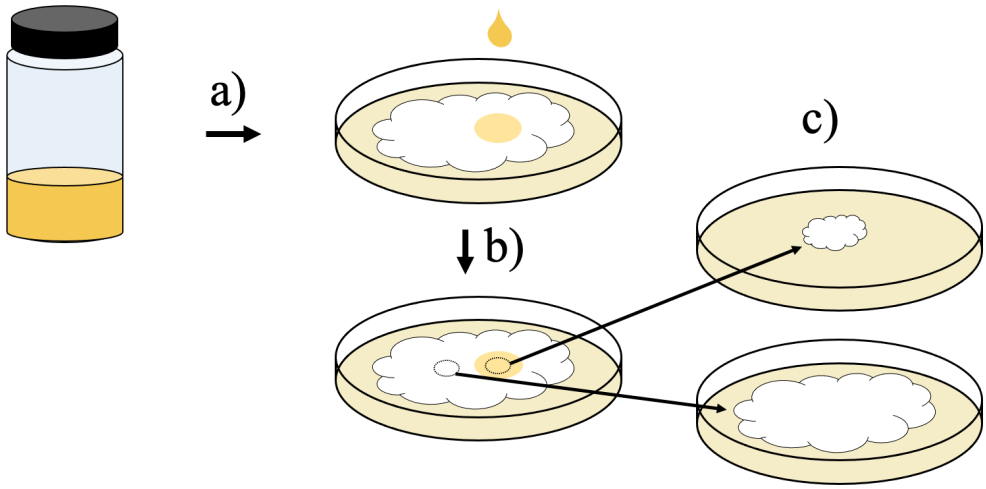

Figure 3.16. Radial growth testing workflow.

Chapter 4: Isolating and Identifying Active Compounds

4.1 Overview

Since crude metabolite extract of S9 is rich in molecules, and elucidating all of them is not feasible, the crude extract was fractionated using preparatory thin-layer chromatography. From there, it was determined which fractions were responsible for the observed inhibition of the White-nose syndrome fungus, *Pseudogymnoascus destructans*. Active compounds were partially purified, and the structure of one of the primary compounds responsible for inhibition was elucidated using a suite of characterisation techniques.

4.2 Background

4.2.1 Principles of Chromatography

Chromatography is a technique that utilises differences in polarity to separate mixtures of compounds. When it was developed in the early 1900s, chromatography was used to separate plant pigments, which were differentiated from one another based on colour, hence the name *chroma*tography.[64] However, since then, its utility has expanded to facilitate the separation of various types of compounds, and for many purposes, including isolation and identification. Some types of chromatography include paper, thin-layer, column, gas, and high-performance liquid chromatography.

While each of these methods have different uses, they all utilise the same principles and two primary components: the stationary phase and the mobile phase. The stationary phase is generally a solid material onto which the sample is loaded. The mobile phase is the solvent that carries the sample through the stationary phase. The mobile and stationary

phases have different polarities, and when chosen correctly, cause the mixed sample to separate based on the strength of the intermolecular forces with the stationary and mobile phases. When the stationary phase is more polar than the mobile phase, it is called normal phase chromatography; if the stationary phase is non-polar, it is referred to as reverse phase.[64]

For example, using normal phase chromatography, a polar compound will be more similar to the stationary phase, and thus will be retained more strongly due to a high number of interactions between the sample and the stationary phase. Whereas if it is more non-polar it will interact more with the mobile phase, thus moving faster and further along the stationary phase. The retention of a compound describes how far along the stationary phase that compound travelled. This is generally reported as a retention time in automated chromatography or as a distance-based retention factor in paper and thin-layer chromatography.

When an ideal stationary and mobile phase combination is chosen for your sample, the compounds being separated will have markedly different retentions; the difference in retention between two compounds is known as the resolution. Overall, the goal of chromatography is to achieve good separation, with well-resolved compounds in the shortest amount of time possible.

4.2.2 Thin-Layer Chromatography

Preparatory thin-layer chromatography, or Prep-TLC is a simple, and rapid way to separate and isolate compounds. In TLC, the stationary phase, as suggested by the name, consists of a thin layer of a solid material, such as silica, adsorbed to an inert backing (like glass or aluminum). The sample is spotted near the bottom of the plate and placed in a TLC

chamber containing a small amount of the mobile phase at the bottom. When the plate is set in the mobile phase, the solvent is wicked up the surface by capillary action, taking the less retained components with it. The plate is removed, and a retention factor is calculated using the ratio of the distance moved by the sample versus the distance travelled by the mobile phase.[65]

Coloured compounds can be visualised on TLC without any aid, but for non-pigmented compounds staining or UV light must be used. Stains, like iodine, potassium permanganate, and bromocresol green, are able to target different types or properties of compounds, and indicate their presence on the plate. However, these methods are destructive to the sample as they undergo reactions for the colours to appear.[65] Since some TLC plates are made with silica containing a material that fluoresces at 254nm, short wave UV light can be used as a non-destructive method to visualise aromatic compounds and other conjugated systems that absorb at this wavelength, thus showing up as a dark spot on a fluorescing plate. While it is rarer, some highly-conjugated compounds will fluoresce themselves under short or long wave UV light. If the compounds can be visualised using non-destructive methods, TLC can be used as a simple but effective method of compound purification and collection. Prep-TLC, which uses a thicker layer of the stationary phase, is primarily used for this type of purification as it allows for more sample to be loaded onto and separated on the plate.

4.2.3 Characterisation Methods

Characterisation refers to the process by which a compound's structure and properties are measured for the purpose of elucidating its identity or confirming its purity. Spectroscopy is a widely used subset of characterisation techniques that can be used to

identify photochemical properties unique to the molecule being studied, as well as determine which elements or functional groups are present in the molecule and their position relative to one another. Spectroscopic techniques measure the interaction between electromagnetic radiation and compounds, where the nature of the interaction is dictated by the frequency of radiation used.[66]

UV-visible absorption spectroscopy, or UV-Vis, involves exposing molecules to ultraviolet (100-400 nm) or visible (400-700 nm) wavelengths of light, which cause excitation of electrons from their ground state. Each wavelength of light has a different quantity of energy, and when the energy of the incident light matches that of potential electronic transitions of the molecule, it is absorbed by the molecule and causes electronic excitation. The excitations are dependent on the energy required to promote an electron from the highest occupied molecular orbital (HOMO) to the lowest unoccupied molecular orbital (LUMO).[67] This can vary depending on the identity of the molecular orbitals present (sigma vs. pi and bonding vs. antibonding), which is dependent on the structure of the molecule. Since structure dictates which wavelengths will be absorbed and the amount of light that can be absorbed, UV-Vis can give some indication as to the identity of a molecule by measuring absorption over a range of wavelengths and determining which are maximally absorbed (λ_{max}) and the probability that an electronic state will become excited (ε, or molar absorptivity).[64,67] These values are related through Beer's Law, $A=\varepsilon cl$, where A is the absorbance value corresponding to λ_{max}, ε is the molar absorptivity specific to λ_{max}, c is the concentration of the sample, and l is the path length of the beam through the sample. While this technique cannot be used alone to identify an unknown molecule, λ_{max} and ε values can be useful for confirmation when compared to known sample spectra.[64]

Infrared spectroscopy (IR) is another form of absorption spectroscopy, which uses mid-infrared light (2.5-25 μm) to cause vibrational excitations along the bonds of molecules.[66] Similar to electronic excitations, vibrational excitations require the absorbed

energy to match the vibrational energy of the bonds. The energy of the bond vibration is dependent on two factors: the identity of the bonded and adjacent atoms and the type of vibration occurring. Since the atoms in the bond determine which energies are absorbed, IR can be used to identify the presence of specific functional groups, or unique chemical moieties consisting of bonds between specific atoms, like O-H bond in alcohols. The types of vibrations that can be measured include symmetrical and asymmetrical stretching and various in- and out-of-plane bending modes, so long as they result in a net dipole change.[66,67] The presence of all characteristic vibrations of a certain functional group can confirm its presence in a molecule, but much like UV-Vis, this is not generally sufficient to identify an unknown compound, as IR does not give information about the relative positioning of the groups or differentiate well between bonds of the same type.

Nuclear magnetic resonance spectroscopy (NMR) is an especially effective tool and is one of the primary characterisation methods used for elucidating the structure of molecules.[66] NMR relies on the properties of charge and spin in atomic nuclei. A magnetic dipole is generated by the "spinning" charge and without external influence, these dipoles will be oriented randomly causing a degenerate state. However, when an external magnetic field is applied, the dipoles will orient parallel to the field, either in the direction (a low energy spin state) or opposite (a high energy spin state) to the applied field. The magnitude of the energy gap between the spin states is proportional to the strength of the magnetic field applied, so a stronger magnetic field causes a greater energy gap. The aligned nuclei are subjected to a radio-frequency pulse, and the frequency that corresponds to the energy transition of each nucleus is absorbed, causing the nuclei to resonate and be detected. The resonant frequencies experienced by all nuclei of the same isotope should be identical, however, the electrons surrounding each nucleus oppose the applied magnetic field, which effectively "shields" the nucleus. So, a nucleus with high electron density will experience the applied magnetic field less strongly, and this resonate at a lower frequency. Electron

density is affected by inductive effects from neighbouring atoms, conjugation, and anisotropy. Through NMR, the differences in electron density, and consequently resonance, can be used to determine the orientation of atoms and their relationship to one another, thus allowing for structural elucidation.[66]

Since organic molecules are consist of hydrocarbon backbones, proton (1H) and carbon-13 (13C, the spin active isotope of carbon) NMR are the most common type of NMR performed. The high abundance of protons in a sample allows for the rapid collection of extremely insightful data. In addition to resonant frequency, or chemical shift, factors like the number of protons in each environment, as well as the number of neighbouring protons and their identity can be gleaned from the spectra using metrics like integration, multiplicity, and coupling constants. Carbon-13 NMR gives less comprehensive results, as the technique is less sensitive due to the low abundance of 13C in any given sample. Carbon-13 NMR spectra are generally proton decoupled (13C NMR{1H}), since the splitting caused by heteronuclear coupling would split the already weak signals. Distortionless enhancement by polarisation (DEPT) NMR can be used to indicate which carbons are primary, secondary, or tertiary. In this method, the angle of the 1H pulse can be altered, causing different proton associated-carbon signals to be suppressed or show up in positive or negative phases. Two-dimensional NMR can be used to gain further insight into the correlation between nuclei in more complex structures. In this method, time-delayed pulses are used to obtain two domains of frequency data, which are plotted on each axis and represented as a contour plot. Signals on these plots indicate correlation between the two peaks and the nature of the correlation is dictated by the type of experiment. Common homonuclear 2D NMR experiments include Correlational Spectroscopy (COSY) and Nuclear Overhauser Effect Spectroscopy (NOESY) which show coupling and spatial proximity between protons, respectively. Heteronuclear Single Quantum Correlation (HSQC) and Heteronuclear Multiple Bond Correlation (HMBC) are usually used to plot

1H and 13C spectra against one another to determine which protons are bonded directly to which carbons and which are separated by multiple bonds. These tools are especially useful when dealing with structurally complex samples like metabolites, that cannot be elucidated or confirmed by 1D NMR.[66]

Another method that is key to structural elucidation or confirmation is high-resolution mass spectrometry (HRMS).[68] Commonly paired with a form of chromatography, HRMS takes pure compounds and converts them to charged gas-phase fragments, which are sorted and detected based on their mass to charge ratio (m/z).[64,68] Hard ionisation methods like, electron ionisation (EI), cause a high degree of fragmentation, but these fragments can give important information about the molecule, since specific fragments are characteristic of certain structures. Soft ionisation methods, like electrospray ionisation (ESI) result in less fragmentation, and generally leave the molecular ion intact.[64] These methods are particularly useful when trying to determine or confirm the exact mass of the compound. Once the fragments are formed, they are sorted in the analyser. A Quadrupole Time-of-Flight (QTOF) analysers accelerate the charged fragments through sets of four parallel rods exerting a range of voltages, which cause the ions to accelerate toward a detector. The mass of the molecules dictates how fast they will travel in the flight tube to reach the detector. The signals obtained from the detector as a function of time are converted to a mass spectrum, which yields information about fragmentation and high-resolution masses that can be used to identify the molecular formula and potential structure of the compound.[64,68]

Finally, x-ray crystallography is a powerful tool for elucidating the structure of a molecule, particularly those with three-dimensional complexity, like biological molecules.[69] In this method, an incident beam of x-rays is directed onto a crystal, and atoms in the crystal will elastically scatter the beam. The angles and intensity of the resultant beams are detected in the form of a diffraction pattern, which can be used to identify where

atoms are in the crystal. Since atomic radii and bond lengths of atoms have been well studied, the diffraction pattern can be used to unambiguously assign a 3D structure to the compound making up the crystal. While this technique has become a gold standard in structural elucidation, it is limited in use since it requires a highly ordered crystal for analysis. For some compounds, attaining a stable, good quality crystal in ambient conditions can be difficult or even impossible.[69]

4.3 Results and Discussion

4.3.1 Crude TLC Separation of Compounds

The separation of the S9 compounds by TLC was initially completed to determine an ideal mobile phase for separation by column chromatography. However, when it was discovered that many of the compounds fluoresced under long wave UV light, and thus could be easily and consistently tracked and collected based on colour and retention factor, TLC became the primary method of compound separation and purification. This method allowed for rapid separation and when desired, the collection of fairly pure compounds in milligram scale yields, which could not be accomplished using benchtop column chromatography.

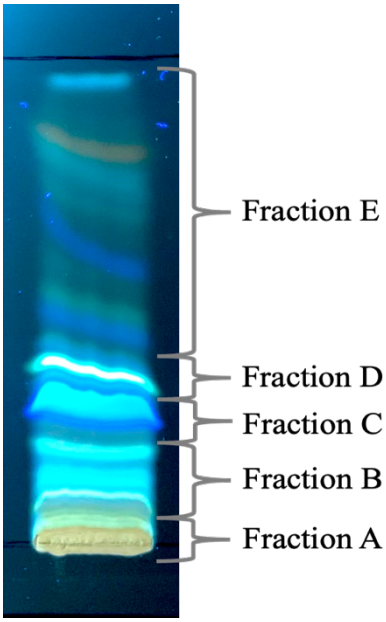

Figure 4.1 Exploratory TLC plate for the separation of S9 compounds under long wave UV light. Stationary phase: 0.25mm silica. Mobile phase: Chloroform.

Based on the exploratory TLC plate, it was clear that S9 was a complex metabolite mixture and isolating and purifying each compound would have been time-consuming, and

unnecessary, since only a few compounds were likely causing the observed inhibition. Therefore, rather than isolating each compound, the plate was separated into five fractions (Figure 4.1).

4.3.2 Identifying and Isolating Active Fractions

The fractions were extracted and applied to the surface of 24 well plates to create thin films of 100 µg of fraction compounds (or a surface concentration of 52.6 µg/cm^2) and the plates were inoculated with *Pd*. Day 10 inhibition scores were determined for each fraction, compared to a methanol treated control. For the purpose of fraction prioritisation, 50% inhibition was set as the threshold to warrant further investigation. Fraction C showed the strongest inhibition of *Pd* with an inhibition score of 100%; this fraction likely contains the compound(s) responsible for the primary fungistatic activity of S9 that was previously observed. Fractions B and E also showed considerable inhibition of *Pd* with scores of 55.5 and 68.7% respectively, while Fractions A and D showed less than 25% inhibition (Figure 4.2).

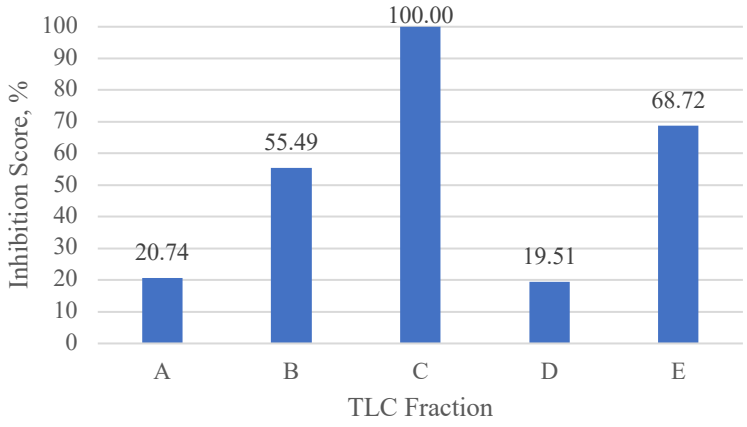

Figure 4.2. Day 10 inhibition scores of *Pd* on media treated with 100 µg thin films of five TLC separated S9 extract fractions.

Fractions B, C, and E each underwent a secondary TLC separation using mobile phase mixtures found to best resolve the visible bands in each sample. In the initial chloroform separation, Fractions B and C were well retained by the polar silica and showed evidence of band overlap, so a more polar solvent mixture was needed to better resolve the compounds in each fraction. For the more highly retained Fraction B, a chloroform-methanol (9:1) mixture was used, while for the less polar Fraction C, a chloroform-acetonitrile mixture (20:1) was used; the non-polar Fraction E was separated with a dichloromethane-chloroform (1:1) mixture (Figure 4.3). Subfractions were collected (Figure 4.4) and assayed using the same method as the initial fractions.

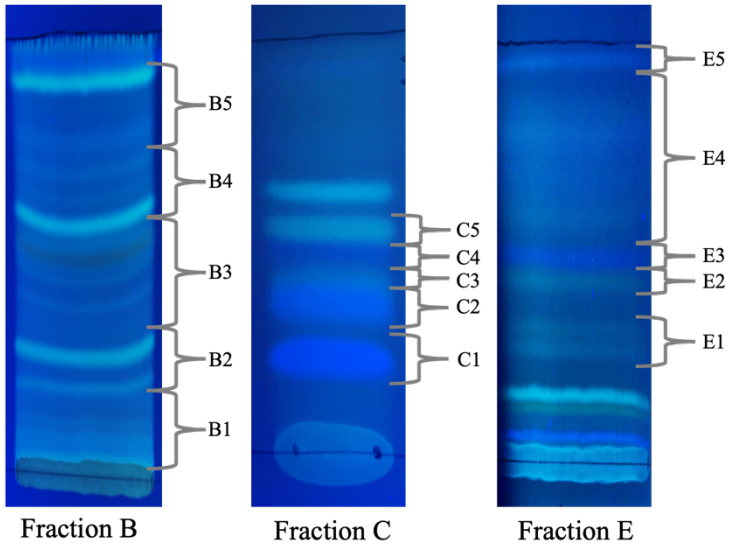

Figure 4.3. TLC separation of S9 Fractions B, C, and E under long wave UV light. Stationary phase: 0.25mm silica.

None of the compounds in Fraction B showed individual inhibition greater than 50%; the observed inhibition in the initial fraction assay was likely due to additive or synergistic effects of the five subfractions, as opposed to being primarily caused by a single compound. On the other hand, the 100% inhibition by fraction C seems to be caused by four effective compounds; both C1 and C2 on their own are sufficient to cause 100% inhibition, while C4 and C5 are effective secondary inhibitory compounds with scores of 78.1 and 82.0% respectively. The 68.7% inhibition in Fraction E seems to be primarily due to Subfractions E1 and E2.

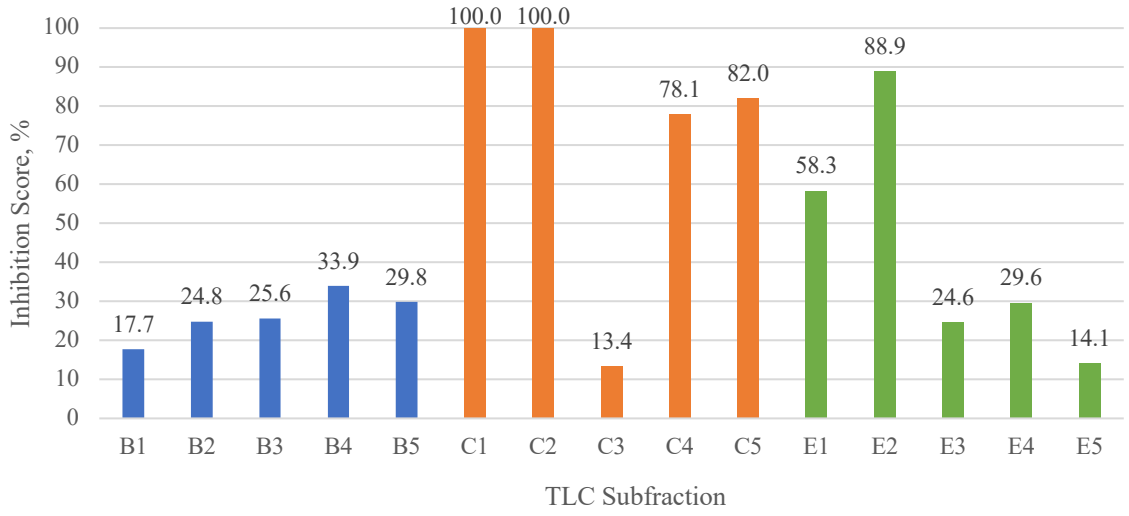

Figure 4.4. Day 10 inhibition scores of *Pd* on media treated with 100 µg thin films of 15 TLC separated S9 extract subfractions.

Purification and full characterisation could not be completed for most of the compounds due to limited yield, but liquid chromatography paired with high-resolution mass spectrometry (LC/HRMS) was performed on each active subfraction to identify the molecular masses and fragmentation patterns of the compounds within it. The LC/HRMS profiles revealed that further purification of the fractions and subfractions was necessary, as some subfractions contained traces of their adjacent subfractions compounds. Since the compounds could not be quantified, it is not known how much their presence would have impacted the assays, but it is probable that active compounds may have skewed the results of the inhibition assay higher in adjacent subfractions—particularly for highly potent subfractions. By cross-referencing the mass and fragment data with antifungal compounds known to be produced by *Penicillium spp*., tentative identities were determined for some of the subfraction compounds. Subfraction C1 contained three compounds with mass and fragment data matches to four griseofulvin derivatives: dechlorogriseofulvin (M+Na) with m/z 341.1022 (Calculated for $C_{17}H_{18}O_6Na^+$: 341.09956), griseofulvin and isogriseofulvin

(M+Na) with m/z 375.0598 and 375.0624 (Calculated for $C_{17}H_{17}ClO_6Na^+$: 375.0606), and dehydrogriseofulvin (M+Na) with m/z 373.0442 (Calculated for $C_{17}H_{15}ClO_6Na^+$: 373.04493). Griseofulvin was originally isolated from a culture of *Penicillium griseofulvum* in 1939 and again in 1946 from *Penicillium janczewskii* as a compound called "curling factor", before they were identified to be the same compound in 1947.[70] It is a known fungistatic antibiotic used as an oral treatment against dermophytes like *Trichophyton, Microsporum, and Epidermophyton floccosum.*[71] When administered orally, it concentrates in keratinised cells, affecting mitosis of attacking dermophytes and has no effect on bacteria, yeast, or other pathogenic fungi.[71,72] However, *in vitro* griseofulvin has shown activity against some fungal plant pathogens, causing issues with hyphal extension like excessive branching, stunting, curling, and gross malformation.[70]

A compound present in both C2 and C4 was tentatively identified as a tryptoquivaline derivative (M+Na) with m/z 569.1979 and 569.1984 (Calculated for $C_{29}H_{30}N_4O_7Na^+$: 569.2006).[73] Tryptoquivaline is a tremorgenic, a mycotoxin causing tremors in vertebrate species, previously shown to be secreted by *Penicillium spp*.[74,75] The remaining compounds did not have strong mass matches or fragmentation to support identification; this is likely due to overlapping signals caused by incomplete separation of compounds. Further purification of the sample and optimisation of the LC and MS fragmentation conditions would result in better matches to known antifungals and, if enough of each pure compound could be obtained, further characterisation by NMR could confirm identity.

4.3.3 Characterisation of Subfraction C1

Early in the process of compound separation, crystal formation was noticed on the edge of a concentrated methanolic S9 extract as a result of very slow evaporation of the solvent. This crystal was collected and analysed by x-ray crystallography (performed by Tanner George), and the compound was determined to be griseofulvin ($C_{17}H_{17}ClO_6$, Figure 4.5).

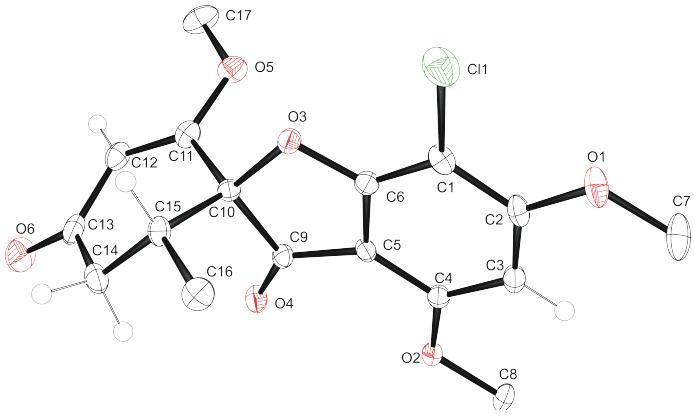

Figure 4.5. Molecular structure of griseofulvin obtained by X-ray crystallography. Ellipsoids are shown at a 50% probability level.

The crystals were dissolved in deuterated chloroform and used to obtain NMR spectra. The ^{1}H and $^{13}C\{^{1}H\}$ NMR spectra and assignments were consistent with previous characterisation of griseofulvin by Townley, with the exception of four carbon assignments.[76] A correlation between peaks at 3.99 ($H^{(b)}$) and 56.4 ppm and 4.04 ($H^{(c)}$) and 57.0 ppm in the ^{1}H-^{13}C HSQC spectrum were used to assign carbons $C^{(16)}$ and $C^{(15)}$ respectively. The presence of a positive peak at 89.5 ppm in the DEPT-135 ^{13}C NMR spectrum, as well as correlation with the 6.14 ppm ($H^{(g)}$) peak in the ^{1}H-^{13}C HSQC spectrum resulted in its assignment as $C^{(13)}$, while the 90.5 ppm was absent from the DEPT-135 ^{13}C NMR spectrum and showed correlation with 5.55 ($H^{(h)}$), 2.47-2.35 ($H^{(f1)}$), and 0.97 ppm ($H^{(d)}$) in the ^{1}H-^{13}C HMBC spectrum, resulting in its assignment as $C^{(7)}$ (Figure 4.6). In the assignment by Townley, the assignment of the two aforementioned pairs were flipped.

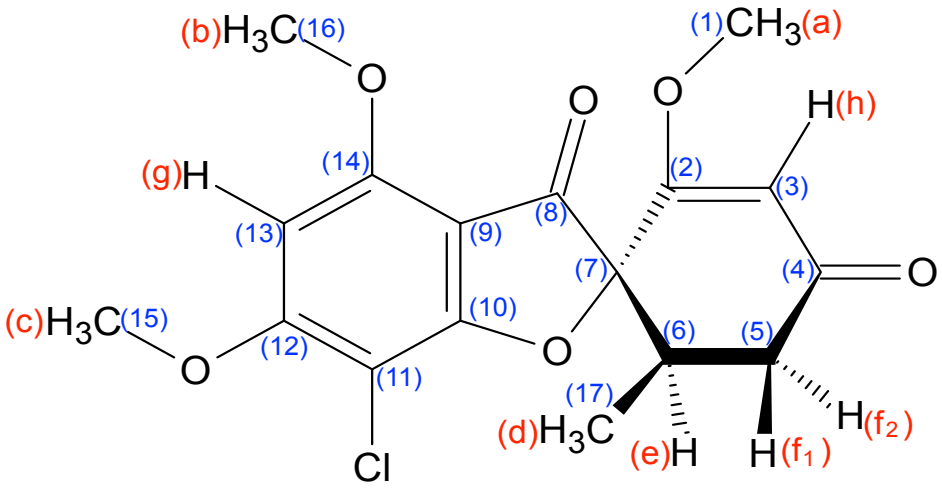

Figure 4.6. Structure of griseofulvin with proton and carbon NMR assignments.

Through the LC/HRMS experiment discussed in the previous section, griseofulvin was confirmed as one of the primary active compounds in Subfraction C1. As a result, this subfraction underwent full characterisation and comparison to a purchased griseofulvin standard (summarised in Section 4.6.4). Retention factor, IR and UV-Vis data collected for C1 was consistent with the purchased griseofulvin standard and the literature, and confirmed that griseofulvin was the main component of Subfraction C1.

The melting range of C1 (205.5-212.8 °C) is both lower and broader than the standard and the literature for griseofulvin, indicating that C1 is not pure. [76] This is supported by the additional peaks in the fingerprint region of the IR spectrum (Figure 4.7) and signals in the LC chromatogram of C1 compared to the griseofulvin standard (Figure 4.8).

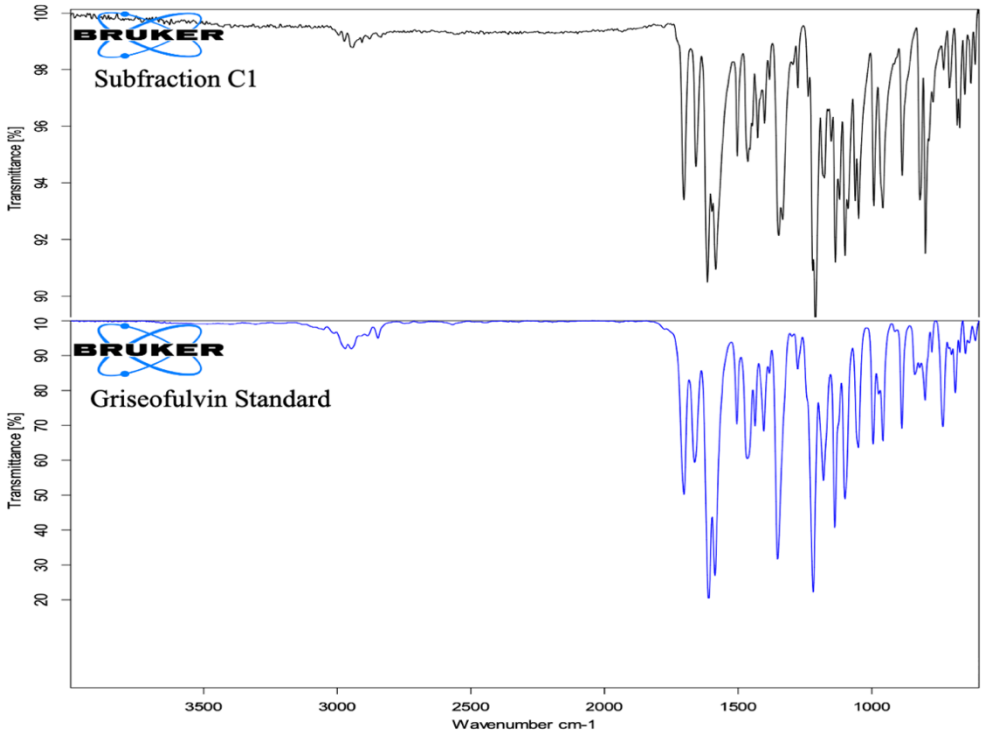

Figure 4.7. IR spectra (powder) of Subfraction C1 and a griseofulvin standard.

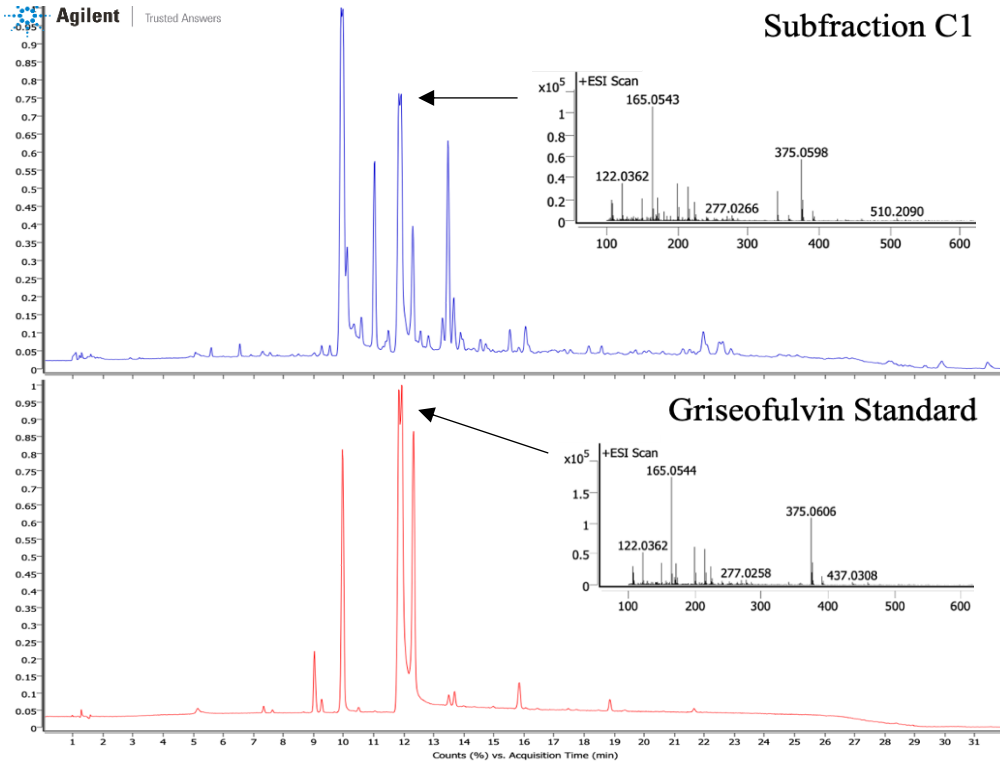

Figure 4.8. Total ion chromatogram and +ESI mass spectrum of the 11.9 min peak of Subfraction C1 and a griseofulvin standard.

Subfraction C1 and the griseofulvin standard had similar retention times on the LC chromatogram (11.901 and 11.929 min, respectively) with identical fragmentation (Figure 4.8). Three griseofulvin derivatives and two unidentified impurities in the C1 LC chromatogram are also present in the standard: Impurity 1 (m/z 361.0441) at 9.6 min, dechlorogriseofulvin (Figure 4.9b) at 10.0 min, dehydrogriseofulvin (Figure 4.9c) at 12.4 min, isogriseofulvin (Figure 4.9d) at 13.5 min, and Impurity 8 (m/z 599.1140) at 23.8 min. Other unidentified impurities in C1 include Impurity 2 (m/z 358.0761) at 11.1 min, Impurity 3 (m/z 393.0699) at 12.9 min, Impurity 4 (m/z 510.2102) at 14.3 min, Impurity 5 (m/z 407.0856) at 16.1 min, Impurity 6 (m/z 540.2196) at 17.0 min, and Impurity 7 (m/z 453.1274) at 18.5 min.

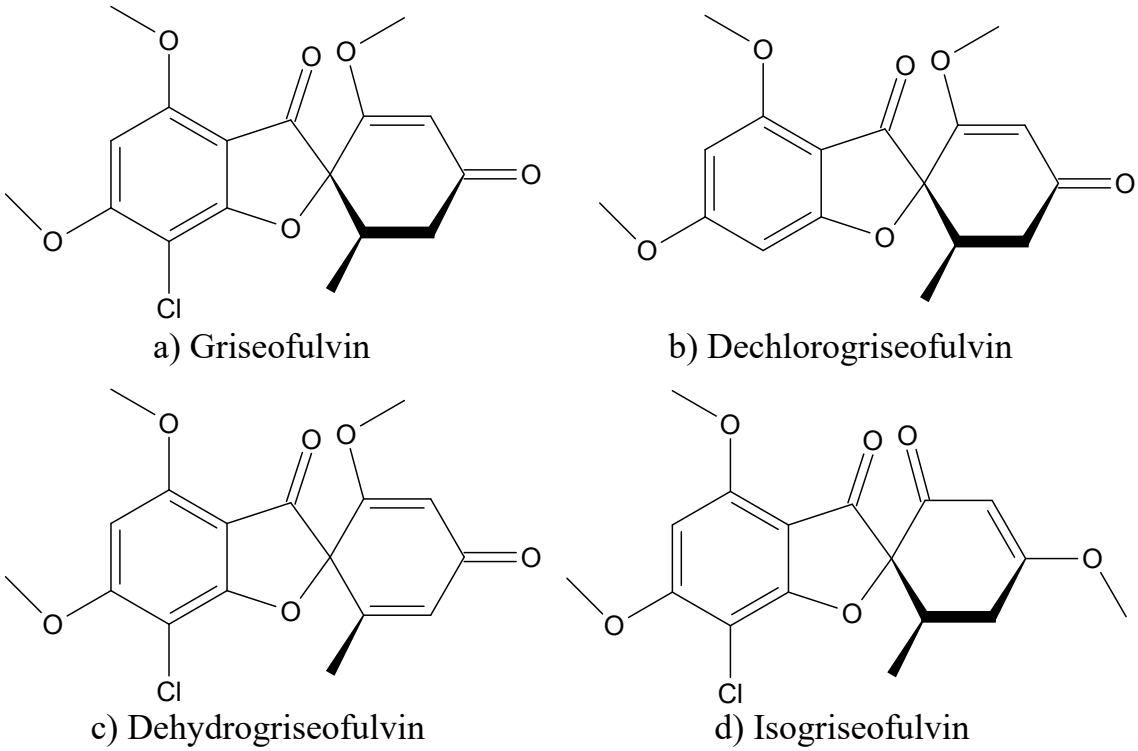

Figure 4.9. Griseofulvin and derivatives.

4.3.4 Concentration Assay of Subfraction C1

The minimum inhibitory concentration for Subfraction C1 against *Pd* was established for comparison to the S9 Crude. Thin films consisting of 0, 5, 10, 25, 50, 75, 100, 150, 200, and 250 µg of Subfraction C1 solid were applied to 24 well plates (surface area of 1.9 cm^2) and inoculated with *Pd.* Due to the limited amount of subfraction C1 collected, an assay against *Pr* could not be completed. Fungistatic activity against *Pd* was observed at all treatment concentrations; successive decreases in rate with increased concentration was observed, with minimal difference in lag time for the days it could be calculated (Table 4.1 and Figure 4.10).

Table 4.1. Growth data for *Pd* on media topically treated with Subfraction C1.

Mass of C1 in film, µg	**Surface concentration of C1, µg/cm²**	***P. destructans***	
		Growth rate, %Area/day	**Lag time, days**
0	0.0	5.64*	5.4
5	2.6	2.46*	5.3
10	5.3	1.78*	5.0
25	13.2	0.79*	-
50	26.3	0.04*	-
75	39.5	0.06*	-
100	52.6	0.00	-
150	78.9	0.00	-
200	105.3	0.00	-
250	131.6	0.00	-

* Deceleration was not observed. All points following acceleration were used to calculate slope.

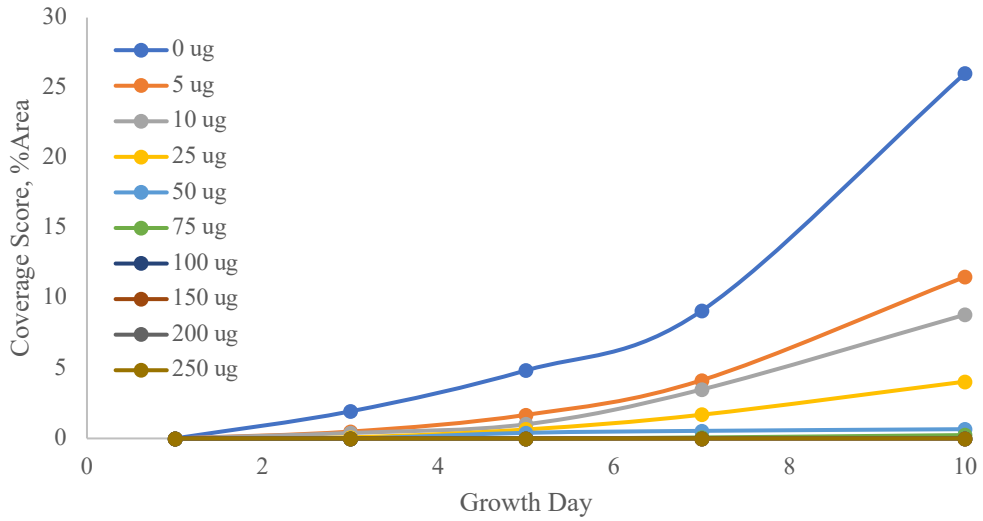

Figure 4.10. Growth curves of percent plate coverage of *Pd* on various masses of Subfraction C1 applied to the media as thin films

While the crude S9 extract is only causes a significant decrease in overall growth of *Pd* on a film of 10 µg or greater, Subfraction C1 shows a significant decrease at all concentrations (Figure 4.11).

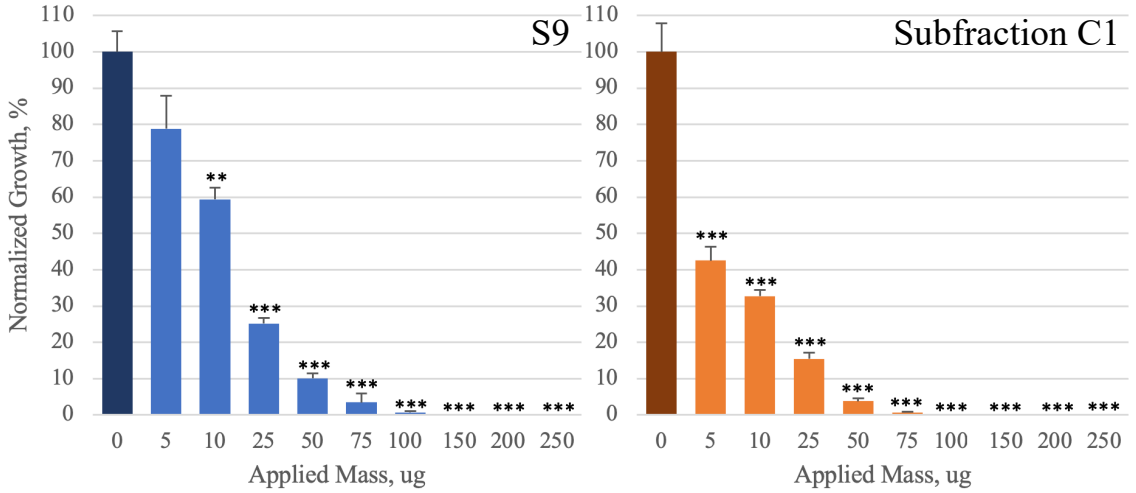

Figure 4.11. Normalised growth scores of Day 10 *Pd* grown on various masses of S9 extract (blue) and Subfraction C1 (orange) applied to the media as thin films. The error bars represent the standard deviation for the averaged overall growth measurements (n=3). Data were analyzed using a *t*-test method. ** $P < 0.001$ and *** $P < 0.0001$.

The MIC of Subfraction C1 against *Pd* on Day 10 of growth was achieved with the 100 µg film or 52.6 µg/cm^2 surface concentration, 50 µg lower than the MIC established for Crude S9 (Figure 4.12). Compared to crude S9, Subfraction C1 shows more potent activity at all treatment concentrations. This supports the theory that C1 is primarily responsible for the observed activity of crude S9. In the S9 crude sample, C1 only makes up a fraction of the solids applied, resulting in less inhibition compared to pure C1.

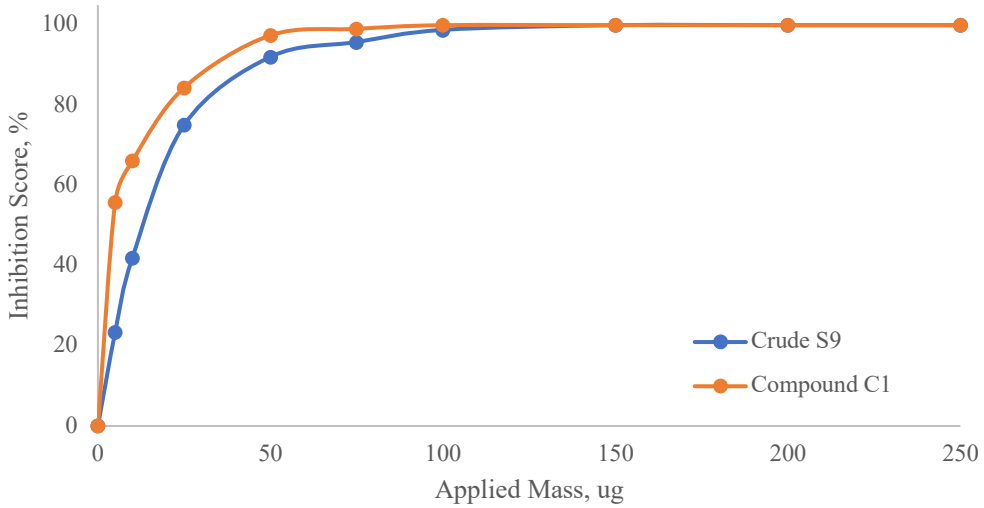

Figure 4.12 Day 10 inhibition scores of *Pd* grown on various concentrations of media topically treated with S9 extract (blue) and Subfraction C1 (orange).

4.4 Conclusions

The separation and subsequent assays of the crude extract of S9 (*Penicillium canescens*) contains a complex mixture of compounds—multiple of which had inhibitory activity again *Pd*. From the initial separation, all five fractions caused some degree of inhibition against *Pd*, with fractions B (55.5%), C (100.0%), and E (68.7% inhibition) causing significant inhibition compared to the control. When further separated and assayed, Fraction B

consisted of five minimally active subfractions (17.7-33.8% inhibition), suggesting that the significant activity observed for Fraction B is a result of synergistic effects between some or all of these subfractions. Fraction E contained two subfractions, E1 and E2, with significant activity (>50% inhibition), which are likely responsible for the activity observed in the whole Fraction E assay. Four of the five subfractions from Fraction C had potent activity (>75%) against *Pd*, with two (C1 and C2) showing complete (100%) inhibition, indicating that these likely contain the primary inhibitory compounds responsible for the observed activity of the S9 extract. Subfraction C1 was fully characterised and determined to be griseofulvin, a known antifungal compound. The MIC for Subfraction C1 against *Pd* was achieved with a 100 µg film (a 52.6 µg/cm^2 surface concentration) as compared to the 150 µg film required to reach the MIC for the crude S9 extract.

4.5 Future Works

To fully characterise the remaining compounds with potential activity, a larger quantity of higher purity samples for each subfraction would need to be collected. Using thicker 2.5mm Prep-TLC plates would increase the amount of sample able to be loaded, separated, and collected from the plate, and fine-tuning of the mobile phase would help further separate compounds within the subfractions to purify. Once this is achieved, MIC can also be established for each compound, and isolated compounds can be mixed to determine if there is an effective combination with even more potent synergistic inhibitory activity against *Pd* for the development of a WNS treatment. Before it can be used as a treatment *in situ*, it should be confirmed that it is safe for bats, as they are fervent groomers, and minimally effective against the rest of the bat microbiome to prevent further dysbiosis.

4.6 Experimental

4.6.1 Crude TLC Separation of Compounds

All organic solvents were purchased from Fisher Scientific and used as received. A preliminary separation of the crude S9 extract was performed on EMD Millipore silica gel 60 F_{254}, 0.5 mm thickness, 20x20 cm glass-backed Prep-TLC plates. A line was drawn along the plate ~2 cm from the bottom; 25 mg of the crude extract was loaded along the bottom of the plate, ~1 cm from the edge, using a pasture pipette. The bottom edge of the plate was dipped in acetone, which was allowed to carry the sample band up ~1cm to the marked origin line, then evaporated from the plate. This was repeated twice more until the sample band was less than 5 mm thick and centred on the origin line. The plate was then placed in a covered TLC chamber containing ~1 cm of chloroform. The plate was allowed to develop then removed from the chamber; the solvent front was marked, and the compounds were visualised by short (254 nm) and long-wave (365 nm) UV light using a handheld UV Lamp (UVP UVGL-58, 6 watt).

The plate was separated into five fractions based on retention factors; the silica from each fraction was collected by scraping it off the plate using the edge of a microspatula. Compounds were extracted from the silica using methanol and filtered through a frit; the filtrate was dried by rotary evaporation, then made up to 2 mg/mL in methanol. Retention factors were calculated using the following equation:

$$Rf = \frac{distance\ travelled\ by\ compound}{distance\ traveled\ by\ solvent\ front}$$

***R_f* ($CHCl_3$):** Fraction A: 0.00-0.07, Fraction B: 0.07-0.24, Fraction C: 0.24-0.34, Fraction D: 0.34-0.37, and Fraction E: 0.37-1.00.

4.6.2 Identifying and Isolating Active Fractions

To determine which fractions were active and necessitated further purification, topical prophylactic assays were performed using the collected fraction solutions. Due to the limited yield of each fraction, the assay was only completed for *Pd* growth. The fraction samples were filtered through 0.22 μm cellulose acetate syringe filters into autoclaved vials; 50 μL of each fraction was applied to the surface of three wells each and the plate was tilted to ensure even coverage of the extract on the surface of the well (1.9 cm^2). The solvent was allowed to evaporate, leaving behind a thin 100 μg film of the fraction compounds evenly coating the surface of the wells. A liquid culture of *Pd* (1.72 mg/mL) was used to inoculate the plates, using a volume of 25 μL per well. The plates were incubated at 14.0 ± 1.0 °C, and photographs were taken on days 1, 3, 5, 7, and 10 and Day 10 percent inhibition was calculated for each fraction.

Fractions with percent inhibition scores greater than 50% were purified further by TLC. The same TLC procedure was completed on the fractions with potential activity, only altering the mobile phase used for the separation. For the fractions that were poorly retained on the initial plate (low polarity fractions), a 1:1 mixture of chloroform-dichloromethane was used as a mobile phase. For mildly and highly retained compounds, a 20:1 mixture of chloroform-acetonitrile and a 9:1 chloroform-methanol, respectively, were used as mobile phases. Subfractions were collected and tested using the same assay method described above, photographs were taken on Days 1, 3, 5, 7, and 10, and Day 10 percent inhibition was calculated for each subfraction. Subfractions were considered active if they yielded a percent inhibition score greater than 50%.

***R_f* (9:1 $CHCl_3$, MeOH):** Subfraction B1: 0.00-0.18, Subfraction B2: 0.18-0.28, Subfraction B3: 0.28-0.53, Subfraction B4: 0.53-0.70, and Subfraction B5: 0.70-0.91.

***R_f* (20:1 $CHCl_3$, MeCN):** Subfraction C1: 0.22, Subfraction C2: 0.36, Subfraction C3: 0.42, Subfraction C4: 0.47, and Subfraction C5: 0.53.

***R_f* (1:1 $CHCl_3$, DCM):** Subfraction E1: 0.25-0.33, Subfraction E2: 0.43, Subfraction E3: 0.48, Subfraction E4: 0.51-0.94, and Subfraction E5: 0.951.

4.6.3 Characterisation of Active Subfraction Components

Each active subfraction was spotted on a 0.25mm silica TLC plate using 10µL capillary tubes. The plates were developed using a mixture of 10:10:1 chloroform-dichloromethane-acetonitrile, and retention factors were calculated.

High resolution mass spectrometry (HRMS) was used to determine the exact mass (to 4 decimal places) and fragmentation pattern of the compounds in the active subfractions. HRMS was performed on an Agilent 1260 Infinity II HPLC paired with an Agilent 6530 quadrupole time-of-flight (QTOF) mass spectrometer. All active subfractions, as well as the crude S9 extract and a Griseofulvin standard (97.4 ± 0.4% Pharmaceutical Secondary Standard), were made up to 2 mg/mL in HPLC-grade methanol and filtered through 0.45um cellulose acetate syringe filters into 1.8mL LC vials. The samples were injected at a volume of 1.5µL onto a Poroshell 120EC C18 (3 x 150 mm, 2.7 µm) column at 30°C. HPLC-grade water with 0.1% formic acid (Solvent A) and 95% HPLC-grade acetonitrile in water with 0.1% formic acid (Solvent B) were used in a gradient mobile phase system. At a flow rate of 0.5mL/min, the sample was eluted using a linear increase from 20% to 35% of Solvent B over 5 min, followed by an increase from 35% to 75% Solvent B over 20 min, an increase from 75% to 100% Solvent B over 2 min, then the mobile phase was held at 100% Solvent

B for an additional 10 min. The QTOF was calibrated to positive electrospray ionisation (+ESI) mode (Gas Temp: 350°C, Drying Gas: 12L/min, Nebuliser 60psi, VCap: 3000V) and the QTOF was set to MS Mode with a 100-1700m/z mass range (Collision energy: 42V, Fragmentor: 175V, Skimmer: 65V, and Oct 1 RF Vpp: 750V). Data was collected as Total Ion Chromatograms (TIC), with MS fragmentation data stored as centroid and profile plots. The retention time, proposed molecular ion, and base peak for highly represented compounds (by peak area) in the active subfractions are reported below.

Table 4.2. TLC and LC-QTOF (HRMS) data for S9 subfractions.

Subfraction	Retention factor (in 10:10:1 $CHCl_3$, DCM, MeCN)	Retention Time(s), min	Proposed Molecular Ion(s), m/z	Base Peak(s), m/z
C1	0.223	10.001	341.1022	341.1022
		11.901	375.0598	165.0543
		12.363	373.0442	321.0158
		13.538	375.0624	240.0178
C2	0.323	12.597	393.0699	255.0054
		20.613	569.1979	197.1052
C4	0.432	13.138	341.0982	245.0811
		20.637	569.1984	197.1063
C5	0.510	14.989	484.1463	244.0719
		15.620	398.2404	302.1856
E1	0.711	18.186	385.1245	301.0694
		18.970	419.0848	335.0326
E2	0.843	29.229	549.3748	107.0724

4.6.4 Full Characterisation of Subfraction C1

Only subfraction C1 was isolated to purity with a high enough yield to complete the remaining analyses. Solvent was removed from the sample by rotatory evaporation and the remaining C1 solid was finely ground in a mortar and pestle. A Cole-Parmer Electrothermal IA9000 Series Melting Point Apparatus, set to a 1 °C per minute ramping speed was used to collect the melting point of C1, in triplicate. A Bruker ALPHA Fourier Transform Infrared Spectrometer was used to obtain an IR spectrum of the powder sample. A 5 μg/mL sample of C1 was made up in methanol and UV-Vis absorption spectra were collected in a 10 mm quartz cuvette on a Cary 50 Bio Spectrophotometer blanked with methanol. These analyses were also completed on the griseofulvin standard for comparison; a 2.5 μg/mL sample was used for UV-Vis analysis.

Crystals of C1 were obtained via slow evaporation crystallisation with methanol as a solvent. The X-ray crystallography was performed by Tanner George. A crystal was selected and attached to the tip of a MicroLoop with paratone-N oil and measured on a Bruker D8 VENTURE diffractometer equipped with a PHOTON III CMOS detector using monochromated Mo Kα radiation (λ = 0.71073 Å) from an Incoatec micro-focus sealed tube at 100 K.

For analysis by nuclear magnetic resonance, approximately 50 mg of compound C1 was dissolved in 1 mL of deuterated chloroform (Chloroform-d or $CDCl_3$). The sample was then filtered into an NMR tube and a Bruker 300 MHz Ultrashield NMR spectrometer at 298 K was used to collect NMR spectra. For all ^{1}H and ^{13}C NMR experiments, the chemical shifts (δ, ppm) were referenced internally to $CDCl_3$ relative to trimethylsilane (TMS, δ = 0 ppm).[77] Proton decoupled {1H} and distortionless enhancement by polarisation transfer

(DEPT) carbon NMR experiments were run; DEPT-135 shows CH and CH_3 carbons as positive phase peaks, CH2 carbons as negative phase peaks, and excludes quaternary carbon peaks completely from the spectrum. Two-dimensional NMR experiments were also run to confirm the peak assignments; heteronuclear single-quantum correlation (HSQC) spectroscopy was used to detect correlation between the ^{1}H and ^{13}C nuclei across a single bond, while heteronuclear multiple-bond correlation (HMBC) spectroscopy detects correlations across 2-4 bonds. Spectra were consistent with the literature.[76]

Subfraction C1 – Griseofulvin (2S,6'R)-7-chloro-2',4,6-trimethoxy-6'-methyl-3H,4'H-spiro[1-benzofuran-2,1'-cyclohex-2'-ene]-3,4'-dione

Appearance: White, crystalline powder.

R_f (10:10:1 $CHCl_3$, DCM, MeCN): C1: 0.223, Griseofulvin Standard: 0.223

IR (Powder): Signal strength: w=weak, m=medium, s=strong, and vs=very strong; 3007 (w, C-H stretch; sp^2), 2995 (w, C-H stretch; sp^2), 2974 (w, C-H stretch; sp^3), 2941 (w, C-H stretch; sp^3), 2907 (w, C-H stretch; sp^3), 2879 (w, C-H stretch; sp^3), 2836 (w, C-H stretch; sp^3), 1703 (s, C=O stretch; benzofuranone ring carbonyl), 1658 (m, C=O stretch; cyclohexeneone ring carbonyl), 1615 (s, C=C stretch; aromatic), 1598 (s, C=C stretch; aromatic), 1584 (s, C=C stretch; aromatic), 1504 (m, C=C stretch; aromatic), 1464 (m, C-H bend; methylene), 1437 (m, C-H bend; methyl), 1348 (s), 1333 (s), 1221 (vs, C-O stretch; aryl ether), 1211 (vs, C-O stretch; aryl ether), 1177 (m), 1152 (w), 1136 (s, C-O stretch; methoxy), 1120 (m), 1100 (s, C-O stretch; methoxy), 1089 (m), 1062 (m), 1049 (m), 993 (m), 959 (m), 887 (m), 820 (m), 799 cm^{-1} (s).

UV (methanol): C1 and Griseofulvin Standard: λ_{max} at 290.9nm (ε= 56267.6 and 54225.4 $Lmol^{-1}cm^{-1}$), Lit: λ_{max} at 291nm.[76]

HRMS: C1: 375.0598 m/z, Griseofulvin Standard: 375.0606m/z. Calc for $C_{17}H_{17}O_6ClNa^+$: 375.0611m/z.

m.p.: C1: 205.5-212.8 °C, Griseofulvin Standard: 217.6-220.4 °C. **Lit. m.p.:** 217-224 °C.[76]

^{1}H NMR ($CDCl_3$): Multiplicity: s=singlet, d=doublet, and m=multiplet; δ 6.14 (s, 1H, $H^{(g)}$), 5.55 (s, 1H, $H^{(h)}$), 4.04 (s, 3H, $H^{(c)}$), 3.99 (s, 3H, H^b), 3.63 (s, 3H, $H^{(a)}$), 3.11-2.98 (m, 1H, $H^{(f2)}$), 2.90-2.70 (m, J_{HH}=6.7Hz, 1H, $H^{(e)}$), 2.47-2.35 (m, 1H, $H^{(f1)}$), 0.97 ppm (d, J_{HH}=6.7Hz, 3H, $H^{(d)}$).

^{13}C{1H} NMR ($CDCl_3$): δ 197.0 ($R_2\underline{C}$=O, $C^{(4)}$), 192.5($R_2\underline{C}$=O, $C^{(8)}$), 170.8 ($\underline{C}$-OCH_3, $C^{(2)}$), 169.6 ($C^{(10)}$), 164.6 ($\underline{C}$-OCH_3, $C^{(12)}$), 157.8 ($\underline{C}$-OCH_3,$C^{(14)}$), 105.2 ($C^{(9)}$), 104.9 ($R_3\underline{C}H$, $C^{(3)}$), 97.3 ($C^{(11)}$), 90.8 ($C^{(7)}$), 89.5($R_3\underline{C}H$, $C^{(13)}$), 57.0 ($RO\underline{C}H_3$, $C^{(15)}$), 56.7 ($RO\underline{C}H_3$, $C^{(1)}$), 56.4 ($RO\underline{C}H_3$, $C^{(16)}$), 40.1 ($R_2\underline{C}H_2C^{(5)}$), 36.4 ($R_3\underline{C}H$, $C^{(6)}$), 14.2 ppm ($R\underline{C}H_3$, $C^{(17)}$).

^{13}C NMR ($CDCl_3$): + and – indicate peak phase; δ 104.9 (+, $R_3\underline{C}H$, $C^{(3)}$), 89.5(+, $R_3\underline{C}H$, $C^{(13)}$), 57.0 (+, $RO\underline{C}H_3$, $C^{(15)}$), 56.7 (+, $RO\underline{C}H_3$, $C^{(1)}$), 56.4 (+, $RO\underline{C}H_3$, $C^{(15)}$), 40.1 (-, $R_2\underline{C}H_2$, $C^{(5)}$), 36.4 (+, $R_3\underline{C}H$, $C^{(6)}$), 14.2 ppm (+, $R\underline{C}H_3$, $C^{(17)}$).

X-ray Crystallography: Selected bond lengths (Å) and angles (°): Cl(1)-C(1) 1.710(4), O(1)-C(2) 1.342(5), O(2)-C(4) 1.345(5), O(3)-C(6) 1.355(5), O(3)-C(10) 1.446(5), O(5)-C(11) 1.341(6), O(4)-C(9) 1.208(5), O(6)-C(13) 1.237(6); C(6)-O(3)-C(10) 107.7(3), O(3)-C(6)-C(5) 114.5(4), O(3)-C(10)-C(11) 110.5(3), O(3)-C(10)-C(15) 107.6(3), C(11)-C(10)-C(9) 110.7(3), C(11)-C(10)-C(15) 109.6(3), C(15)-C(10)-C(9) 113.0(3).

Table 4.3 Summary of crystallographic data for S9 Griseofulvin.

Chemical formula	$C_{17}H_{17}ClO_6$	**Formula mass**	352.75
Temperature/K	100.0	**Wavelength/Å**	0.71073
Crystal system	Tetragonal	**Space group**	$P4_1$
Unit cell dimensions		**Unit Cell Volume/ Å^3**	1541.85(8)
a/Å	8.8491(2)	**Number of formulas per Unit Cell, Z**	4
b/Å	8.8491(2)	**Crystal size/mm^3**	0.4 x 0.4 x 0.27
c/Å	19.6899(4)	**R(int)**	0.0401
Reflections collected	13788	**Independent reflections**	4668
Absorption correction	Semi-empirical from equivalents	**Final R indices [I>2s(I)]**	R_1 = 0.0545
Refinement method	Full-matrix least-squares on F^2		$wR(F^2)$= 0.1396
Data / restraints / parameters	4668 / 1 / 221	**Final R indices (all data)**	R_1 = 0.0726
Goodness-of-fit on F^2	1.055		$wR(F^2)$= 0.1782

4.6.5 Minimum-effective Concentration Test of Subfraction C1

Pd was grown in triplicate on YMA media with Subfraction C1 applied to the surface of each well. Dilutions of Subfraction C1 were prepared and filtered through 0.22 µm cellulose acetate syringe filters into autoclaved vials; 100 µL of the solution was applied to the surface of three wells each on 24-well plates, which were tilted to ensure even coverage of the compounds on the surface of each well (1.9 cm^2). The solvent was allowed to evaporate, leaving behind 0, 5, 10, 25, 50, 75, 100, 150, 200, and 250 µg films of the Subfraction C1 metabolite solids evenly coating the surface of the wells. A liquid culture of *Pd* (1.75 mg/mL) was used to inoculate wells on each of the surface concentrations using a volume of 25 µL per well. The plates were incubated at 14.0 ± 1.0 °C, and photographs were taken on Days 1, 3, 5, 7, and 10. Growth curves were created, and Day 10 percent inhibition was calculated for each surface concentration.

Chapter 5: Mechanism of Action of S9 Metabolites

5.1 Overview

To determine how the active molecules affect the growth of *Pd* compared to other *Pseudogymnoascus spp.*, comparative transcriptome analysis was completed on S9-treated and untreated *Pd* and *Pr*. By looking at RNA and the transcriptome, it can be determined how the active compounds affect gene expression, and if it may have any effect on protein, enzyme, or metabolite production. Transcriptome analysis on S9, the microbe producing the active compounds may help identify the genes—or biosynthetic gene clusters—and molecular machinery that is used to produce the compounds. This insight would aid in developing a benchtop synthesis method for the compound, should it need to be upscaled or derivatised.

5.2 Background

5.2.1 Gene Expression and Transcriptomics

Originally detailed by Francis Crick in 1958, the central dogma of molecular biology states that information in a cell is transferred from nucleic acid to nucleic acid, and nucleic acid to protein, implying a set sequence for the expression of proteins, based on the genomic blueprint.[78] This relationship is simplified as genes or DNA is transcribed into RNA, which are then translated into proteins. However, the genome is complex, and every encoded gene is not always expressed into a gene product. Rather, the timing, location, and degree of gene expression are regulated at every step outlined in the central dogma—leading to phenotypic variation.

One way to investigate gene expression is through the transcriptome. The transcriptome consists of the RNA transcribed by the genome at a point in time in a cell, including the coding mRNA and non-coding RNA transcripts. Transcriptomics, or the study of the transcriptome, gives indication as to what genes are "turned on", what proteins are being produced, and to what degree the expression is occurring. Transcriptomics is especially useful in comparative studies, whereby the RNA of treated and untreated specimens is extracted and sequenced, and the amounts and types of gene products are compared to understand how the treatment affects the specimen. This technique is known as RNA-Seq.[79,80] RNA-Seq utilises next generation sequencing (NGS) technology to determine the sequence and quantity of RNA expressed at a given moment of time—like a snapshot of gene expression. Aside from differential gene expression, RNA-Seq can also be used to understand alternative splicing events and post-transcriptional modifications that cannot be observed using DNA sequencing, like polyadenylation and 5' capping.[81,82]

5.2.2 The RNA-Seq Process

Experimental Design

RNA-Seq can be split into three distinct stages: sample preparation, sequencing, and analysis. While all three stages rely on a planned experimental design, it is especially crucial in the sample preparation stage. To adequately test a null hypothesis using RNA-seq, appropriate control specimens must be prepared for comparison to understand the effect of the treatment, and enough replicates of the controls and treatments must be tested to identify which changes are statistically significant. RNA-Seq only takes a snapshot of the RNA at the point of extraction, so the timing of the extraction is also a key factor, as it must fall into the effective window of the treatment.

Preparing RNA Samples

RNA extraction is generally completed using some form of a phenol-chloroform separation.[83] When added to lysed cells, acidic phenol solubilises biological components, and when chloroform is added, a biphasic separation occurs. The organic phase and interphase contain the DNA and protein from the sample, while the aqueous phase holds the RNA. This RNA can be collected and further purified to obtain a clean sample. Various methods are used to determine the quality of an RNA sample prior to sequencing, including 260/280 and 260/230 ratios for purity and gel or microcapillary electrophoresis for integrity.[84]

Nucleic acids, like DNA and RNA, have an absorbance maximum at 260 nm, so to determine the purity of the sample, absorbance reading at 260 nm is compared to the reading at 280 nm and 230 nm. Proteins and phenol give absorbance readings at 280 nm, and organic compounds used in the extraction give readings at 230 nm, so a low 260/280 and 260/230 ratios may indicate incomplete purification or washing of the sample after extraction. For a clean, well-purified RNA sample, the 260/280 ratio and 260/230 ratio should fall around 2.0 and 2.0 – 2.2, respectively.[85]

To determine integrity of a total RNA sample, electrophoresis methods are used to separate the RNA. Ribosomal RNA, or rRNA is abundant in total RNA samples, so it is easiest to use as an indicator for degradation. In non-degraded, eukaryotic total RNA samples, the 18S and 28S rRNA bands should be strongly visible on ethidium bromide-stained, denaturing agarose using gel electrophoresis, with the 28S band being twice as intense. If the rRNA bands are faint, smeared, or do not exhibit the 2:1 intensity ratio, the RNA is likely partially degraded. If the sample is a large, low molecular weight smear, the

RNA is completely degraded.[84] Microcapillary electrophoresis also utilises a comparison between the 28S and 18S RNA levels. Rather than relying on subjective observation of band intensity, it uses a microfluidic chip and voltage-based separation paired with a laser-induced fluorescence detector to produce electropherograms. The electropherogram is assigned an RNA integrity number (RIN) based on features such as peak area and peak height of the 18S and 28S signals and degradation marker signals.[84,86]

The final step of sample preparation is selecting the type of RNA to be sequenced. A total RNA sample contains coding RNA (messenger, or mRNA) and non-coding RNA, which consists of rRNA, long-noncoding RNA (lncRNA), and small RNA (micro, miRNA; small interfering, siRNA; and transfer, tRNA). The type(s) of RNA to be sequenced and analysed is dependent on the research question. For example, as previously mentioned, rRNA is abundant in the total RNA, making up over 80% of the total RNA extracted, while mRNA only constitutes 1-2%.[80,82] If mRNA is the component of interest, the rRNA must be depleted in the sample, or the mRNA must be enriched. To deplete rRNA, complimentary oligomers are added to the sample to bind with and precipitate out rRNA, while mRNA enrichment uses oligo dT primers to capture the 3' polyadenylated (PolyA) tails of mRNA to isolate and concentrate the sample in coding RNA.[82] However, if the sample is partially degraded, some of the mRNA might be separated from their PolyA tails, which would cause non-representative enrichment of the sample. Enrichment would also exclude non-polyadenylated transcripts that may be of interest, like non-PolyA mRNA, lncRNA and small RNA, but may lead to better gene expression quantification when based on 3' PolyA mRNA alone.[82]

RNA Sequencing

Once appropriate RNA samples with high integrity and purity are obtained, they can be sequenced. First, fragmented RNA is reverse transcribed to complementary DNA (cDNA), and the synthesised cDNA is fitted with adaptor sequences at the end of the fragments to label which sample the fragment belongs to, allowing multiple samples to be sequenced at once.[87] The cDNA is amplified by polymerase chain reaction (PCR), gel purified, then sequenced using high-throughput sequencing technologies. One example is the Illumina sequencing platform, where adapter-bound DNA is captured in a flow cell using oligomers complementary to the adapters. The fragments are amplified into clonal clusters to create hundreds of reverse and forward strands of each fragment of DNA through bridge amplification. The reverse strands are washed away, and primers are attached to the forward strand adapters. Through a sequencing by synthesis (SBS) method, polymerases add fluorescently tagged deoxynucleoside triphosphates (dNTPs) one base at a time to the bound strands, with each of the four bases (adenine, thymine, guanine, and cytosine) emitting a unique fluorophore. The platform records the identity of the base added each round for each cluster, and the process is repeated until a certain read length (number of bases) is reached. Once the first read is complete, the complementary reverse strands are resynthesised, and the forward strands are washed away. The SBS method is repeated on the reverse strand to create a second read, which together with the forward read creates a complete paired-end read library.[87]

Assessing Quality of the Raw Reads

Prior to analysis, quality control checks of the reads should be completed. FastQC is a tool commonly used to assess raw read quality.[88] While there are many modules in the

FastQC program to understand the quality of the reads, the following eight (italicised) modules are useful in identifying and diagnosing problems in the RNA-Seq process up to this point.

Per Base Sequencing Quality is one of the most important QC metrics for raw reads. In this process, a Phred score is assigned to each sequenced base call and represents the probability that the base was called incorrectly. The Phred quality score, Q, is related to the base calling error probability, P, by the equation $Q = -10 \log_{10} P$. Thus, a Phred quality score of 30 indicates a 1 in 1000 probability of error, or a 99.9% base call accuracy, while a score of 40 indicates a 1 in 10000 probability of error or 99.99% base call accuracy. Generally, a score greater than 30 indicates good quality reads.

Per Sequence Quality Score reports the average Phred score across all of the sequences. If a portion of the sequences have a low quality, this could indicate an issue with a portion of the flow cell on which the RNA was sequenced. *Per Tile Sequence Quality* utilises sequence identifiers on the read specific to each tile in a flow cell to assess the quality of sequences from each tile. This can help confirm whether loss of quality was associated with one part of the flow cell, or if it was a systematic problem.

Sequence Length Distribution gives the distribution of fragment sizes in the reads. This module will generally give a single length for Illumina sequencing, as sequence length is dictated by the number of rounds of base calling performed in the SBS process.

Per Base Sequence Content indicates the proportion of each of the four bases' positions in the raw read. The proportions should be fairly equal among the bases—within 10% at all positions—and be representative of the overall proportion of each base in the genome. However, RNA-Seq libraries tend to be imbalanced at the start of the read, tending

toward enrichments of certain bases at certain positions in the first 12 bases of each run. This is a result of the biased fragmentation process used prior to sequencing and leads to most RNA-Seq libraries failing this module. This issue cannot be fixed by trimming, but it does not seem to cause adverse effects in later analysis, so it can largely be ignored as long as the rest of the read positions are fairly consistent.

Overrepresented sequences which make up greater than 0.1% of the total sample can also skew the proportions along the length of the read. These sequences may be biologically significant repeated motifs, residues from the adapters used (which are generally recognised by the FASTQC program), contamination, or a result of biased fragmentation. *Adapter Content* specifies the proportion of reads with an adapter sequence and the position of the adapter in the read. If less than 5% of the reads have adapter sequences at the end, no trimming is required prior to analysis.

Finally, *Per Base GC Content* indicates the distribution of GC over all of the sequences. This should be a smooth normalised plot centred at the expected % GC content of the organism, but overrepresented sequences can cause the graph to appear as sharp peaks on a normal distribution.[88,89]

Assembling the Transcriptome

Once the raw reads are obtained and confirmed to be of high quality, the transcriptome can be assembled. This can be done with or without a reference transcriptome or genome. Without a reference genome, *de novo* transcriptome assembly must be completed using programs like Trinity, which use complex multistep algorithms to turn high quality reads into full length transcripts. This program uses de Bruijn graphs to determine all linear sequences, or potential transcripts, that can be constructed from

overlapping fixed length sequences in the reads. These potential transcripts are scored based on the actual reads using a dynamic programming procedure to identify the most probable full length transcripts.[90] When a reference transcriptome for the species already exists, reads can be mapped directly to it, allowing for quantification of known, annotated transcripts. However, this method does not allow for the discovery of novel transcripts not yet annotated on the available reference transcriptome.[80,89] If a reference genome is available, programs like STAR (Spliced Transcripts Aligned to a Reference) can be used to find the genomic origin of each read.[91] One major challenge of aligning to a genome is that post transcriptional modifications, specifically splicing, prevents exact overlap between the length of a processed mRNA read and the gene(s) its sequence originated from; splice-aware alignment software like STAR take this into account. Rather than only aligning whole reads that match the genome exactly, STAR searches for the longest sequence in the read that can be mapped to the genome, or the Maximal Mappable Prefix (MMP), and uses this as a seed to anchor the read. The program then searches for the next longest sequence in the unmapped section of the same read and repeats the mapping process. If an exact match of a section cannot be found, the previous seed is extended to determine if the unmappable portion of the read is due to mismatching or insertion-deletion events (indels).[91] If the extended seed can align well after the mismatch, it is mapped, but if it does not align well, the read sequence is clipped. This clipped section generally represents contaminating sequences like adapters or poor-quality reads. The seeds that are mapped to the same region of the genome are clustered and then stitched together based on the best alignment for the read, taking into account the placement of singly mapped MMP "anchor" seeds, location and size of gaps, and presence of mismatches and indels.[89,91]

RNA-Seq Data Analysis

Once the reads have been aligned and assembled into a transcriptome, the process of extracting meaningful information from the data can begin. Both quantitative and qualitative information can be extracted from RNA-Seq data. Quantitative methods, like differential gene expression (DGE) analysis, can be used to help understand how a treatment impacted relative expression of genes or isoforms, while qualitative analysis, or annotation, allows for the identification of expressed genes to determine which functions or pathways are impacted.

Prior to downstream analyses, the gene expression levels from the RNA-Seq data must be determined. This is done by counting the number of reads mapped to each site. However, reads are often not uniquely mapped to a single site, and in many quantification methods, are not included in the counts.[80] Programs like RNA-Seq by Expectation-Maximisation (RSEM) use statistical methods like Expectation-Maximisation produce an estimate for gene and isoform expression that include these ambiguous reads.[80,92] RSEM outputs a gene- and isoform-level estimate, with an estimate of the number of fragments (counts) and fraction of transcripts (in transcripts per million, TPM) originating from each gene or isoform.[92]

Now that the expression data has been prepared, the variability in the datasets can be explored. Ideally, intergroup variability, or variability between treatment groups and controls, is higher than intragroup variability.[80,93] This is normally visualised using principal component analysis (PCA), which plots the principal components describing the most variance in the sample against one another. In this plot, high intergroup and low intragroup variability would be observed if datapoints formed distinct clusters consisting

of data originating from each treatment. This type of plot is also useful for identifying outliers that may impact other downstream analyses. Pearson's correlation is another measure of variability that reveals the linear relationship between two variables based on differences in their mean and standard deviation. The correlation coefficient of the variables can be plotted as a heatmap to assess variability between or within groups to further confirm grouping or identify outliers prior to analysis.[93]

Once variability has been assessed, outliers have been removed, and replicates have been grouped, DGE analysis can be completed. When identifying DGE between two groups, like a treatment and a control, programs using negative binomial models. DESeq is one such program that tests the null hypothesis that a gene will not be differentially expressed between the two groups. If the genes are significantly differentially expressed, the hypothesis will be rejected. DESeq outputs the $\log_2$ fold change for each gene, as well as a p-value. This data can be visualised as a volcano plot (log fold change vs. $-\log_{10}$ P value), to identify which show differential gene expression that is statistically significant.[80,93,94]

To extract biological information and determine what these differentially expressed genes mean in terms of the mechanism or effect of the treatment, the transcripts must be annotated. If the reference genome or transcriptome is well annotated, this process is simple, but for most species, annotation must be performed manually. Blast2GO is a useful platform for high-throughput functional annotation that can perform BLAST (Basic Local Alignment Search Tool) searching, GO (gene ontology) term mapping, and annotation.[93,95]

First, a BLASTx search is completed to identify matches to similar known sequences; BLAST2GO can be connected to multiple different databases, like the NCBI

nonredundant protein database or SwissProt for BLAST searching. Then, the GO term mapping is performed to find GO terms associated hits obtained from the BLAST search. GO consists of three domains: molecular function, biological processes, and cellular components. Each GO term contains an indication as to which domain it falls with, then a unique term name. Finally, the genes are annotated by selecting from the GO terms obtained from the mapping based on statistical significance. This data can then be visualised to understand the proportions of genes related to different metabolic and cellular processes to give biological insight into the data sets being compared. The process of identifying these over-represented or depleted gene types is known as Gene Set Enrichment Analysis (GSEA) and can be used to identify biological pathways or mechanisms through which an applied treatment has effects.[95]

5.2.3 Applications of Transcriptomics in Assessing Antimicrobial Activity

Transcriptomic studies have been utilised to investigate the mechanism of antimicrobials on target microbes for a variety of applications in the health and food sectors. With the concerning rise of antibiotic resistant pathogens, employing new approaches to drug development and discovery is imperative. Most clinically applied antibiotics are derivatives of just 22 classes of novel antimicrobial structures, with only two of these classes being developed since 2000.[96] The current model of creating analogues of existing classes, as opposed to discovering new structures, makes it easier to get a product to market, but only serves as a short-term solution. Since the structures and thus the mechanisms of the new derivative antibiotics are so similar to previously used antibiotics, bacteria are able to rapidly develop resistance to the drugs. To truly combat antibiotic resistance, new classes of antibiotics with unique mechanisms of action need to be developed on a constant basis.

Using transcriptomics, antimicrobials with clinical potential can be studied to assess what the mechanism of action is and used to infer how susceptible the drug would be to acquired resistance by target microbes. Varney *et al.* revisited the potential of antibiotic metal complexes, which were described as early as 1950 but never made it to market due to a lack of development.[97] It was determined that a ruthenium(II) complex showed comparable antibiotic activity against a pathogenic *Escherichia coli* strain to clinically available antibiotics, with *E. coli* showing slower rates of resistance. Using transcriptomic analysis, it was determined that the ruthenium(II) complex utilizes a multi-mechanism mode of action, targeting internal components used in aerobic respiration and metabolite production, as well as membrane function. The connection between the slower evolution of resistance and multi-targeted mechanism of the ruthenium complex gives credibility to the idea that mechanistic diversity should be a priority in new antibiotic candidates.

Transcriptomics has also been used to explore the mechanism of known but not widely understood natural antibiotics, including honey and essential oils.[98,99] While these natural treatments have been used for millennia, there have been no reports on developed bacterial resistance.[99] However, due to the lack of mechanistic understanding about these treatments, they are not generally used it a clinical setting. The success of these natural antibiotic substances is proposed to be the result of the composite nature of the samples. Rather than containing single drug-like compounds, they contain a complex profiles of multiple potential antibiotic compounds that can work synergistically to produce a multi-targeted antibiotic mechanism. Manuka honey, for example, consists of multiple compounds, which, when tested independently, do not account for the overall antimicrobial activity of the honey.[99] Transcriptomic analysis confirmed the multi-mechanistic effect of

the honey, revealing that multiple functions and metabolic pathways are impacted, including the response to DNA damage, aerobic respiration, and quorum sensing.

While essential oils are less complex than honey, usually only consisting of a few major chemical components, they still have fairly broad antimicrobial activity. Through transcriptomic analysis, it was determined that target microbes treated with thyme essential oil had more differentially expressed genes that one of its main components, carvacrol, though both widely effected gene expression, impacting genes associated with energy metabolism, oxidative stress response, and fatty acid biosynthesis.[98]

Overall, there is great value in not just identifying, but mechanically understanding potential antimicrobial remedies. By understanding how the treatment works, we can determine the range of target microbes it can be used against, the risks or likelihood of developed resistance, and how and where the drug would best be applied. Finally, evidence suggests that for future drug development, priority should be given to candidates with multi-mechanistic modes of action to increase the longevity of the clinical and practical use and prevent the rise of resistant pathogens.

5.3 Results and Discussion

5.3.1 RNA Isolation and Sequencing

RNA was extracted in triplicate from control and S9-extract treated *Pseudogymnoascus destructans* (*Pd* and *Pd*S9) and *Pseudogymnoascus roseus (Pr and Pr*S9*),* as well as the *Penicillium* strain S9. The concentration, A260/280, and A260/230 of each sample was measured (Table 5.1) to ensure they fell within the guidelines set by the sequencing company Genome Quebec (>30 ng/μL, 1.7-2.1, and 2.0-2.2, respectively). Several of the samples fell outside the A260/280 and A260/230 ratio ranges, however,

Genome Quebec accepted the samples and performed a more comprehensive, independent quality control check, which all fifteen of the samples below passed. The number of raw reads obtained for each sample is summarised in Table 5.1. All 15 samples had an average *Per Sequence Quality Score* of 36 indicating high-accuracy base calling for all sequenced samples.

Table 5.1 Summary of RNA-Seq data.

Sample	260/280	260/230	Concentration, ng/µL	#Reads	Genes Detected
*Pd*_1	2.07	2.35	697.6	69 947 930	8334
*Pd*_2	2.09	2.36	1788.0	74 153 448	8382
*Pd*_3	2.08	2.38	1373.9	73 410 408	8300
*Pr*_1	2.20	2.15	55.5	70 482 311	6181
*Pr*_2	1.88	1.93	83.0	74 651 286	6199
*Pr*_3	1.86	2.22	59.9	66 004 567	6181
*Pd*S9_1	2.17	2.31	1385.2	67 162 858	8305
*Pd*S9_2	2.13	2.27	2334.2	71 840 925	8132
*Pd*S9_3	2.12	2.12	1204.7	58 994 115	7942
*Pr*S9_1	2.00	2.20	319.4	61 442 459	5940
*Pr*S9_2	2.05	2.47	668.8	63 344 934	5973
*Pr*S9_3	2.05	2.44	552.7	67 932 012	5982
S9_1	1.83	2.06	113.7	63 243 797	-
S9_2	1.90	1.88	356.2	79 173 266	-
S9_3	1.84	2.03	218.2	68 743 811	-

5.3.2 Alignment and Analysis

The reads for the *Pd, Pd*S9, *Pr,* and *Pr*S9 samples were all mapped to the reference genome for *Pseudogymnoascus destructans*, since no reference genome for *Pr* exists and the number of genes detected. Control and treated *Pd* samples expressed an average of 8339 and 8129 genes out of the 9620 known *Pd* genes, indicating a sufficient read depth to measure *Pd* gene expression. While the number of genes in the *Pr* genome is unknown, most sequenced *Pseudogymnoascus* species have ~10000 genes, indicating that the detected genes in the treated and *Pr* samples might only make up a fraction of the genes

actually expressed. This could be a result of using a non-*Pr* reference genome, as some of the reads might not have correctly mapped to the Pd genome, causing them to be rejected due to low quality.

Compared to control *Pd*, 873 genes were differentially expressed in the *Pd*S9 treated group, while 2579 were differentially expressed between the Pr control and *Pr*S9 treated groups. Since neither variance testing nor enrichment analysis of these data have been performed, the significance of these values cannot be commented on.

5.4 Future work

Further analysis of the control and treated *Pd* and *Pr* data must be completed to explore the effect of the S9 treatment on gene expression in *Pseudogymnoascus* species. First, PCA should be completed to understand patterns of variance and global transcriptomic patterns in the data. To validate the DGE data, quantitative PCR (qPCR) should be performed on a few stably and differentially expressed genes to quantify expression, then the expression trends can be compared to the trends yielded by the RNA-seq data. Visual representations of the DGE data, like volcano plots or heat maps, should be constructed to allow for a more meaningful understanding of the degree and significance of the differential expression. From there, the provided GO terms should be used to perform enrichment analysis to identify potential targets for the active S9 compounds. Based on the known mechanism of one of the identified active compounds in the S9 extract, griseofulvin, it is hypothesised that enrichment analysis will reveal differential expression in genes involved in mitosis, nucleic acid synthesis, and cell wall synthesis.

Finally, once the remaining active compounds produced by S9 are identified, the S9 transcriptome may be used to determine the biosynthetic pathways the fungus uses to make the active compounds. The value of S9 as a biocontrol agent is derived from its status as a fungus native to bat caves in the region of study (Eastern Canada), but since WNS is widespread and the micro-ecology of affected locations differ, site specific, active fungal

strains need to be found. Using the pathway data from the active S9 compounds, the genomes of other bat associated fungi can be mined for similar pathways to identify more species or strains from different regions that can be used as biocontrol agents against *Pd* and bat WNS.

5.5 Experimental

5.5.1 Treatment of *Pd* with S9 Metabolites

Six plates each of *Pd* and *Pr* were allowed to grow for two weeks, and then three of each were treated by dropping 50 µL of 100 mg/mL methanolic S9 extract on the surface of the fungi. The treatment was allowed to sit for one day. Three S9 plates were also grown for three weeks. The result was three plates of S9-treated *Pd*, three plates of control *Pd* (for baseline comparison), three plates of S9-treated *Pr* (as *Pr* had previously shown resistance to the action of S9), three plates of control *Pr,* and three plates of S9 (for determination of transcriptomic metabolite sources).

5.5.2 RNA Extraction

The work in this section was primarily designed and completed by Lindsay N. Donovan. A 150 mg sample of fungi was taken from each of the aforementioned plates, and placed in a homogenising tube. The tube and sample were cooled in liquid nitrogen, then the sample was ground into a fine powder. A volume of 1000 µL of TRIzol (phenol and guanidinium isothiocyanate) was added to the tube and the sample was ground until evenly dispersed; the sample mixture was transferred to a 2 mL microcentrifuge tube. A volume of 100 µL of beta-mercaptoethanol (BMer) buffer (4 g Tris-HCl, 2 g NaCl, 1 mL BMer, 250mL dH_2O, pH 9.5) was added to each sample, vortexed for 1 min, then allowed to incubate at room temperature (~21 °C) for 5 min. A volume of 200 µL of chloroform

was added to each sample, incubated at room temperature for 5 min, then centrifuged at 12000 g for 15 min at room temperature. The resulting solution consisted of a colourless top layer, a solid interface, and a pink bottom layer; the colourless top layer was transferred into a new tube and the old tube was discarded. To the new tube, 500µL of isopropanol was added, cooled on ice for 10min, vortexed for 1min, then centrifuged at 12000g for 15min at room temperature. The supernatant was discarded and 1mL of ice-cold 100% ethanol was added to the pellet and incubated at -80°C for 20min. The sample was briefly vortexed, then centrifuged at 12000g for 20min at room temperature. The supernatant was discarded and 500µL of ice-cold 75% ethanol was added to the pellet and briefly vortexed, then centrifuged at 7500g for 5min at room temperature. The previous step was repeated a second time, then the supernatant was removed without disturbing the pellet. The sample was allowed to airdry for 5min—not letting the pellet go completely dry. The resulting RNA pellet was resuspended in 50µL of nuclease-free water, briefly vortexed, then stored in the -80°C freezer.

The quality of the RNA samples was assessed using gel electrophoresis on 1% agarose-TAE-Bleach gels (1g agarose powder, 1 mL 6% bleach, 0.5 µg/mL ethidium bromide, made up to 100mL in Tris-acetate-EDTA).[100] NanoDrop 1000 Spectrophotometer was used to determine the concentration and purity of the sample. Samples with a concentration >30 ng/µL and A260/280 and A260/230 >2 were deemed acceptable for sequencing. In triplicate samples of 15 µL of RNA from *Pd* (non-treated), *Pr* (non-treated), *Pd*S9 (1 day, S9 extract treated *Pd*), and *Pr*S9 (1 day, S9 extract treated *Pr*) were sequenced by GenomeQuebec on a NovaSeq 6000 (S2 PE100) Analyser.

5.5.3 Sequence Analysis

Raw stranded transcriptome FASTQ files for the treated and untreated *Pd* and *Pr* were sent to Canada's Michael Smith Genome Science Centre (Vancouver, Canada) for alignment and differential expression analysis. The sequences were aligned to the reference genome of *Pseudogymnoascus destructans* (assembly ASM164126v1) by STAR to the full read length.[91,101] Isoform and gene expression was quantified from the aligned transcriptome using RSEM.[92] Differential expression analysis was completed using DESeq (v 1.39.0) with a noise filter threshold of 25 reads and a p-value (FDR) of 5%.[102] Expression was compared between the treated and untreated samples of the same fungi (untreated *Pd* vs. treated *Pd and* untreated *Pr* vs. treated *Pr*), then between the two fungi (treated *Pd* vs. treated *Pr* and untreated *Pd* vs. untreated *Pr*).

Since no assigned GO terms were available for either fungus, Blast2GO was used to search and annotate genes of interest.[95] Differentially expressed genes were run through BLASTx sequence similarity searches of the NCBI non-redundant protein database. GO terms were mapped and annotated in using the respective functions built into Blast2GO.[95]

Chapter 6: References

(1) U.S. Fish & Wildlife Service. 2017.
(2) U.S. Fish & Wildlife Service. White-nose syndrome occurrence map https://www.whitenosesyndrome.org/where-is-wns (accessed Jul 9, 2021).
(3) Kolwich, J. BSc Honours, Saint Mary's University, Halifax, NS, 2019.
(4) Altringham, J. D.; McOwat, T.; Hammond, L. In *Bats: from evolution to conservation*; Oxford University Press: Oxford New York, 2011; Vol. 2, pp 1–36.
(5) Tudge, C. In *The variety of life: a survey and a celebration of all the creatures that have ever lived*; Oxford University Press: London ; New York, 2000; pp 433–460.
(6) Sears, K. E.; Behringer, R. R.; Rasweiler, J. J.; Niswander, L. A. *Proceedings of the National Academy of Sciences* **2006**, *103* (17), 6581–6586.
(7) Altringham, J. D.; McOwat, T.; Hammond, L. In *Bats: from evolution to conservation*; Oxford University Press: Oxford New York, 2011; Vol. 2, pp 195–238.
(8) Boyles, J. G.; Cryan, P. M.; McCracken, G. F.; Kunz, T. H. *Science* **2011**, *332* (6025), 41–42.
(9) Altringham, J. D.; McOwat, T.; Hammond, L. In *Bats: from evolution to conservation*; Oxford University Press: Oxford New York, 2011; Vol. 2, pp 97–112.
(10) Nagel, A.; Nagel, R. *Comparative Biochemistry and Physiology Part A: Physiology* **1991**, *99* (3), 323–326.
(11) Carey, H. V.; Andrews, M. T.; Martin, S. L. *Physiological Reviews* **2003**, *83* (4), 1153–1181.
(12) Rosner, E.; Voigt, C. C. *Journal of Experimental Biology* **2017**, jeb.168096.
(13) Lennarz, W. J.; Lane, M. D. Elsevier/Academic Press: Amsterdam, 2013.
(14) Cryan, P. M.; Meteyer, C.; Boyles, J. G.; Blehert, D. S. *BMC Biology* **2010**, *8* (1), 135.
(15) Blehert, D. S.; Hicks, A. C.; Behr, M.; Meteyer, C. U.; Berlowski-Zier, B. M.; Buckles, E. L.; Coleman, J. T. H.; Darling, S. R.; Gargas, A.; Niver, R.; Okoniewski, J. C.; Rudd, R. J.; Stone, W. B. *Science* **2009**, *323* (5911), 227.
(16) Andrea, G. *Nova Scotia Government*. April 2011.
(17) Broders, H. Welcome to the Nova Scotia Bat Conservation Site http://www.batconservation.ca/.
(18) Warnecke, L.; Turner, J. M.; Bollinger, T. K.; Misra, V.; Cryan, P. M.; Blehert, D. S.; Wibbelt, G.; Willis, C. K. R. *Biology Letters* **2013**, *9* (4).
(19) Verant, M. L.; Meteyer, C. U.; Speakman, J. R.; Cryan, P. M.; Lorch, J. M.; Blehert, D. S. *BMC Physiology* **2014**, *14* (1).
(20) Reeder, D. M.; Frank, C. L.; Turner, G. G.; Meteyer, C. U.; Kurta, A.; Britzke, E. R.; Vodzak, M. E.; Darling, S. R.; Stihler, C. W.; Hicks, A. C.; Jacob, R.; Grieneisen, L. E.; Brownlee, S. A.; Muller, L. K.; Blehert, D. S. *PLoS ONE* **2012**, *7* (6), e38920.
(21) Minnis, A. M.; Lindner, D. L. *Fungal Biology* **2013**, *117* (9), 638–649.
(22) Gargas, A.; Trest, M.; Christensen, M.; Volk, T. J.; Blehert, D. S. 2009; Vol. 108.

(23) Chaturvedi, V.; Springer, D. J.; Behr, M. J.; Ramani, R.; Li, X.; Peck, M. K.; Ren, P.; Bopp, D. J.; Wood, B.; Samsonoff, W. A.; Butchkoski, C. M.; Hicks, A. C.; Stone, W. B.; Rudd, R. J.; Chaturvedi, S. *PLoS ONE* **2010**, *5* (5), e10783.
(24) Verant, M. L.; Boyles, J. G.; Waldrep, W.; Wibbelt, G.; Blehert, D. S. *PLoS ONE* **2012**, *7* (9), e46280.
(25) Reynolds, H. T.; Barton, H. A. *PLoS ONE* **2014**, *9* (1), e86437.
(26) Puechmaille, S. J.; Wibbelt, G.; Korn, V.; Fuller, H.; Forget, F.; Mühldorfer, K.; Kurth, A.; Bogdanowicz, W.; Borel, C.; Bosch, T.; Cherezy, T.; Drebet, M.; Görföl, T.; Haarsma, A.-J.; Herhaus, F.; Hallart, G.; Hammer, M.; Jungmann, C.; Le Bris, Y.; Lutsar, L.; Masing, M.; Mulkens, B.; Passior, K.; Starrach, M.; Wojtaszewski, A.; Zöphel, U.; Teeling, E. C. *PLoS ONE* **2011**, *6* (4), e19167.
(27) Lorch, J. M.; Meteyer, C. U.; Behr, M. J.; Boyles, J. G.; Cryan, P. M.; Hicks, A. C.; Ballmann, A. E.; Coleman, J. T. H.; Redell, D. N.; Reeder, D. M.; Blehert, D. S. *Nature* **2011**, *480* (7377), 376–378.
(28) Rachowicz, L. J.; Hero, J.-M.; Alford, R. A.; Taylor, J. W.; Morgan, J. A. T.; Vredenburg, V. T.; Collins, J. P.; Briggs, C. J. *Conservation Biology* **2005**, *19* (5), 1441–1448.
(29) Rajkumar, S. *Emerging Infectious Diseases* **2011**, *17* (7), 1273–1276.
(30) Ren, P.; Haman, K. H.; Last, L. A.; Rajkumar, S. S.; Keel, M. K.; Chaturvedi, V. *Emerging Infectious Diseases* **2012**, *18* (5), 883–885.
(31) Palmer, J. M.; Kubatova, A.; Novakova, A.; Minnis, A. M.; Kolarik, M.; Lindner, D. L. *G3* **2014**, *4* (9), 1755–1763.
(32) Wibbelt, G.; Kurth, A.; Hellmann, D.; Weishaar, M.; Barlow, A.; Veith, M.; Prüger, J.; Görföl, T.; Grosche, L.; Bontadina, F.; Zöphel, U.; Seidl, H.-P.; Cryan, P. M.; Blehert, D. S. *Emerging Infectious Diseases* **2010**, *16* (8), 1237–1243.
(33) Puechmaille, S. J.; Verdeyroux, P.; Fuller, H.; Gouilh, M. A.; Bekaert, M.; Teeling, E. C. *Emerging Infectious Diseases* **2010**, *16* (2), 290–293.
(34) Martínková, N.; Bačkor, P.; Bartonička, T.; Blažková, P.; Červený, J.; Falteisek, L.; Gaisler, J.; Hanzal, V.; Horáček, D.; Hubálek, Z.; Jahelková, H.; Kolařík, M.; Korytár, L.; Kubátová, A.; Lehotská, B.; Lehotský, R.; Lučan, R. K.; Májek, O.; Matějů, J.; Řehák, Z.; Šafář, J.; Tájek, P.; Tkadlec, E.; Uhrin, M.; Wagner, J.; Weinfurtová, D.; Zima, J.; Zukal, J.; Horáček, I. *PLoS ONE* **2010**, *5* (11), e13853.
(35) Zukal, J.; Bandouchova, H.; Brichta, J.; Cmokova, A.; Jaron, K. S.; Kolarik, M.; Kovacova, V.; Kubátová, A.; Nováková, A.; Orlov, O.; Pikula, J.; Presetnik, P.; Šuba, J.; Zahradníková, A.; Martínková, N. *Scientific Reports* **2016**, *6* (1).
(36) Warnecke, L.; Turner, J. M.; Bollinger, T. K.; Lorch, J. M.; Misra, V.; Cryan, P. M.; Wibbelt, G.; Blehert, D. S.; Willis, C. K. R. *Proceedings of the National Academy of Sciences* **2012**, *109* (18), 6999–7003.
(37) Leopardi, S.; Blake, D.; Puechmaille, S. J. *Current Biology* **2015**, *25* (6), R217–R219.
(38) Drees, K. P.; Lorch, J. M.; Puechmaille, S. J.; Parise, K. L.; Wibbelt, G.; Hoyt, J. R.; Sun, K.; Jargalsaikhan, A.; Dalannast, M.; Palmer, J. M.; Lindner, D. L.; Marm Kilpatrick, A.; Pearson, T.; Keim, P. S.; Blehert, D. S.; Foster, J. T. *mBio* **2017**, *8* (6).
(39) Meteyer, C. U.; Barber, D.; Mandl, J. N. *Virulence* **2012**, *3* (7), 583–588.

(40) Lilley, T. M.; Prokkola, J. M.; Johnson, J. S.; Rogers, E. J.; Gronsky, S.; Kurta, A.; Reeder, D. M.; Field, K. A. *Proceedings of the Royal Society B: Biological Sciences* **2017**, *284* (1848), 20162232.
(41) Rapin, N.; Johns, K.; Martin, L.; Warnecke, L.; Turner, J. M.; Bollinger, T. K.; Willis, C. K. R.; Voyles, J.; Misra, V. *PLoS ONE* **2014**, *9* (11), e112285.
(42) Field, K. A.; Johnson, J. S.; Lilley, T. M.; Reeder, S. M.; Rogers, E. J.; Behr, M. J.; Reeder, D. M. *PLOS Pathogens* **2015**, *11* (10), e1005168.
(43) Moore, M. S.; Reichard, J. D.; Murtha, T. D.; Nabhan, M. L.; Pian, R. E.; Ferreira, J. S.; Kunz, T. H. *PLoS ONE* **2013**, *8* (3), e58976.
(44) Johnson, J. S.; Reeder, D. M.; Lilley, T. M.; Czirják, G. Á.; Voigt, C. C.; McMichael, J. W.; Meierhofer, M. B.; Seery, C. W.; Lumadue, S. S.; Altmann, A. J.; Toro, M. O.; Field, K. A. *Ecology and Evolution* **2015**, *5* (11), 2203–2214.
(45) Fleming, A. *Bull. World Health Organ.* **2001**, *79* (8), 780–790.
(46) Horrocks, N. P. C.; Matson, K. D.; Tieleman, B. I. *Integrative and Comparative Biology* **2011**, *51* (4), 563–576.
(47) Lemieux-Labonté, V.; Simard, A.; Willis, C. K. R.; Lapointe, F.-J. *Microbiome* **2017**, *5* (1).
(48) Cornelison, C. T.; Gabriel, K. T.; Barlament, C.; Crow, S. A. *Mycopathologia* **2014**, *177* (1–2), 1–10.
(49) Cornelison, C. T.; Keel, M. K.; Gabriel, K. T.; Barlament, C. K.; Tucker, T. A.; Pierce, G. E.; Crow, S. A. *BMC Microbiology* **2014**, *14* (1).
(50) Zhang, T.; Chaturvedi, V.; Chaturvedi, S. *PLOS ONE* **2015**, *10* (10), e0141316.
(51) Singh, A.; Lasek-Nesselquist, E.; Chaturvedi, V.; Chaturvedi, S. *Microbiome* **2018**, *6* (1), 139.
(52) Micalizzi, E. W.; Mack, J. N.; White, G. P.; Avis, T. J.; Smith, M. L. *PLOS ONE* **2017**, *12* (6), e0179770.
(53) Hoyt, J. R.; Cheng, T. L.; Langwig, K. E.; Hee, M. M.; Frick, W. F.; Kilpatrick, A. M. *PLoS ONE* **2015**, *10* (4), e0121329.
(54) Cheng, T. L.; Mayberry, H.; McGuire, L. P.; Hoyt, J. R.; Langwig, K. E.; Nguyen, H.; Parise, K. L.; Foster, J. T.; Willis, C. K. R.; Kilpatrick, A. M.; Frick, W. F. *Journal of Applied Ecology* **2017**, *54* (3), 701–708.
(55) Fischer, N. M.; Altewischer, A.; Ranpal, S.; Dool, S.; Kerth, G.; Puechmaille, S. J. preprint; Ecology, 2021.
(56) Deacon, J. W. 4th ed.; Blackwell Pub: Malden, MA, 2006.
(57) American Type Culture Collection, 2013.
(58) Zhang, M.; Gu, L.; Zheng, P.; Chen, Z.; Dou, X.; Qin, Q.; Cai, X. *J Clin Lab Anal* **2020**, *34* (1).
(59) Langvad, F. *Journal of Microbiological Methods* **1999**, *37* (1), 97–100.
(60) Avena, C. V.; Parfrey, L. W.; Leff, J. W.; Archer, H. M.; Frick, W. F.; Langwig, K. E.; Kilpatrick, A. M.; Powers, K. E.; Foster, J. T.; McKenzie, V. J. *Frontiers in Microbiology* **2016**, *7*.
(61) Hoyt, J. R.; Langwig, K. E.; Okoniewski, J.; Frick, W. F.; Stone, W. B.; Kilpatrick, A. M. *EcoHealth* **2015**, *12* (2), 330–333.
(62) Schneider, C. A.; Rasband, W. S.; Eliceiri, K. W. *Nat. Methods* **2012**, *9* (7), 671–675.
(63) Sausen, C. W.; Bochman, M. L. *BioEssays* **2021**, *43* (8), 2100108.

(64) Skoog, D. A.; Holler, F. J.; Crouch, S. R. Seventh edition.; Cengage Learning: Boston, 2018.
(65) Nichols, L. 2nd ed.; 2017.
(66) Field, L. D.; Sternhell, S.; Kalman, J. R. Fifth edition.; Wiley: Chichester, West Sussex, 2013.
(67) Ouellette, R. J.; Rawn, J. D. First edition.; Elsevier: Amsterdam ; Boston, 2014.
(68) Pitt, J. J. *Clin Biochem Rev* **2009**, *30* (1), 19–34.
(69) Tro, N. J. Fifth edition.; Pearson Education, Inc: Hoboken, NJ, 2020.
(70) Napier, E. J.; Turner, D. I.; Rhodes, A. *Annals of Botany* **1956**, *20* (3), 461–466.
(71) Nigam, P. S.; Singh, A. In *Encyclopedia of Food Microbiology*; Elsevier, 2014; pp 570–578.
(72) Gull, K.; Trinci, A. P. J. *Nature* **1973**, *244* (5414), 292–294.
(73) Clardy, J.; Springer, J. P.; Buechi, G.; Matsuo, K.; Wightman, R. *J. Am. Chem. Soc.* **1975**, *97* (3), 663–665.
(74) Frisvad, J. C.; Larsen, T. O.; Dalsgaard, P. W.; Seifert, K. A.; Louis-Seize, G.; Lyhne, E. K.; Jarvis, B. B.; Fettinger, J. C.; Overy, D. P. *International Journal of Systematic and Evolutionary Microbiology* **2006**, *56* (6), 1427–1437.
(75) Grijseels, S.; Nielsen, J. C.; Randelovic, M.; Nielsen, J.; Nielsen, K. F.; Workman, M.; Frisvad, J. C. *Sci Rep* **2016**, *6* (1), 35112.
(76) Townley, E. R. In *Analytical Profiles of Drug Substances*; Elsevier, 1979; Vol. 8, pp 219–249.
(77) Fulmer, G. R.; Miller, A. J. M.; Sherden, N. H.; Gottlieb, H. E.; Nudelman, A.; Stoltz, B. M.; Bercaw, J. E.; Goldberg, K. I. *Organometallics* **2010**, *29* (9), 2176–2179.
(78) Crick, F. H. *Symp Soc Exp Biol* **1958**, *12*, 138–163.
(79) Wang, Z.; Gerstein, M.; Snyder, M. *Nat Rev Genet* **2009**, *10* (1), 57–63.
(80) Conesa, A.; Madrigal, P.; Tarazona, S.; Gomez-Cabrero, D.; Cervera, A.; McPherson, A.; Szcześniak, M. W.; Gaffney, D. J.; Elo, L. L.; Zhang, X.; Mortazavi, A. *Genome Biol* **2016**, *17* (1), 13.
(81) Ozsolak, F.; Milos, P. M. *Nat Rev Genet* **2011**, *12* (2), 87–98.
(82) Zhao, S.; Zhang, Y.; Gamini, R.; Zhang, B.; von Schack, D. *Sci Rep* **2018**, *8* (1), 4781.
(83) Rio, D. C.; Ares, M.; Hannon, G. J.; Nilsen, T. W. *Cold Spring Harbor Protocols* **2010**, *2010* (6), pdb.prot5439-pdb.prot5439.
(84) Wieczorek, D.; Delauriere, L.; Schagat, T. Methods of RNA Quality Assessment. http://www.promega.co.uk/resources/pubhub/methods-of-rna-quality-assessment/.
(85) Matlock, B. Assessment of Nucleic Acid Purity (Technical Note 52646) https://assets.fishersci.com/TFS-Assets/CAD/Product-Bulletins/TN52646-E-0215M-NucleicAcid.pdf.
(86) Sheng, Q.; Vickers, K.; Zhao, S.; Wang, J.; Samuels, D. C.; Koues, O.; Shyr, Y.; Guo, Y. *Briefings in Functional Genomics* **2016**, elw035.
(87) Illumina, Inc. 2017.
(88) Andrews, S. FastQC: A Quality Control Tool for High Throughput Sequence Data. http://www.bioinformatics.babraham.ac.uk/projects/fastqc/.

(89) Harvard Chan Bioinformatics Core. Introduction to RNA-Seq using high-performance computing. https://hbctraining.github.io/Intro-to-rnaseq-hpc-salmon-flipped/schedule/links-to-lessons.html.
(90) Grabherr, M. G.; Haas, B. J.; Yassour, M.; Levin, J. Z.; Thompson, D. A.; Amit, I.; Adiconis, X.; Fan, L.; Raychowdhury, R.; Zeng, Q.; Chen, Z.; Mauceli, E.; Hacohen, N.; Gnirke, A.; Rhind, N.; di Palma, F.; Birren, B. W.; Nusbaum, C.; Lindblad-Toh, K.; Friedman, N.; Regev, A. *Nat Biotechnol* **2011**, *29* (7), 644–652.
(91) Dobin, A.; Davis, C. A.; Schlesinger, F.; Drenkow, J.; Zaleski, C.; Jha, S.; Batut, P.; Chaisson, M.; Gingeras, T. R. *Bioinformatics* **2013**, *29* (1), 15–21.
(92) Li, B.; Dewey, C. N. *BMC Bioinformatics* **2011**, *12* (1), 323.
(93) Koch, C. M.; Chiu, S. F.; Akbarpour, M.; Bharat, A.; Ridge, K. M.; Bartom, E. T.; Winter, D. R. *Am J Respir Cell Mol Biol* **2018**, *59* (2), 145–157.
(94) Harvard Chan Bioinformatics Core. Introduction to DGE. https://hbctraining.github.io/DGE_workshop_salmon_online/schedule/links-to-lessons.html.
(95) Conesa, A.; Gotz, S.; Garcia-Gomez, J. M.; Terol, J.; Talon, M.; Robles, M. *Bioinformatics* **2005**, *21* (18), 3674–3676.
(96) Coates, A. R.; Halls, G.; Hu, Y. *British Journal of Pharmacology* **2011**, *163* (1), 184–194.
(97) Varney, A. M.; Smitten, K. L.; Thomas, J. A.; McLean, S. *ACS Pharmacol. Transl. Sci.* **2021**, *4* (1), 168–178.
(98) Siroli, L.; Braschi, G.; de Jong, A.; Kok, J.; Patrignani, F.; Lanciotti, R. *J Appl Microbiol* **2018**, *125* (5), 1308–1320.
(99) Bouzo, D.; Cokcetin, N. N.; Li, L.; Ballerin, G.; Bottomley, A. L.; Lazenby, J.; Whitchurch, C. B.; Paulsen, I. T.; Hassan, K. A.; Harry, E. J. *mSystems* **2020**, *5* (3).
(100) Aranda, P. S.; LaJoie, D. M.; Jorcyk, C. L. *ELECTROPHORESIS* **2012**, *33* (2), 366–369.
(101) Drees, K. P.; Palmer, J. M.; Sebra, R.; Lorch, J. M.; Chen, C.; Wu, C.-C.; Bok, J. W.; Keller, N. P.; Blehert, D. S.; Cuomo, C. A.; Lindner, D. L.; Foster, J. T. *Genome Announc* **2016**, *4* (3).
(102) Anders, S.; Huber, W. *Genome Biol* **2010**, *11* (10), R106.